Optimal Design of Orthotropic Piezoelectric Membranes and Plates Using Particle Swarms

by
Matthew James Stuart Joubert

Dissertation presented for the degree of *Master of Engineering (Mechanical) in the Faculty of Engineering at Stellenbosch University*

Promotor: Mr S. Parker and Prof A. A. Groenwold

April 2014

Declarations

By submitting this thesis electronically, I declare that the entirety of the work contained therein is my own, original work, that I am the sole author thereof (save to the extent explicitly otherwise stated), that reproduction and publication thereof by Stellenbosch University will not infringe any third party rights and that I have not previously in its entirety or in part submitted it for obtaining any qualification.

Date:.....

Abstract

Optimal Design Of Orthotropic Piezoelectric Membranes And Plates Using Particle Swarms

M.J.S. Joubert

Department of Mechanical and Mechatronic Engineering,
University of Stellenbosch,
Private Bag X1, Matieland 7602, South Africa.

Thesis: MEng (Mech)

March 2014

Over the past 50 years smart materials have made their appearance in many structures. The thermopiezoelectric ceramic is one of these smart materials. When thermal effects are considered negligible, then the materials are classified as piezo-ceramic and piezoelectric materials. These so called piezo-ceramics are used as actuator and sensor components in many structures. The use of these components with composite materials is significant due to their application in the aerospace and aeronautics fields. The interaction that the piezoelectric material has with a composite body can be improved in order to reduce the energy requirement of the material for deformation. An objective in the optimisation of composite material structures is to minimise compliance or maximise stiffness $\mathbf{u}^T\mathbf{f}$, with the laminate ply orientations as design variables, where $\mathbf{u}$ and $\mathbf{f}$ are displacement and force vectors, respectively.

Here, the objective is not the maximisation of stiffness but the maximisation of compliance, with typical constraints being failure criteria. These failure criteria can include theories such as the maximum principle stress, the Tsai-Hill or Tsai-Wu failure theories. The compliance is maximised to accentuate any piezoelectric movement and is for theoretical treatment only.

Piezoelectric materials once polarized the materials becomes quasi-isotropic. The piezoelectric materials are isotropic in the plane normal to the direction of the voltage being applied and have altered properties normal to this plane. This change in the material properties can be exploited so that the layup can be altered in orientation to improve performance. The idea is to improve the mechanical capabilities of the structure subject to an electrical input or *vice versa*.

In the works by both Carrera *et al.* and Piefort, First Order Shear Deformation Theory (FSDT) is used in finite element analysis to characterise the structural and electrical behaviour of a plate or

shell. FSDT, also known as the Mindlin-Reissner theory, is a plate bending theory that assumes a transverse shear distribution through the thickness of the plate. This theory is considered an improvement on the standard theories such as the Kirchoff or Timoshenko theories.

Many optimisation techniques exist and are classed as either being direct search or gradient based methods. Particle Swarm Optimisation (PSO) is a direct search method. It mimics the behaviour of a flock of birds or school of fish in their attempt to find food. The PSO's mathematical statement characterises a set of initial unknown particles within a designated search space that are compared to a set of local best particles and a single global best particle. This comparison is used to update the swarm each run cycle.

Regression is a procedure whereby a set of testing data is used to fit a pseudo-function that represents the form the data should take in practice. The aim of this work is to optimise the piezoelectric-composite layer interaction to improve the overall compliance of a structure.

Extensive modelling is performed and tested with peer reviewed literature to demonstrate its accuracy.

Opsomming

Optimale Ontwerp van Ortotropiese Piezo-elektriese Membrane en Plate deur Partikelswerms

("Optimal Design Of Orthotropic Piezoelectric Membranes And Plates Using Particle Swarms ")

Projek voorstel

M.J.S. Joubert

Departement Meganiese en Megatroniese Ingenieurswese,
Universiteit van Stellenbosch,
Privaatsak X1, Matieland 7602, Suid-Afrika.

Tesis: MIng (Meg)

Maart 2014

Oor die afgelope 50 jaar het slim materiale hulle verskyning gemaak in verskeie strukture. Termopiezo-elektriese keramieke is een van hierdie nuwe materiale. Wanneer termiese effekte onbeduidend is, word hierdie materiale as piezo-elektriese materiale geklassifiseer. Hierdie sogenaamde piezo-keramieke word gebruik as aandrywers en sensoriese onderdele in verskeie strukture. Die kombinasie van hierdie onderdele met saamgestelde materiale het belangrike toepassings in die ruimte- en lugvaartkunde. Die interaksie van die piezo-elektriese materiale met die saamgestelde materiaal strukture kan verbeter word om die energie-vereistes van die materiaal vir vervorming te verminder. 'n Tipiese doel in die optimering van saamgestelde materiaalstrukture is om styfheid $\mathbf{u}^T\mathbf{f}$ te maksimeer met die gelamineerde laag-oriëntasies as ontwerpsveranderlikes, waar $\mathbf{u}$ en $\mathbf{f}$ onderskeidelik verplasing en kragvektor voorstel.

In teenstelling met die optimering van die samestelling wat voorheen gedoen is, is die doel hier nie die maksimering van styfheid nie, maar die minimering van styfheid, met falingskriteria as tipiese beperkings. Die falingskriteria sluit die volgende in: die maksimum spanningsteorie, en die Tsai-Hill of Tsai-Wu falingsteorieë. Die styfheid word geminimeer om piezo-elektriese verplasing te versterk, maar word hierin net teoreties bekyk.

Sodra piezo-elektriese materiale gepolariseer word, word hulle quasi-isotropies. Die piezo-elektriese materiale is isotropies in die vlak gelyk aan die rigting van die stroomspanning wat daarop toegepas word en het ander eienskappe normaal tot die vlak. Die verandering in die materiaal se eienskappe kan gebruik word sodat beide die saamgestelde materiaal en die piezo-elektriese laag se oriëntasie aangepas kan word vir verbeterde werkverrigting. Die idee is om

die meganiese vermoëns te verbeter van ’n struktuur wat onderwerp word aan ’n elektriese inset of *vice versa*.

In die literatuur van beide Carrera et al. en Piefort word Eerste Orde Skuifvervormings Teorie (EOST) gebruik in eindige element analises om die strukturele en elektriese gedrag van ’n plaat of dop te karakteriseer. EOST, ook bekend as Mindlin-Reissner teorie, is ’n plaat buigings-teorie wat ’n dwarsvervormingverspreiding aanneem deur die dikte van die plaat. Hierdie teorie word gesien as ’n verbetering op die standaard teorieë soos bv. Kirchoff of Timoshenko se teorieë.

Daar bestaan baie optimeringstegnieke wat geklassifiseer word as ’direkte soek’ of ’helling-gebaseerde’ metodes. Partikel swerm-optimering (PSO) is ’n direkte soekmetode. Dit boots die gedrag van ’n swerm voëls of ’n skool visse in hulle poging om kos te vind, na. PSO se wiskundige stelling karakteriseer ’n aanvanklike stel onbekende partikels binne ’n afgebakende soekgebied wat vergelyk word met ’n stel van die beste plaaslike partikels sowel as ’n enkele beste globale partikel. Die vergelykings word gebruik om die swerm met elke siklus op te dateer.

Regressie is ’n metode waarin toetsdata gebruik word om ’n benaderde funksie te konstrueer wat ongeveer voorspel hoe die regte funksie lyk. Die doel van hierdie werk is om die piezo-elektriese saamgestelde laag te optimeer en die interaksie van die totale gedrag van die struktuur te verbeter.

Uitgebreide modellering word uitgevoer en getoets met eweknie-beoordeelde literatuur om die akkuraatheid en korrektheid te bewys.

Contents

List of Figures

List of Tables

List of Algorithms

Chapter 1

Introduction

In the transport industry, comprising of aerospace, automotive, locomotive and marine, improving aerodynamics results in millions of dollars in savings [14]. With this in mind, it is not surprising that the manufacturers pour significant resources into this field of study. Generally, aerodynamic improvements are made through the redesign of the skin or specified contact regions where problems arise [15]. These regions are normally identified through the use of commercial software.

More central to the authors interest is the field of adaptive shape control of aerofoils/wings. It is theorised that shape control in this region could improve fuel consumption by up to 15% [16]. At this juncture the question is how can this shape control be achieved?

Smart materials in general comprise a field of research that has gained major popularity in the last 50 years or so [17]. They fall under the categories of materials that change shape due to temperature, electricity, magnetic fields, light or acidity [18]. Central to this thesis, is the piezoelectric field of smart materials where mechanical strains are linked to the electrical input/output of the material.

The general, piezoelectric materials are used in small structures and actuators [19]. This however does not limit their use entirely to small structures, large scale use has been achieved where a piezoelectric film has significantly altered the shape of a large structure through bending [20]. It is therefore possible that this large scale use could also be implemented into the shape control of aerofoils or wings. This could, initially, be attempted on drones and unmanned aircraft where the use of composites for aerofoils is prominent. Often, when piezoelectric materials are used in relatively large structures, they are used in conjunction with a composite layup [1]. This thesis will focus on the theory behind the utilisation of the piezo-composite layup along with its optimised numerical applications to simple structures. Thus, this research's major objective is:

Optimising the piezoelectric-composite layer interaction to improve the overall compliance of a structure.

The primary objectives to affect this outcome are:

- Incorporate piezoelectric material model into the finite element method.
- Program a solver for membrane piezoelectric finite element models.

- Enhance the program to incorporate piezoelectric plate models.
- Prove a comprehensive knowledge of optimisation methods.
- Extend the program to incorporate an optimisation scheme to allow for the improvement of the piezoelectric composite structure.
- Critically analyse the results of the program and review the data.

On completion of this thesis the reader should have a thorough knowledge of the general workings of piezoelectric finite element analysis and at least one optimisation scheme. A more general knowledge of the finite element and optimisation fields along with their programming methods should be realised.

With this in mind, Chapter 2 gives a brief introduction to the literature that was used in the research of this thesis's outcomes. Please be advised however, that chapter 2 is not a traditional literary review but rather an outline to the research path taken. It is written in this manner due to the space constraints within this thesis.

Chapter 3 pertains to the research done in the finite element method along with the results of the programming. This chapter explains the general and piezoelectric finite element methods in stages that are directly comparable to one another. This is done in order to improve understanding of the more problematic piezoelectric principles.

In Chapter 4 optimisation is explained. One optimisation method is chosen and explained in detail. Test cases are demonstrated and the results pertaining to these test cases obtained from the author's program are compared to external published results.

Chapter 5 is where the optimisation will be combined with the piezoelectric finite element method. This is achieved by coupling the finite element solver and the objective function to produce a compliance result that can then be maximised. At this point the author will attempt to improve the speed and performance of the program through the use of basic linear algebra subroutines (BLAS), Open Multi-Processing (OpenMP) and Regression. The BLAS and OpenMP will be utilised through reprogramming of areas that require the most time (assessed through profiling of the program). The regression will be implemented through coupling with the FEA and optimiser resulting in a reduction of FEA runs. After this, multiple test cases will be run and the results will be detailed and explained. The test cases that have been run pertain to the results shown in Chapter 3 and an improvement is expected.

Finally, a conclusion will be drawn and a break down of the objectives will be stated.

Chapter 2

Literature

Generally in theses, a literature review is called upon to explain the work that is already common knowledge. In this thesis, this definition will be altered slightly because most of the processes used are in existing fields of research and although the knowledge is not common, it is considered to be common enough. This section will describe the research that was conducted by giving a very short explanation on each topic. The topics are finite element analysis, both general and piezoelectric, optimisation, regression and programming.

2.1 General Finite Element Analysis (FEA)

The starting point for this research was in finite element analysis. For the introduction Cook's work 'Finite Element Modelling for Stress Analysis' explained the basis of the finite element method and Cook *et al.* presented it in more detail in 'Concepts and Applications of Finite Elements' [12; 21]. Both of these books explained the classical approach to the finite element method, although, for a more in depth approach the works by Reddy gave an understandable look at the deeper principles [22; 23; 24]. Two other works, one by Zienkiewicz and Taylor and the other by Solin *et al.*, were useful although in most areas they proved to be for the extremely advanced reader and were used to enhance understanding [25; 26]. The last book of interest was a work by Dlowinski *et al.* that explained energy methods [27]. This work proved influential in grasping the more problematic variational concepts.

Most of the definition of the Finite Element Method (FEM) was extracted from the works above. Additional information obtained from the papers by Bathe and Dvorkin detailed an expansion to the shear stress in plate elements [5; 6]. Another paper by Macneal and Harder detailed a standard for testing of finite elements [28]. The last paper of major significance was by Di and Ramm detailing the definition of the hybrid finite elements [29].

2.2 Piezoelectric Finite Element Analysis

The major area of research was on piezoelectric finite element analysis. This was due to the large quantity of papers pertaining to this field of research. Benjeddou published a survey of piezoelectric elements in 2000 in which 113 papers were cited [30]. Since then many more works have been published.

Piezoelectric formulations are generally based on composite layered materials and the books by Kaw and Reddy give thorough explanation of these subjects [3; 23]. Allik and Hughes published a paper on the formulation of a piezoelectric tetrahedral element [31]. Although the tetrahedral element was not used the explanation given on the formulation was the building block for the understanding of piezoelectric formulations. In 2001 Piefort published a thesis on 'Simplified Plate and Shell Elements for Piezoelecrtic Finite Element Analysis' [13]. This work proved to be very beneficial and formed the basis of the work done on piezoelectrics in this thesis.

In 2009 Brischetto published a thesis on 'Multi-Field Problems for Plates and Shells' [32]. Carrera *et al.* built upon this by publishing a book in 2011 on 'Plates, Shells and Smart Structures' where the complete formulation for a piezoelectric material is defined [1]. The works mentioned above are all finite element prioritised. To build upon the fundamental principles of piezoelectric theory a more scientific approach was assessed.

The scientific work was used to supplement understanding and Maxwell released a thesis in 2009 where the micro-mechanical principles of piezoelectric materials are explained [33]. Maxwell's work had a strong theoretical basis and moved on to nanocomposites. At this juncture, an internal description from Morgan Ceramics was used to further elaborate on the practical engineering applications of the materials [19].

The term piezoelectric is a simplification from thermopiezoelectric ceramics materials where the heating component is ignored and although this was touched upon in the works by Carrera *et al.* and Piefort it was later simplified for the finite element models [34; 13]. Lee released an internal paper from NASA on the 'Finite Element Analysis of Active and Sensory Thermopiezoelectric Composite Materials' in 2001. This paper shows the full workings of these materials [35].

2.3 Optimisation

The optimisation field is ever growing and a thorough introduction to this field is given by Rao [36]. The general area of interest is the particle swarm optimisation method due to its simplicity of application in this proof of concept thesis. Rao detailed the general method along with the programming techniques. Following Rao's in book suggestion the penalty method application to the particle swarm was researched in a paper by Liu and Lin [37]. In this paper a momentum based particle swarm method was suggested which proved beneficial in application.

The particle swarm method was researched through programming logic, and trial and error. As such most of the papers found, beyond those already mentioned, were researched as problems or inaccuracies arose. One such group of papers were those by Wilke *et al.* on the differences between the linear and classical update rules [38; 39]. Another was on boundary handling methods by Padhye and Deb [40].

2.4 Regression

On researching regression techniques a basic statistical method was first studied. This method was the response surface methodology [41]. Following the attempted application of the methodology using linear regression techniques it was noted that the regression would have to be altered for every different finite element (FE) model due to the multi-modal problem.

To avoid the continuous changes a more adaptive technique would have to be used. To facilitate this, machine learning techniques were researched [42; 43]. This research lead to the study of two highly adaptive techniques based on neural networks and single linear feed-forward networks namely the extreme learning machine (ELM) and the general regression neural network (GRNN) [11; 44; 45; 46]. Following this research it was decided that the GRNN should be implemented in this thesis taking into consideration its adaptability.

2.5 Programming

The last and probably most important section of research was the actual programming. The importance of which is highly relevant as the programming was extensive and about 65% of the time spent on this thesis was in this field. Due to space constraints the program is only supplied in its briefest form in the text.

A basic finite element and optimisation routine was coded. For these tasks the books by Ferreira and Rao were used in conjunction with MATLAB [47; 36].

Once a complete working model of the finite element optimiser was achieved, the code was translated into FORTRAN 95 in order to achieve greater speed. To support this process the book by Ellis *et al.* was extremely useful in its easy to understand descriptions [48]. Following this more speed is always preferable and multi-processor optimisation was implemented through the use of OpenMP which was learnt at a course, attended during the research period, that was presented by the centre for high performance computing in Cape Town [49]. This allowed for the full parallel utilisation of all the cores in any computer. To supplement the speed supplied by the multiprocessing the basic linear algebra subroutines (BLAS) were implemented following direction from the Linear Algebra Package (LAPACK) website [50]. This package supplied preprogrammed programs that have been created for speed in the solving of linear algebra problems.

Chapter 3

Finite Element Analysis

3.1 Standard QUAD 4 Membrane Formulation

In all basic formulations there are alternate means of arriving at the same solution. Although the methods used may differ, if the mathematical logic is sound no problems arise. Two such approaches will be explained in this section. The approaches will be the variational mathematical solution (from here on called the variational formulation) and the finite element approximate numerical solution (from here on called the finite element formulation) to any arbitrary problem.

3.1.1 Variational Formulation

The variational formulation arises from continuum mechanics, using an energy method approach, the underlying mechanics of a structure can be represented with a mathematical equation. This equation can then be solved analytically. Solving problems in this manner proves costly because the problems are simply too large. Therefore FEMs are used. Having knowledge of the theory of a variational formulation in structural mechanics is necessary for full understanding of finite element methods.

The basic principle of variational formulations begin with the statement for total potential energy [12; 26]:

$$\Pi = U + W_p, \tag{3.1}$$

where Π is the total potential energy, U is the internal energy and W_p is the potential energy of applied loads [26]. Using variational mathematics and taking

$$\delta W_p = -\delta W \tag{3.2}$$

as the internal energy generally acts against the potential of applied loads in elastic systems. The principle of minimum potential energy can be restated as:

$$\delta\Pi = \delta U - \delta W = 0. \tag{3.3}$$

The statement for total potential energy can be redefined as,

$$\Pi = U - W, \tag{3.4}$$

where W is the work done by the loads [26]. Now that the underlying principle has been defined the construction of W and U needs to take place.

3.1.1.1 Variation and Functional Mathematics

It is pertinent at this point to explain what a functional variation is before explaining U or W. A functional is a variable that is itself a function [51]. An example of this is:

$$J = \int_{x_1}^{x_2} G(x, u, u', u'')\, dx, \tag{3.5}$$

where J and G are functionals as J is a function of G and G is a function of x, u, u', u'' [51]. In terms of variations suppose that any tentative solution $\overline{u}$ is equal to the sum of the exact and the variation of the solution:

$$\overline{u} = u + \delta u, \tag{3.6}$$

where δu is the variation [51]. Consequently as δu tends to zero we get the exact solution.

3.1.1.2 Internal Energy

U is defined as the internal energy of a structure. In everyday situations there can be subtle alterations to this internal energy dependent on external influences like heat and electricity [13]. Also, there is the consideration of non-linear compliance and whether or not the structure is under a pre-stress [12]. All of these conditions need to be taken into account when formulating the variational principle.

Following this reasoning U can be constructed. Consider a simple static model of a spring

$$U = \frac{1}{2} k u^2, \tag{3.7}$$

with k being the stiffness and u the displacement [52]. For a simple beam in uni-axial tension it is seen that the beam acts as a spring of sorts and the equation is

$$U = \frac{1}{2} \sigma \epsilon \tag{3.8}$$

and using Hooke's law a form similar to the spring is seen

$$U = \frac{1}{2} E_Y \epsilon^2 = \frac{1}{2} E_Y \left(\frac{\partial u}{\partial x}\right)^2, \tag{3.9}$$

where σ is stress, E_Y is Young's Modulus, ϵ is strain, x is a distance along the beam and u is the displacement in the x-direction [12]. Taking a look at a broader definition lets assume U_0 is the energy of an infinitesimal section of an arbitrary structure. Equation (3.9) can be expanded to define a more general structure:

$$U_0 = \int_0^{\epsilon} \boldsymbol{\sigma}^T \, d\epsilon \tag{3.10}$$

$$= \int_0^{\epsilon_x} \sigma_x \, d\epsilon_x + \int_0^{\epsilon_y} \sigma_y \, d\epsilon_y + \int_0^{\epsilon_z} \sigma_z \, d\epsilon_z + \int_0^{\gamma_{xy}} \tau_{xy} \, d\gamma_{xy}$$

$$+ \int_0^{\gamma_{xz}} \tau_{xz} \, d\gamma_{xz} + \int_0^{\gamma_{yz}} \tau_{yz} \, d\gamma_{yz} \tag{3.11}$$

$$= \frac{1}{2}\boldsymbol{\sigma}^T \boldsymbol{\epsilon} \tag{3.12}$$

here τ and γ are the shear representation of the stress and strain respectively. Again using Hooke's law

$$= \frac{1}{2}\boldsymbol{\epsilon}^T \mathbf{C}_E \boldsymbol{\epsilon}, \tag{3.13}$$

where $\mathbf{C}_E$ is the constitutive relation and the bold symbols indicate matrices or column vectors [12]. If, however, there are initial strains and stresses that the equation must accommodate, the considered stress will change to

$$\boldsymbol{\sigma} = \mathbf{C}_E(\boldsymbol{\epsilon} - \boldsymbol{\epsilon}_0) + \boldsymbol{\sigma}_0. \tag{3.14}$$

Substituting Equation (3.14) into Equation (3.12) then Equation (3.13) yields

$$U_0 = \frac{1}{2}\boldsymbol{\epsilon}^T \mathbf{C}_E \boldsymbol{\epsilon} - \boldsymbol{\epsilon}^T \mathbf{C}_E \boldsymbol{\epsilon}_0 + \boldsymbol{\epsilon}^T \boldsymbol{\sigma}_0, \tag{3.15}$$

where $\boldsymbol{\sigma}_0$ are the initial stresses and $\boldsymbol{\epsilon}_0$ are the initial strains [12]. U_0 however only describes the localised internal energy and this needs to be integrated over the structures volume (Ω) in order to cater for all internal energy in the structure [12]. Thus

$$U = \int_{\Omega} U_0 \, d\Omega, \tag{3.16}$$

which by Equation (3.13) is

$$U = \int_{\Omega} \frac{1}{2}\boldsymbol{\epsilon}^T \mathbf{C}_E \boldsymbol{\epsilon} \, d\Omega \tag{3.17}$$

or which by Equation (3.15) is

$$U = \int_{\Omega} \frac{1}{2}\boldsymbol{\epsilon}^T \mathbf{C}_E \boldsymbol{\epsilon} - \boldsymbol{\epsilon}^T \mathbf{C}_E \boldsymbol{\epsilon}_0 + \boldsymbol{\epsilon}^T \boldsymbol{\sigma}_0 \, d\Omega, \tag{3.18}$$

which describes the internal energy of any simply elastic structure [12].

3.1.1.3 Potential Energy of Applied Loads

The next step is to define the work done on the structure, W. Work done is classified into three categories. The first is body forces, $\mathbf{f}_B$, which are applied over the structure's entire volume (e.g. self weight), the second is tractions, $\mathbf{f}_\Gamma$, applied to the body's outer surfaces (e.g. friction or water pressure) and the last is concentrated loads, $\mathbf{f}_P$, applied to single points (e.g. a force or moment) [51]. These are described as

$$\int_{\Omega} \mathbf{u}^T \mathbf{f}_B \, d\Omega, \int_{\Gamma} \mathbf{u}^T \mathbf{f}_\Gamma \, d\Gamma \text{ and } \mathbf{u}^T \mathbf{f}_P \tag{3.19}$$

respectively, where Γ is the surface where the respective load is applied [12].

3.1.1.4 Potential Energy and its Variation

Following the formulations in the last two subsections, the potential energy equation can be expanded to:

$$\Pi = U - W, \tag{3.20}$$

$$= \int_{\Omega} \frac{1}{2}\boldsymbol{\epsilon}^T \mathbf{C}_E \boldsymbol{\epsilon} - \boldsymbol{\epsilon}^T \mathbf{C}_E \boldsymbol{\epsilon}_0 + \boldsymbol{\epsilon}^T \boldsymbol{\sigma}_0 \, d\Omega - \int_{\Omega} \mathbf{u}^T \mathbf{f}_B \, d\Omega - \int_{\Gamma} \mathbf{u}^T \mathbf{f}_\Gamma \, d\Gamma - \mathbf{u}^T \mathbf{f}_P. \tag{3.21}$$

Furthermore, following the arguments of Equation (3.3) and Section 3.1.1.1, if the variation of potential energy is equal to 0 the solution is exact [26]. Thus, taking the first functional variation of potential energy gives

$$\begin{aligned} 0 = \delta\Pi = &\int_{\Omega} \delta(\boldsymbol{\nabla}\mathbf{u})^T (\mathbf{C}_E(\boldsymbol{\nabla}\mathbf{u}) - \mathbf{C}_E\boldsymbol{\epsilon}_0 + \boldsymbol{\sigma}_0) - \delta\mathbf{u}^T \mathbf{f}_B \, d\Omega \\ &- \int_{\Gamma} \delta\mathbf{u}^T \mathbf{f}_\Gamma \, d\Gamma - \delta\mathbf{u}^T \mathbf{f}_P, \end{aligned} \tag{3.22}$$

where

$$\boldsymbol{\epsilon}^T = (\boldsymbol{\nabla}\mathbf{u})^T \tag{3.23}$$

and the $\boldsymbol{\nabla}$ symbol is used to define the derivative operator later defined in Equation (3.38).

At this juncture integration by parts needs to be completed using a higher order of the basic formula [26; 53]:

$$\int g_{arb}(x)' f_{arb}(x)\,dx = g_{arb}(x)f_{arb}(x) - \int f_{arb}(x)' g_{arb}(x)\,dx, \tag{3.24}$$

which gives rise to:

$$\int_{\Omega} \frac{\partial u}{\partial x} v\,d\Omega = \int_{\Gamma} uv \cdot \upsilon\,d\Gamma - \int_{\Omega} u\frac{\partial v}{\partial x}\,d\Omega. \tag{3.25}$$

From this, the solution to the reduced integral,

$$\int_{\Omega} \delta(\nabla \mathbf{u})^T(\mathbf{C}_E(\nabla \mathbf{u}) - \mathbf{C}_E\boldsymbol{\epsilon}_0 + \boldsymbol{\sigma}_0)\,d\Omega = \int_{\Omega} \delta(\nabla \mathbf{u})^T\boldsymbol{\sigma}\,d\Omega \tag{3.26}$$

can be determined to be

$$\int_{\Omega} \delta(\nabla \mathbf{u})^T\boldsymbol{\sigma}\,d\Omega = \int_{\Gamma} \delta\mathbf{u}^T\mathbf{G}_n^T\boldsymbol{\sigma}\,d\Gamma - \int_{\Omega} \delta\mathbf{u}^T\nabla^T\boldsymbol{\sigma}\,d\Omega, \tag{3.27}$$

where

$$\mathbf{G}_n^T = \begin{bmatrix} n_1 & 0 & 0 & n_2 & 0 & n_3 \\ 0 & n_2 & 0 & n_1 & n_3 & 0 \\ 0 & 0 & n_3 & 0 & n_1 & n_2 \end{bmatrix}, \tag{3.28}$$

where $\mathbf{n} = (n_1, n_2, n_3)$ are direction cosines of the normal boundary to the surface under traction S [26]. This allows for the full expansion to the theoretically solvable solution which is:

$$\begin{aligned} \delta\Pi = &- \int_{\Omega} \delta\mathbf{u}^T\nabla^T(\mathbf{C}_E(\nabla \mathbf{u}) - \mathbf{C}_E\boldsymbol{\epsilon}_0 + \boldsymbol{\sigma}_0) + \delta\mathbf{u}^T\mathbf{f}_B\,d\Omega \\ &+ \int_{\Gamma} \delta\mathbf{u}^T(\mathbf{G}_n^T(\mathbf{C}_E(\nabla \mathbf{u}) - \mathbf{C}_E\boldsymbol{\epsilon}_0 + \boldsymbol{\sigma}_0) - \mathbf{f}_\Gamma)\,d\Gamma - \delta\mathbf{u}^T\mathbf{f}_P, \end{aligned} \tag{3.29}$$

which is the variational problem for any arbitrary problem [12; 26]. With the boundary conditions being

$$\mathbf{u} = \mathbf{u}^* \tag{3.30}$$

for displacement and

$$\mathbf{f}_\Gamma = \mathbf{G}_n^T\boldsymbol{\sigma} = \mathbf{f}_S^* \tag{3.31}$$

for traction respectively, where the * symbol represents a specified body, surface or point [26]. From this type of variational principle many variants/hybrids can be created that explain the problem in slightly different ways. These variants define alternate ways of coming to this point or progressing to the FE Model. Some of these variants are

- the Bubnov-Galerkin method,
- the Hu-Washizu principle,
- the Hellinger-Reissner method,
- the Rayleigh-Ritz method,
- the principle of virtual work,
- the potential energy principle,
- the complementary energy principle,

these by no means encompass all the methods but do include those primarily used to date [54; 55; 56]. From here it is possible to change Equation (3.29) into its weak form and using the Budnov-Galerkin method of solution, to change it to a FE representation. The next section explains the FE development/process of the solution to this variational principle.

3.1.2 FE Formulation Adaptation

The method for the FE Formulation can be derived from the work done in the previous section and is basically an expansion of that work. Here the simplest possible approach will be used to explain the formulation so as to ensure understanding in the chapters to come. The basis for FE is the formula:

$$\mathbf{f} = \mathbf{K}\mathbf{q}, \tag{3.32}$$

where $\mathbf{f}$ defines a vector of known forces, $\mathbf{K}$ defines the calculated stiffness matrix of the structure and $\mathbf{q}$ defines the unknown vector of displacements [21]. All of these variables depend on the number of degrees of freedom (dof's) in the system as well as the number of nodal points and as such $\mathbf{q}$ is not equivalent to $\mathbf{u}$ [57]. The details of these variables will be explained in depth in this section.

3.1.2.1 Defining The System

Nodal points are grouped together in elements of predetermined shape types as in Figure 3.1 [21]. The element is a quadrilateral which can group 4, 8 or 9 nodes depending on the technique used. These techniques are adaptations of either linear or quadratic interpolations along with a standard or hybrid scheme approach [12; 29]. This section deals with only the 4-node linearly interpolated quadrilateral with a standard approach.

The system is a grouping of elements or rather a body that has been discretized into a large number of elements. These bodies can be anything from buildings to bridges to cams or MEMS (Micro-electro-mechanical systems). Once discretized into multiple elements the body can then be stated as a FE model or system. FE systems are in essence only the solution sum of the individual elements displacements. Following this logic, it is inevitable that the development and solution of the individual elements is a sizeable part of the solution.

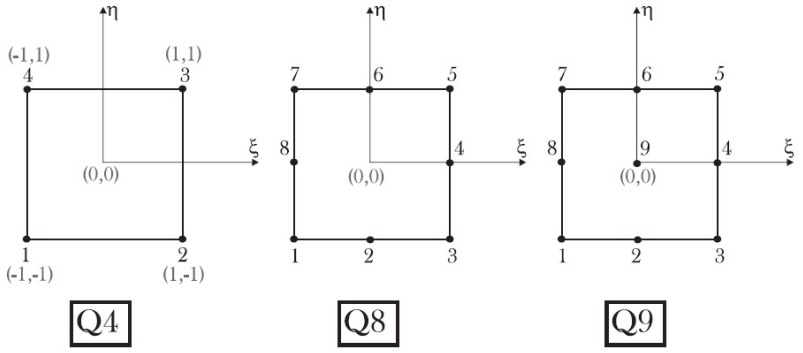

Figure 3.1: Shapes of elements [1]

There are two major approaches to solving systems. The first is to solve them in their global co-ordinates [21]. This proves quite cumbersome as the co-ordinates for each node have to be passed around, the interpolation functions change at each element and also the shapes of the elements become arbitrary [21]. The second approach (called the iso-parametric approach) is to transform the global co-ordinates to a local system (Figure 3.2) that is the same for all elements. This is done using a transformation matrix [12]. This approach proves very useful because the resultant standard solution type can be used to solve for all of the elements [58; 57].

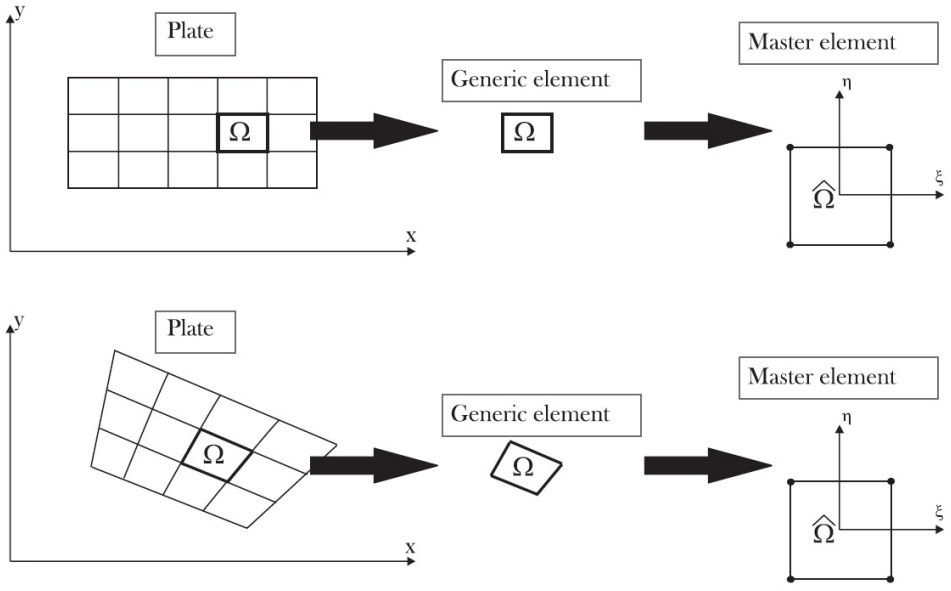

Figure 3.2: System co-ordinate transformation [1]

The further development of the system requires additional details. To initiate this further development the simplified elements can be classified into different types, one of which is the membrane element. This element will be used in this section. Membrane elements have a prescribed set of degrees of freedom (being u and v). Also, let it be assumed that the initial/pre-existing

stresses and strains on the body are negligible. This provides enough information to proceed to the FE mathematical development and to solve a simple system.

3.1.2.2 Mathematical System Definition

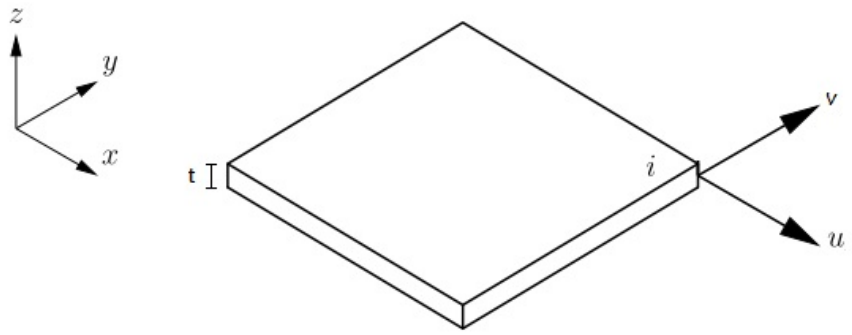

Figure 3.3: A membrane Q4 element [2]

The formulation to a membrane problem will be defined here following Figure 3.3, as it is one of the simpler problems to conceive. To begin it is understood that

$$\mathbf{u} = \mathbf{N}\mathbf{q} \tag{3.33}$$

and differentiating this gives

$$\boldsymbol{\epsilon} = \boldsymbol{\nabla}\mathbf{N}\mathbf{q} = \mathbf{B}\mathbf{q}, \tag{3.34}$$

where

$$\mathbf{N} = \begin{bmatrix} N_1 & 0 & N_2 & 0 & N_3 & 0 & N_4 & 0 \\ 0 & N_1 & 0 & N_2 & 0 & N_3 & 0 & N_4 \end{bmatrix}, \tag{3.35}$$

$$\mathbf{q} = \begin{bmatrix} u_1 & v_1 & u_2 & v_2 & u_3 & v_3 & u_4 & v_4 \end{bmatrix}, \tag{3.36}$$

and

$$\begin{aligned} N_1 &= \frac{1}{4}(1-\xi)(1-\eta), \\ N_2 &= \frac{1}{4}(1+\xi)(1-\eta), \\ N_3 &= \frac{1}{4}(1+\xi)(1+\eta), \\ N_4 &= \frac{1}{4}(1-\xi)(1+\eta), \end{aligned} \tag{3.37}$$

where **N** is the interpolation matrix resulting from nodal interactions [21; 12]. If

$$\boldsymbol{\nabla} = \begin{bmatrix} \dfrac{\partial}{\partial \xi} & 0 \\ 0 & \dfrac{\partial}{\partial \eta} \\ \dfrac{\partial}{\partial \eta} & \dfrac{\partial}{\partial \xi} \end{bmatrix} \tag{3.38}$$

then from Equation (3.34)

$$\mathbf{B} = \begin{bmatrix} N_{1,\xi} & 0 & N_{2,\xi} & 0 & N_{3,\xi} & 0 & N_{4,\xi} & 0 \\ 0 & N_{1,\eta} & 0 & N_{2,\eta} & 0 & N_{3,\eta} & 0 & N_{4,\eta} \\ N_{1,\eta} & N_{1,\xi} & N_{2,\eta} & N_{2,\xi} & N_{3,\eta} & N_{3,\xi} & N_{4,\eta} & N_{4,\xi} \end{bmatrix}, \tag{3.39}$$

where the subscript '$,\xi$' or '$,\eta$' means the partial derivative with respect to '$,\xi$' or '$,\eta$' respectively. These equations assume that the transformation to local coordinates has already taken place [21; 12].

In Section 3.1.2.1 the transformation from global to local co-ordinates was mentioned. This has already been allowed for in the above matrices, however a scaling value needs to be applied. This is done because the elements of an arbitrary size in the global coordinate scheme are scaled to perfect 2×2 square elements in the local coordinate scheme. The square has its centre at (0,0) and a corner at (1,1). This allows for all the points to be commonly known and for the easy application of Gaussian integration which will be explained in detail later in this section.

This scaling term is the determinant of the *Jacobian Matrix*, **J**, which is created as follows:

$$\mathbf{J} = \begin{bmatrix} \sum N_{i,\xi} x_i & \sum N_{i,\xi} y_i \\ \sum N_{i,\eta} x_i & \sum N_{i,\eta} y_i \end{bmatrix} \text{ with } \det(\mathbf{J}) = J_{11}J_{22} - J_{21}J_{12} \tag{3.40}$$

being the determinant of the *Jacobian Matrix* and x and y being the co-ordinates of the nodal points in the global coordinate system [21]. The *Jacobian Matrix* is relevant as it is the means by which the transformation between the co-ordinates occurs. It can be thought of as a simple transformation matrix.

The stiffness matrix, **K**, and the forces, **f**, still need to be determined. In order to obtain the stiffness matrix, a further look at the functional formulation is needed. Looking at Equation (3.29) and applying the simplifications spoken of in Section 3.1.2.1, the equations are as follows:

$$0 = -\int_{\Omega} \delta\mathbf{u}^T \boldsymbol{\nabla}^T \mathbf{C}_E (\boldsymbol{\nabla}\mathbf{u}) + \delta\mathbf{u}^T \mathbf{f}_B \, d\Omega - \int_{\Gamma} \delta\mathbf{u}^T \mathbf{f}_\Gamma \, d\Gamma - \delta\mathbf{u}^T \mathbf{f}_P. \tag{3.41}$$

Furthermore, applying the equalities explained so far in this section produce

$$0 = -\int_{V} \delta(\mathbf{Bq})^T \mathbf{C}_E \mathbf{Bq} + \delta(\mathbf{Nq})^T \mathbf{f}_B \, dV - \int_{S} \delta(\mathbf{Nq})^T \mathbf{f}_\Gamma \, dS - \delta(\mathbf{Nq})^T \mathbf{f}_P. \tag{3.42}$$

The force terms can be moved to the other side of the equals sign to create the form of Equation (3.32). Ignoring the force terms and simplifying further leaves,

$$\text{Force Terms} = -\int_V \delta\mathbf{q}^T\mathbf{B}^T\mathbf{C}_E\mathbf{B}\mathbf{q}\,dV \tag{3.43}$$

$$= \delta\mathbf{q}^T\int_V \mathbf{B}^T\mathbf{C}_E\mathbf{B}\,dV\mathbf{q} \tag{3.44}$$

and let

$$\mathbf{K} = \int_V \mathbf{B}^T\mathbf{C}_E\mathbf{B}\,dV \tag{3.45}$$

where the $\delta\mathbf{q}^T$ term will cancel with the 'Force Terms' equivalent.

One of the last steps before obtaining the displacements is to use the stiffness matrix $\mathbf{K}$ with simplifications into the 2-D local co-ordinate system. This matrix is obtained as follows

$$\mathbf{K} = \int\int \mathbf{B}^T\mathbf{C}_E\mathbf{B}t\,dx\,dy = \int_{-1}^{1}\int_{-1}^{1} \mathbf{B}^T\mathbf{C}_E\mathbf{B}\det(\mathbf{J})t\,d\xi\,d\eta, \tag{3.46}$$

where t is the thickness of the membrane [12]. At this point it is pertinent to say a little on numerical integration. It can be shown that the integration

$$I = \int_{-1}^{1} \varphi\,d\xi, \tag{3.47}$$

$$\approx \omega_1\varphi_1 + \omega_2\varphi_2 + \ldots + \omega_n\varphi_n, \tag{3.48}$$

where the ω's in this case are the weights and φ's are the integration sampling points for the *Gauss Quadrature Integration Scheme* [59; 12]. Table 3.1 lists the first three orders of scheme data.

Order n	Degree of Precision Precision	Sampling point locations φ_i	Weight factors ω_i
1	1	0	2
2	3	$\pm\frac{1}{\sqrt{3}}$	1
3	5	$\pm\sqrt{0.6}$ 0	5/9 8/9

Table 3.1: Gauss quadrature integration scheme points and weights [12]

Applying this integration scheme directly to the **K** matrix will produce

$$\mathbf{K}(\varphi_1, \varphi_2, \ldots) = \sum_x \sum_y \mathbf{B}^T \mathbf{C}_E \mathbf{B} \det(\mathbf{J}) \omega_x \omega_y t. \tag{3.49}$$

Now that the integration is completed the only thing left to do is to solve the system. Therefore rearranging Equation (3.32) gives the solution

$$\mathbf{q} = \mathbf{K}^{-1}\mathbf{f}. \tag{3.50}$$

As the system is solved other data can be extrapolated from the results by, in essence, reversing the scheme of things. Equation (3.34) shows how strain is obtained and Equation (3.14) shows how stress is obtained. From these stress can be extrapolated from the resulting data as

$$\boldsymbol{\sigma} = \mathbf{C}_E(\boldsymbol{\epsilon} - \boldsymbol{\epsilon}_0) + \boldsymbol{\sigma}_0 = \mathbf{C}_E(\mathbf{Bq} - \boldsymbol{\epsilon}_0) + \boldsymbol{\sigma}_0 = \mathbf{C}_E\mathbf{Bq} \tag{3.51}$$

on the grounds of no initial strains or stresses [12].

3.1.3 The Basic Programming Structure

The previous section details the mathematical formulation for a single element. This will be applied to each element in an arbitrary body and as more elements are associated with the body the matrices will get larger and larger. When more than a couple of elements are used it becomes advisable to use computers to solve the system numerically. In order to accomplish this a numerical model needs to be constructed using some mathematical based programming language (MATLAB, Fortran, C++) [58; 57].

The structure of the numerical model is given in the pseudo code of Algorithm 1, which is abbreviated quite substantially. One of the most important parts of the construction of the matrix K is the indexing of the smaller local element matrix into the larger global stiffness matrix. This is done by keeping careful note of the elements and their assembly. The rest follows a logical

structure that is coupled to the mathematical process [57].

Algorithm 1: FEM basic structure for displacement solution of Q4 membrane element

```
1  begin
2      Declaration of Control Parameters;
3      Declaration of Constitutive Relation;
4      Declaration of Mesh;
5      Declaration of Force Inputs;
6      Initialization of Total Matrices;
7      Declaration of Gaussian Integration Scheme;
8      for 1⟶element total do
9          for 1⟶nodes per element do
10             Extract Element Nodal Data;
11         end
12         Initialization of Sub-Matrix Structures;
13         for first dimensional integration do
14             Extract x Sampling Points and Weights;
15             for second dimentional integration do
16                 Extract y Sampling Points and Weights;
17                 Solve for K using Equation (3.49) and Summing;
18                 i.e. K = K + math;
19             end
20         end
21         Assemble 1 Large Stiffness Matrix Using Indices;
22     end
23     Solve for Displacements using Equation (3.50);
24     Derivation of Stresses;
25 end
```

As stated in line 24 of Algorithm 1, the output data is extracted depending on what is needed and many algorithms exist depending on the desired output [26]. For instance Von Mises stresses will differ from residual heat, and if only displacement is needed the stress algorithm is not needed.

3.1.4 The Hybrid Form

The hybrid form of the FE formulation of Section 3.1.2.2 is an offshoot of the standard variational formulation using the Hellinger-Reissner principle [29]. The Hellinger-Reissner principle uses Hooke's law to change Equation (3.29) into the stress form [29]

$$\Pi_{HR} = \int_{\Omega} \boldsymbol{\sigma}^T \mathbf{C}_E^{-1} \boldsymbol{\sigma} + \boldsymbol{\sigma}^T \boldsymbol{\nabla} \mathbf{u} \, d\Omega - \int_{\Gamma} \mathbf{f}_{\Gamma}^T \mathbf{u} \, d\Gamma, \tag{3.52}$$

where assuming stress is derived as

$$\boldsymbol{\sigma} = \mathbf{P}\boldsymbol{\beta} \tag{3.53}$$

and the rest of the initial equations before Equation (3.41) remain valid then in much the same way as Equations 3.41 to 3.45

$$\begin{aligned}\Pi_{HR} = &-\frac{1}{2}\boldsymbol{\beta}_{HR}^T \int_\Omega \mathbf{P}^T \mathbf{C}_E^{-1} \mathbf{P}\, d\Omega\, \boldsymbol{\beta}_{HR} + \boldsymbol{\beta}_{HR}^T \int_\Omega \mathbf{P}^T \mathbf{B}_{HR}\, d\Omega \mathbf{q} \\ &- \Big(\int_\Gamma \mathbf{N}^T \mathbf{f}_\Gamma\, d\Gamma\Big)^T \mathbf{q},\end{aligned} \tag{3.54}$$

which can be further simplified to

$$\Pi_{HR} = -\frac{1}{2}\boldsymbol{\beta}_{HR}^T \mathbf{H}_{HR} \boldsymbol{\beta}_{HR} + \boldsymbol{\beta}_{HR}^T \mathbf{G}_{HR} \mathbf{q} - \mathbf{R}_{HR}^T \mathbf{q}. \tag{3.55}$$

To find the stiffness matrix, in this case the systems stationary position, being when $\delta\beta$ and δq are zero, must be computed [29]. This results in

$$\boldsymbol{\beta}_{HR} = -\mathbf{H}_{HR}^{-1} \mathbf{G}_{HR} \mathbf{q}, \;\; \mathbf{K}\mathbf{q} = \mathbf{R}_{HR} \text{ and } \mathbf{K} = \mathbf{G}_{HR}^T \mathbf{H}_{HR}^{-1} \mathbf{G}_{HR} \tag{3.56}$$

from Equation (3.55) [29]. From this solution various offshoots of stress analysis can be performed depending on the required clarity, for more details see [29].

3.2 Standard PIEZO QUAD 4 Membrane Formulation

In Section 3.1 the basic membrane formulation for a Q4 element was detailed. Following on from this, this Section details the formulation of a similar element, namely the P4 element. This element caters for piezoelectric responses and allows for a change in displacement caused by the coupling of both mechanical and electrical effects. Again, as in Section 3.1, the basic formulation will be explained initially and expansion to the FE membrane model will be explained thereafter.

It must be said however that the logic behind the formulation of the piezoelectric effect has its basis in crystal lattice formulations, specifically in bi-ionic crystal structure. For more information on this see references [60; 13]. For brevity this chapter will assume that the coupling equations,

$$\begin{aligned}\boldsymbol{\sigma} &= \mathbf{C}_E \boldsymbol{\epsilon} - \mathbf{e}^T \mathbf{E} \\ \mathbf{D} &= \mathbf{e}\boldsymbol{\epsilon} + \boldsymbol{\gamma}_\epsilon \mathbf{E}\end{aligned} \tag{3.57}$$

have already been validated [1; 61]. In Equation (3.57), $\boldsymbol{\sigma}$ and $\mathbf{D}$ are the mechanical and electrical stresses respectively, $\boldsymbol{\epsilon}$ and $\mathbf{E}$ mechanical and electrical strains respectively, and $\mathbf{C}_E$, $\mathbf{e}$ and $\boldsymbol{\gamma}_\epsilon$ are the elastic, piezoelectric coupling and electrical permittivity constitutive relations respectively. Here the subscript E is used for identification as a constitutive relation and not as an index.

3.2.1 PIEZO Variational Formulation

The PIEZO Variational Formulation differs in most parts from Section 3.1.1. In the first place it has to allow for both the electric and piezoelectric effects along with the already shown elasticity. There is much literature on piezoelectric finite element formulations and a variety of subtly different approaches to getting to the variational form [30; 1]. One of the most complete description is in a thesis by Vincent Piefort [13]. This is the method that will be elaborated upon here. This method begins with the electrical enthalpy equation,

$$H = U - E_i D_i, \tag{3.58}$$

where H is the electrical enthalpy and this is used due to the pyro-electric coupling in the Gibbs equation not being needed [62]. The conservation of energy results in the first law of thermodynamics

$$dU = \sigma_{ij}\, d\epsilon_{ij} + E_i\, dD_i, \tag{3.59}$$

taking the first derivative of Equation (3.58) gives

$$dH = dU - E_i\, dD_i - D_i\, dE_i \tag{3.60}$$

from the product rule [62; 63]. Combining Equations 3.59 and 3.60 gives

$$dH = \sigma_{ij}\, d\epsilon_{ij} - D_i\, dE_i, \tag{3.61}$$

finally expanding Equation (3.61) using the chain rule the following identities are shown

$$\sigma_{ij} = \frac{\partial H}{\partial \epsilon_{ij}} \text{ and} \tag{3.62}$$

$$D_i = -\frac{\partial H}{\partial E_i}. \tag{3.63}$$

Here subscripts i and j, and in further instances k and l are indices that are an indication of the dimensionality of each situation [13; 26].

The next step in this process is to obtain the elastically equivalent true form of H from linear piezoelectric theory. This step has its basis in physics and is derived using a similar theory to the above equation set. Initially, however, the Gibbs equation is used instead of the Enthalpy equation. The second derivative of the Gibbs equation is then taken and when expanded with the adaptation of the chain rule three thermopiezoelectric coupling equations using independent variables are derived. These equations lead to a simplification to the linear thermopiezoelectric equation [1; 13]. Without further explanation, a simplification of this equation to only use the Enthalpy terms is used. In this simplification the heating effects are ignored. The equation is as follows [13],

$$H = \frac{1}{2} C_{E\,ijkl} \epsilon_{ij} \epsilon_{kl} - e_{E\,kij} E_k \epsilon_{ij} - \frac{1}{2} \gamma_{E\,ij} E_i E_j \tag{3.64}$$

and simplification of this equation into matrix form yields

$$\mathbf{H} = \frac{1}{2}\{\boldsymbol{\epsilon}^T\boldsymbol{\sigma} - \mathbf{E}^T\mathbf{D}\}. \tag{3.65}$$

This completes the formulation of the enthalpy component of the formulation which can also be looked at as the potential energy component. There is a relevant kinetic energy component in piezoelectrics theory which is represented by [64; 13]:

$$V_K = \frac{1}{2}mv^2, \tag{3.66}$$

which in variables previously described converts to:

$$\mathbf{V}_K = \frac{1}{2}\rho\dot{\mathbf{u}}\dot{\mathbf{u}}, \tag{3.67}$$

where, $\mathbf{V}$ is kinetic energy, and $\dot{\mathbf{u}}$ is the time derivative of $\mathbf{u}$ and by using Equations 3.67 and 3.65 in the Lagrangian

$$\mathcal{L} = \int_V \{\mathbf{T}_K - \mathbf{H}\}\, dV \tag{3.68}$$

$$= \int_V \{\frac{1}{2}\rho\dot{\mathbf{u}}\dot{\mathbf{u}} - \frac{1}{2}\{\boldsymbol{\epsilon}^T\boldsymbol{\sigma} - \mathbf{E}^T\mathbf{D}\}\}\, dV. \tag{3.69}$$

Using the Hamiltonian principle

$$0 = \delta\int_{t_1}^{t_2}\{\mathcal{L} + W\}\, dt \tag{3.70}$$

where $\mathcal{L}$ is the Lagrangian. The work has yet to be defined and is based on the same principles as observed in Section 3.1.1.3 [31]. This can yet again be expanded to functional form as,

$$\delta\mathbf{W} = \{\delta\mathbf{u}\}^T\mathbf{f} - \delta\boldsymbol{\phi}\mathbf{r}, \tag{3.71}$$

where, r is the charge density and ϕ is the potential, which are analogous with force and displacement in the mechanical system respectively. This can then be expanded to

$$\delta\mathbf{W} = \int_\Omega \{\delta\mathbf{u}\}^T\mathbf{f}_B\, d\Omega + \int_{\Gamma_1}\{\delta\mathbf{u}\}^T\mathbf{f}_\Gamma\, d\Gamma_1 + \{\delta\mathbf{u}\}^T\mathbf{f}_P$$
$$- \int_\Omega \{\delta\boldsymbol{\phi}\}\mathbf{r}_B\, d\Omega - \int_{\Gamma_2}\{\delta\boldsymbol{\phi}\}\mathbf{r}_\Gamma\, d\Gamma_2 - \{\delta\boldsymbol{\phi}\}\mathbf{r}_P. \tag{3.72}$$

Proceeding to the full variational principle using the Hamiltonian principle [31]. The functional of the Lagrangian term needs to be obtained in the same way as in Section 3.1.1.4 producing (in matrix form) [13]

$$\begin{aligned} 0 = -\int_{\Omega} &[\rho\{\delta\mathbf{u}\}^T\ddot{\mathbf{u}} - \{\delta\boldsymbol{\epsilon}\}^T\mathbf{C}_E\boldsymbol{\epsilon} + \{\delta\boldsymbol{\epsilon}\}^T\mathbf{e}\mathbf{E} + \{\delta\mathbf{E}\}^T\mathbf{e}\boldsymbol{\epsilon} \\ &+ \{\delta\mathbf{E}\}^T\boldsymbol{\gamma}_\epsilon\mathbf{E} + \{\delta\mathbf{u}\}^T\mathbf{f}_B - \delta\phi\mathbf{r}_B]\,d\Omega + \int_{\Gamma_1}\{\delta\mathbf{u}\}^T\mathbf{f}_\Gamma\,d\Gamma_1 \\ &+ \{\delta\mathbf{u}\}^T\mathbf{f}_P - \int_{\Gamma_2}\delta\phi\mathbf{r}_\Gamma\,d\Gamma_2 - \delta\phi\mathbf{r}_P. \end{aligned} \tag{3.73}$$

3.2.2 PIEZO FE Formulation Adaptation

Many of the equations in Section 3.1.2 apply in this section as well because there are still elastic effects that take place. The difference is in the piezoelectric and electric considerations. Redoing all of the formulation at this stage plays an important role in the overall comparison of the FE adaptation.

Again, as in the beginning of Section 3.1.2, the formulation begins with the isoparametric linear interpolation in the Equations 3.37. The difference, however, also begins here as, although the relation

$$\mathbf{u} = \mathbf{N}_m\mathbf{q}_m \tag{3.74}$$

still stands, it is appended by the relation

$$\phi = \mathbf{N}_e\mathbf{q}_e \tag{3.75}$$

for the electric effect, where

$$\mathbf{N}_m = \begin{bmatrix} N_1 & 0 & N_2 & 0 & N_3 & 0 & N_4 & 0 \\ 0 & N_1 & 0 & N_2 & 0 & N_3 & 0 & N_4 \end{bmatrix}, \text{ and} \tag{3.76}$$

$$\mathbf{N}_e = \begin{bmatrix} N_1 & N_2 & N_3 & N_4 \end{bmatrix}, \tag{3.77}$$

with the q values being the displacements with respect to both mechanical and electrical effects represented by indices m and e respectively [65]. This leads to the addition of new terms, in comparison to the work detailed in Section 3.1.2, as the interpolation relations are key to the FE solution. Differentiating the displacements to obtain strain yield

$$\boldsymbol{\epsilon} = \mathbf{B}_m\mathbf{q}_m, \tag{3.78}$$

$$\mathbf{E} = \mathbf{B}_e\mathbf{q}_e, \tag{3.79}$$

where

$$\mathbf{B}_m = \boldsymbol{\nabla}_m\mathbf{N}_m, \tag{3.80}$$

$$\mathbf{B}_e = \boldsymbol{\nabla}_e\mathbf{N}_e \tag{3.81}$$

and

$$\boldsymbol{\nabla}_m = \begin{bmatrix} \dfrac{\partial}{\partial \xi} & 0 \\ 0 & \dfrac{\partial}{\partial \eta} \\ \dfrac{\partial}{\partial \eta} & \dfrac{\partial}{\partial \xi} \end{bmatrix}, \tag{3.82}$$

$$\boldsymbol{\nabla}_e = \begin{bmatrix} \dfrac{\partial}{\partial \xi} \\ \dfrac{\partial}{\partial \eta} \end{bmatrix}. \tag{3.83}$$

Taking a step back to the variational principle of Equation (3.73), the new forms of displacement and strain can be inserted into the variational form to obtain

$$\begin{aligned} 0 = &- \int_{\Omega} [\rho \delta \{\mathbf{N}_m \mathbf{q}_m\}^T \ddot{\mathbf{u}} - \delta \{\mathbf{B}_m \mathbf{q}_m\}^T \mathbf{C}_E \mathbf{B}_m \mathbf{q}_m \\ &+ \delta \{\mathbf{B}_m \mathbf{q}_m\}^T \mathbf{e} \mathbf{B}_e \mathbf{q}_e + \delta \{\mathbf{B}_e \mathbf{q}_e\}^T \mathbf{e} \mathbf{B}_m \mathbf{q}_m + \delta \{\mathbf{B}_e \mathbf{q}_e\}^T \boldsymbol{\gamma}_\epsilon \mathbf{B}_e \mathbf{q}_e \\ &+ \delta \{\mathbf{N}_m \mathbf{q}_m\}^T \mathbf{f}_B - \delta \mathbf{N}_e \mathbf{q}_e{}^T \mathbf{r}_B] \, d\Omega + \int_{\Gamma_1} \delta \{\mathbf{N}_m \mathbf{q}_m\}^T \mathbf{f}_\Gamma \, d\Gamma_1 \\ &+ \delta \{\mathbf{N}_m \mathbf{q}_m\}^T \mathbf{f}_P - \int_{\Gamma_2} \delta \{\mathbf{N}_e \mathbf{q}_e\}^T \mathbf{r}_\Gamma \, d\Gamma_2 - \delta \{\mathbf{N}_e \mathbf{q}_e\}^T \mathbf{r}_P \end{aligned} \tag{3.84}$$

and by the law for transposed groups [66]

$$\begin{aligned} = &- \int_{\Omega} [\rho \delta \mathbf{q}_m^T \mathbf{N}_m^T \ddot{\mathbf{u}} - \delta \mathbf{q}_m^T \mathbf{B}_m^T \mathbf{C}_E \mathbf{B}_m \mathbf{q}_m + \delta \mathbf{q}_m^T \mathbf{B}_m^T \mathbf{e} \mathbf{B}_e \mathbf{q}_e \\ &+ \delta \mathbf{q}_e^T \mathbf{B}_e^T \mathbf{e} \mathbf{B}_m \mathbf{q}_m + \delta \mathbf{q}_e^T \mathbf{B}_e^T \boldsymbol{\gamma}_\epsilon \mathbf{B}_e \mathbf{q}_e + \delta \mathbf{q}_m^T \mathbf{N}_m^T \mathbf{f}_B - \delta \mathbf{q}_e^T \mathbf{N}_e^T \mathbf{r}_B] \, d\Omega \\ &+ \int_{\Gamma_1} \delta \mathbf{q}_m^T \mathbf{N}_m^T \mathbf{f}_\Gamma \, d\Gamma_1 + \delta \mathbf{q}_m^T \mathbf{N}_m^T \mathbf{f}_P - \int_{\Gamma_2} \delta \mathbf{q}_e^T \mathbf{N}_e^T \mathbf{r}_\Gamma \, d\Gamma_2 - \delta \mathbf{q}_e^T \mathbf{N}_e^T \mathbf{r}_P \end{aligned} \tag{3.85}$$

and simplifying further into the substituted stiffness matrices gives

$$\begin{aligned} = &- \{\delta \mathbf{q}_m\}^T \mathbf{M} \ddot{\mathbf{u}} + \{\delta \mathbf{q}_m\}^T \mathbf{K}_m \mathbf{q}_m - \{\delta \mathbf{q}_m\}^T \mathbf{K}_p \mathbf{q}_e - \{\delta \mathbf{q}_e\}^T \mathbf{K}_p^T \mathbf{q}_m \\ &- \{\delta \mathbf{q}_e\}^T \mathbf{K}_e \mathbf{q}_e + \{\delta \mathbf{q}_m\}^T \mathbf{f} - \{\delta \mathbf{q}_e\}^T \mathbf{r}, \end{aligned} \tag{3.86}$$

where

$$\mathbf{M} = \int_{\Omega} \rho \mathbf{N}_m^T \, d\Omega, \tag{3.87}$$

$$\mathbf{K}_m = \int_{\Omega} \mathbf{B}_m^T \mathbf{C}_E \mathbf{B}_m \, d\Omega, \tag{3.88}$$

$$\mathbf{K}_p = \int_{\Omega} \mathbf{B}_m^T \mathbf{e} \mathbf{B}_e \, d\Omega, \tag{3.89}$$

$$\mathbf{K}_e = -\int_{\Omega} \mathbf{B}_e^T \boldsymbol{\gamma}_\epsilon \mathbf{B}_e \, d\Omega, \tag{3.90}$$

$$\mathbf{f} = -\int_{\Omega} \mathbf{N}_m^T \mathbf{f}_B \, d\Omega + \int_{\Gamma} \mathbf{N}_m^T \mathbf{f}_\Gamma \, d\Gamma + \mathbf{N}_m^T \mathbf{f}_P \tag{3.91}$$

and

$$\mathbf{r} = -\int_{\Omega} \mathbf{N}_e^T \mathbf{r}_B \, d\Omega + \int_{\Gamma} \mathbf{N}_e^T \mathbf{r}_\Gamma \, d\Gamma + \mathbf{N}_e^T \mathbf{r}_P. \tag{3.92}$$

This whole variational formulation simplification can once again be simplified into an extension of the form for Newton's Second Law

$$\mathbf{M}\ddot{\mathbf{u}} + \mathbf{K}\mathbf{u} = \mathbf{f}, \tag{3.93}$$

where extension in matrix form which includes the electric and piezoelectric effects looks like

$$\begin{bmatrix} \mathbf{M} \\ 0 \end{bmatrix} \ddot{\mathbf{u}} + \begin{bmatrix} \mathbf{K}_m & \mathbf{K}_p \\ \mathbf{K}_p^T & \mathbf{K}_e \end{bmatrix} \begin{bmatrix} \mathbf{u} \\ \phi \end{bmatrix} = \begin{bmatrix} \mathbf{f} \\ \mathbf{r} \end{bmatrix}. \tag{3.94}$$

In keeping with most formulations, simplifications can be made at this point, which is after the FE formulation is complete but before it is applied. The first simplification is that the eigenvalues/vibratory responses will not be computed unless specifically needed. By ignoring the mass, $\mathbf{M}$, a quasi-static problem is assumed, rather than a vibratory response (which is a by-product). The second simplification is that the element type used as described in the beginning of this chapter is a thin membrane and as such only a 2-D response is needed. These assumptions simplify the Equations 3.87 to 3.92 by removing one dimension of the integration step. Lastly, through the process of numerical integration as described in Section 3.1.2.2 Equation (3.49) the

final equations for the stiffness and loading matrices can be determined to be [31]

$$\mathbf{K_m}(\phi_1, \phi_2) = \sum_x \sum_y \mathbf{B}_m^T \mathbf{C}_E \mathbf{B}_m \det(\mathbf{J}) w_x w_y t, \tag{3.95}$$

$$\mathbf{K_p}(\phi_1, \phi_2) = \sum_x \sum_y \mathbf{B}_m^T \mathbf{e} \mathbf{B}_e \det(\mathbf{J}) w_x w_y t, \tag{3.96}$$

$$\mathbf{K_e}(\phi_1, \phi_2) = -\sum_x \sum_y \mathbf{B}_e^T \boldsymbol{\gamma}_\epsilon \mathbf{B}_e \det(\mathbf{J}) w_x w_y t, \tag{3.97}$$

$$\begin{aligned}\mathbf{f}(\phi_1, \phi_2) = &-\sum_x \sum_y \mathbf{N}_m^T \mathbf{f}_B \det(\mathbf{J}) w_x w_y t + \sum_y \mathbf{N}_m^T \mathbf{f}_\Gamma \det(\mathbf{J}) w_y t \\ &+ \sum_x \mathbf{N}_m^T \mathbf{f}_\Gamma \det(\mathbf{J}) w_x t + \mathbf{N}_m^T \mathbf{f}_P\end{aligned} \tag{3.98}$$

and

$$\begin{aligned}\mathbf{r}(\phi_1, \phi_2) = &-\sum_x \sum_y \mathbf{N}_e^T \mathbf{r}_B \det(\mathbf{J}) w_x w_y t + \sum_y \mathbf{N}_e^T \mathbf{r}_\Gamma \det(\mathbf{J}) w_y t \\ &+ \sum_x \mathbf{N}_e^T \mathbf{r}_\Gamma \det(\mathbf{J}) w_x t + \mathbf{N}_e^T \mathbf{r}_P.\end{aligned} \tag{3.99}$$

These equations can now be employed in a numerical model in order to solve membrane systems. The next section explains the numerical process for employing this mathematical model.

3.2.3 Adaptation To Programming Thinking

The programming algorithm is similar to Algorithm 1 and it only differs in that it is expanded to allow for the new terms. Looking at the expanded Algorithm 2, the differences become clear.

Algorithm 2: FEM basic structure for displacement solution of P4 membrane Element

```
1  begin
2      Declaration of Control Parameters;
3      Declaration of Constitutive Relation;
4      Declaration of Mesh;
5      Declaration of Force Inputs;
6      Initialization of Total Matrices;
7      Declaration of Gaussian Integration Scheme;
8      for 1⟶element total do
9          for 1⟶nodes per element do
10             Extract Element Nodal Data;
11         end
12         Initialization of Sub-Matrix Structures;
13         for first dimensional integration do
14             Extract x Sampling Points and Weights;
15             for second dimensional integration do
16                 Extract y Sampling Points and Weights;
17                 Solve for K using Math of Equations 3.95 to 3.99;
18                 i.e. k_m = k_m + math;
19                 i.e. k_p = k_p + math;
20                 i.e. k_e = k_e + math;
21             end
22         end
23         Assemble 3 Large Stiffness Matrices Using Indexing(K_m, K_p and K_e);
24     end
25     Assemble Stiffness Matrix as in Equation (3.94);
26     Solve for Displacements using Equation (3.50) Noting that the Matrix Definitions
       Differ from Algorithm 1;
27 end
```

By completing the algorithm in this manner the mechanical and electrical displacements can be kept apart. This allows for the easy handling of the results in the latter parts of the program.

3.2.4 The Piezoelectric Hybrid Formulations

In the P4 element there are 3 alternate hybrid element formulations. These hybrids can be seen by interchanging the 4 independent variables available in the coupling equations (Equation (3.57)). A similar derivation to that in Section 3.2.1 is used in order to get the FE starting point for each method. Therefore the standard formulation from Section 3.2.1 must be modified

to account for the starting point.

Using the alternate choices of independent variables in the coupling equations the three other forms can be given as [13]

$$\begin{aligned} \boldsymbol{\epsilon} &= \mathbf{S}_E\boldsymbol{\sigma} + \mathbf{d}^T\mathbf{E} \\ D &= \mathbf{d}\boldsymbol{\sigma} + \gamma_\sigma\mathbf{E}, \end{aligned} \tag{3.100}$$

$$\begin{aligned} \boldsymbol{\epsilon} &= \mathbf{S}_D\boldsymbol{\sigma} + \mathbf{g}\mathbf{D} \\ \mathbf{E} &= \mathbf{g}\boldsymbol{\sigma} + \beta_\sigma\mathbf{D} \end{aligned} \tag{3.101}$$

and

$$\begin{aligned} \boldsymbol{\sigma} &= \mathbf{C}_D\boldsymbol{\epsilon} - \mathbf{h}^T\mathbf{D} \\ \mathbf{E} &= -\mathbf{h}\boldsymbol{\epsilon} + \beta_\epsilon\mathbf{D}. \end{aligned} \tag{3.102}$$

Although the process whereby the variational principle is obtained will not be looked at, it is necessary to show the FE usage. Firstly the new variables used need to be defined in terms of the first coupling equations where the values of the matrices are relatively widely known. Using these variables the new variables can be explained as

$$\begin{bmatrix} \mathbf{S}_D & \mathbf{g}^T \\ -\mathbf{g} & \beta_\sigma \end{bmatrix} = \begin{bmatrix} \mathbf{C}_E & -\mathbf{e}^T \\ \mathbf{e} & \gamma_\epsilon \end{bmatrix}^{-1}, \tag{3.103}$$

$$\begin{bmatrix} \mathbf{C}_D & -\mathbf{h}^T \\ -\mathbf{h} & \beta_\epsilon \end{bmatrix} = \begin{bmatrix} \mathbf{C}_E + \mathbf{e}^T\gamma_\epsilon^{-1}\mathbf{e} & -[\gamma_\epsilon^{-T}e]^T \\ -\gamma_\epsilon^{-T}\mathbf{e} & \gamma_\epsilon^{-1} \end{bmatrix} \tag{3.104}$$

and

$$\begin{bmatrix} \mathbf{S}_E & -\mathbf{d} \\ -\mathbf{d} & \gamma_\sigma \end{bmatrix} = \begin{bmatrix} \mathbf{C}_E^{-1} & -\mathbf{e}\mathbf{C}_E^{-1} \\ -\mathbf{e}\mathbf{C}_E^{-1} & \gamma_\epsilon - \mathbf{e}\mathbf{C}_E^{-1}\mathbf{e}^T \end{bmatrix}, \tag{3.105}$$

the subscripts in this case refer to the independent variable that is constant for determination of the primary variables [61]. Before these constitutive relations can be expanded into the FE formulations it is pertinent to show the variational principle that can then be converted [61].

$$\boldsymbol{\Pi}_D = \int_\Omega \Big[\frac{1}{2}\begin{bmatrix} \boldsymbol{\nabla}_m\mathbf{u} \\ \mathbf{D} \end{bmatrix}^T \begin{bmatrix} \mathbf{C}_D & -\mathbf{h}^T \\ -\mathbf{h} & \beta_\epsilon \end{bmatrix} \begin{bmatrix} \boldsymbol{\nabla}_m\mathbf{u} \\ \mathbf{D} \end{bmatrix} + \mathbf{D}^T\boldsymbol{\nabla}_e\phi - (-\rho\ddot{\mathbf{u}})^T\mathbf{u}\Big]d\Omega - \mathbf{f}, \tag{3.106}$$

$$\boldsymbol{\Pi}_\sigma = \int_\Omega \Big[\frac{-1}{2}\begin{bmatrix} \boldsymbol{\sigma} \\ \boldsymbol{\nabla}_e\phi \end{bmatrix}^T \begin{bmatrix} \mathbf{S}_E & -\mathbf{d} \\ -\mathbf{d} & \gamma_\sigma \end{bmatrix} \begin{bmatrix} \boldsymbol{\sigma} \\ \boldsymbol{\nabla}_e\phi \end{bmatrix} + \boldsymbol{\sigma}^T\boldsymbol{\nabla}_m\mathbf{u} - (-\rho\ddot{\mathbf{u}})^T\mathbf{u}\Big]d\Omega - \mathbf{f} \tag{3.107}$$

and

$$\boldsymbol{\Pi}_{\sigma D} = \int_\Omega \Big[\frac{-1}{2}\begin{bmatrix} \boldsymbol{\sigma} \\ \mathbf{D} \end{bmatrix}^T \begin{bmatrix} \mathbf{S}_D & \mathbf{g}^T \\ -\mathbf{g} & \beta_\sigma \end{bmatrix} \begin{bmatrix} \boldsymbol{\sigma} \\ \mathbf{D} \end{bmatrix} + \begin{bmatrix} \boldsymbol{\sigma} \\ \mathbf{D} \end{bmatrix}^T \begin{bmatrix} \boldsymbol{\nabla}_m\mathbf{u} \\ \boldsymbol{\nabla}_e\phi \end{bmatrix} - (-\rho\ddot{\mathbf{u}})^T\mathbf{u}\Big]d\Omega - \mathbf{f}, \tag{3.108}$$

where $\mathbf{f}$ is the additional surface and point loadings [61]. As in Section 3.1.4, the mechanical and electrical stress terms can be expanded to [29; 61]

$$\boldsymbol{\sigma} = \mathbf{P}_m \boldsymbol{\beta}_m, \quad \mathbf{D} = \mathbf{P}_e \boldsymbol{\beta}_e, \tag{3.109}$$

where

$$\mathbf{P}_m = \begin{bmatrix} \mathbf{I}_3 & \mathbf{T}_m \mathbf{P}_{mh} \end{bmatrix}, \quad \mathbf{P}_e = \begin{bmatrix} \mathbf{I}_2 & \mathbf{T}_e \mathbf{P}_{eh} \end{bmatrix}, \tag{3.110}$$

$$\mathbf{T}_m = \begin{bmatrix} a_1^2 & a_3^2 & 2a_1a_3 \\ b_1^2 & b_3^2 & 2b_1b_3 \\ a_1b_1 & a_3b_3 & a_1b_3 + a_3b_1 \end{bmatrix}, \quad \mathbf{T}_e = \begin{bmatrix} a_1 & b_1 \\ a_2 & b_2 \end{bmatrix}, \tag{3.111}$$

$$\mathbf{P}_{eh} = \begin{bmatrix} \eta \\ \xi \end{bmatrix} \text{ and } \mathbf{P}_{mh} = \begin{bmatrix} \eta & 0 \\ 0 & \xi \\ 0 & 0 \end{bmatrix} \tag{3.112}$$

and in this case

$$\begin{bmatrix} a_1 & b_1 \\ a_2 & b_2 \\ a_3 & b_3 \end{bmatrix} = \frac{1}{4} \begin{bmatrix} -1 & 1 & 1 & -1 \\ 1 & -1 & 1 & -1 \\ -1 & -1 & 1 & 1 \end{bmatrix} \begin{bmatrix} x_1 & y_1 \\ x_2 & y_2 \\ x_3 & y_3 \\ x_4 & y_4 \end{bmatrix}. \tag{3.113}$$

Here $\mathbf{T}_e$ and $\mathbf{T}_m$ are transformation matrices. Using these terms in the variational principles the three different $\mathbf{K}$ matrix formulations can be deduced. They are as follows [61] (the triangular brackets indicate the integral with respect to volume):
for the Π_D variational form where D is assumed

$$\mathbf{K}_D = \begin{bmatrix} \langle \mathbf{B}_m^T \mathbf{C}_D \mathbf{B}_m \rangle & 0 \\ 0 & 0 \end{bmatrix} - \begin{bmatrix} \langle \mathbf{P}_e^T \mathbf{h} \mathbf{B}_m \rangle^T \\ -\langle \mathbf{P}_e^T \mathbf{B}_e \rangle^T \end{bmatrix} \langle \mathbf{P}_e^T \boldsymbol{\beta}_\epsilon \mathbf{P}_e \rangle^{-1} \begin{bmatrix} \langle \mathbf{P}_e^T \mathbf{h} \mathbf{B}_m \rangle & -\langle \mathbf{P}_e^T \mathbf{B}_e \rangle \end{bmatrix}, \tag{3.114}$$

for the Π_σ variational form where σ is assumed

$$\mathbf{K}_\sigma = \begin{bmatrix} \langle \mathbf{P}_m^T \mathbf{B}_m \rangle^T \\ \langle \mathbf{P}_m^T \mathbf{d}^T \mathbf{B}_e \rangle^T \end{bmatrix} \langle \mathbf{P}_m^T \mathbf{S}_E \mathbf{P}_m \rangle^{-1} \begin{bmatrix} \langle \mathbf{P}_m^T \mathbf{B}_m \rangle & \langle \mathbf{P}_m^T \mathbf{d}^T \mathbf{B}_e \rangle \end{bmatrix} - \begin{bmatrix} 0 & 0 \\ 0 & \langle \mathbf{B}_e^T \boldsymbol{\gamma}_\sigma \mathbf{B}_e \rangle \end{bmatrix} \tag{3.115}$$

and for the $\Pi_{\sigma D}$ variational form where both $\sigma$and D are assumed

$$\mathbf{K}_{\sigma D} = \int_V \begin{bmatrix} \langle \mathbf{P}_m^T \mathbf{B}_m \rangle & 0 \\ 0 & \langle \mathbf{P}_e^T \mathbf{B}_e \rangle \end{bmatrix}^T \begin{bmatrix} \langle \mathbf{P}_m^T \mathbf{S}_D \mathbf{P}_m \rangle & \langle \mathbf{P}_m^T \mathbf{g}^T \mathbf{P}_e \rangle \\ \langle \mathbf{P}_e^T \mathbf{g} \mathbf{P}_m \rangle & -\langle \mathbf{P}_e^T \boldsymbol{\beta}_\sigma^T \mathbf{P}_e \rangle \end{bmatrix}^{-1} \begin{bmatrix} \langle \mathbf{P}_m^T \mathbf{B}_m \rangle & 0 \\ 0 & \langle \mathbf{P}_e^T \mathbf{B}_e \rangle \end{bmatrix} dV, \tag{3.116}$$

in each of these cases it is important to know how to obtain the $\boldsymbol{\beta}$ values as they are needed in the stress calculation [61]. The methods of obtaining the $\boldsymbol{\beta}$ values are

$$\boldsymbol{\beta}_{e\,D} = \langle \mathbf{P}_e^T \boldsymbol{\beta}_\epsilon \mathbf{P}_e \rangle^{-1} \begin{bmatrix} \langle \mathbf{P}_e^T \mathbf{h} \mathbf{B}_m \rangle & -\langle \mathbf{P}_e^T \mathbf{B}_e \rangle \end{bmatrix} \begin{bmatrix} \mathbf{q}_m \\ \mathbf{q}_e \end{bmatrix}, \tag{3.117}$$

$$\boldsymbol{\beta}_{m\,\sigma} = \langle \mathbf{P}_m^T \mathbf{S}_E \mathbf{P}_m \rangle^{-1} \begin{bmatrix} \langle \mathbf{P}_m^T \mathbf{B}_m \rangle & \langle \mathbf{P}_m^T \mathbf{d}^T \mathbf{B}_e \rangle \end{bmatrix} \begin{bmatrix} \mathbf{q}_m \\ \mathbf{q}_e \end{bmatrix} \tag{3.118}$$

and

$$\begin{bmatrix} \beta_{m\sigma D} \\ \beta_{e\sigma D} \end{bmatrix} = \begin{bmatrix} \langle \mathbf{P}_m^T \mathbf{S}_D \mathbf{P}_m \rangle & \langle \mathbf{P}_m^T \mathbf{g}^T \mathbf{P}_e \rangle \\ \langle \mathbf{P}_e^T \mathbf{g} \mathbf{P}_m \rangle & -\langle \mathbf{P}_e^T \beta_\sigma^T \mathbf{P}_e \rangle \end{bmatrix}^{-1} \begin{bmatrix} \langle \mathbf{P}_m^T \mathbf{B}_m \rangle & 0 \\ 0 & \langle \mathbf{P}_e^T \mathbf{B}_e \rangle \end{bmatrix} \begin{bmatrix} \mathbf{q}_m \\ \mathbf{q}_e \end{bmatrix} \tag{3.119}$$

follow from Equation 3.114 to 3.116, respectively.

3.3 Orthotropic Materials and Classical Laminate Theory

Most piezoelectric materials are used in composite layups where a thin sheet of piezoelectric material can alter the shape of the structure. Therefore, it is necessary to have some insight into the workings of composites.

Classical Laminate Theory (CLT) is a field that spans a vast amount of research which will only be touched upon herein. This section will present the basics of orthotropic material formations, followed by the CLT formulations equations for a single ply. Thereafter, equations for the multi-layer case are presented.

3.3.1 Materials

Most of the preceding formulations have dealt with the elastic constitutive relation in the form of an isotropic material. When dealing with composite materials this is not always the case hence, a new constitutive relation needs to be discussed.

In isotropic materials it is assumed that the material properties are the same in all directions. In composites these usually differ in at least one of the three directions. More specifically in orthotropic materials, it is assumed that there are three mutually perpendicular planes of material symmetry [3].

The three dimensional composite stiffness matrix is a 6×6 dense matrix made up of the dimensional Youngs moduli, E, the Shear moduli, G and the Poisons ratios, v. Following the assumption of an orthotropic material the total number of variables used is reduced and the stiffness matrix is of the form

$$\mathbf{S} = \mathbf{C}_E^{-1} = \begin{bmatrix} \frac{1}{E_1} & -\frac{v_{12}}{E_1} & -\frac{v_{13}}{E_1} & 0 & 0 & 0 \\ -\frac{v_{21}}{E_2} & \frac{1}{E_2} & -\frac{v_{23}}{E_2} & 0 & 0 & 0 \\ -\frac{v_{31}}{E_3} & -\frac{v_{32}}{E_3} & \frac{1}{E_3} & 0 & 0 & 0 \\ 0 & 0 & 0 & \frac{1}{G_{23}} & 0 & 0 \\ 0 & 0 & 0 & 0 & \frac{1}{G_{31}} & 0 \\ 0 & 0 & 0 & 0 & 0 & \frac{1}{G_{12}} \end{bmatrix}, \tag{3.120}$$

which reduces to the form

$$\mathbf{C}_E = \begin{bmatrix} \frac{S_{22}}{S_{11}S_{22} - S_{12}^2} & -\frac{S_{12}}{S_{11}S_{22} - S_{12}^2} & 0 \\ -\frac{S_{12}}{S_{11}S_{22} - S_{12}^2} & \frac{S_{11}}{S_{11}S_{22} - S_{12}^2} & 0 \\ 0 & 0 & -\frac{1}{S_{66}} \end{bmatrix} \tag{3.121}$$

for the 2-dimensional case, where [3]

$$\boldsymbol{\epsilon} = \mathbf{S}\boldsymbol{\sigma} \text{ and } \boldsymbol{\sigma} = \mathbf{C}_E\boldsymbol{\epsilon}. \tag{3.122}$$

3.3.2 A Single Layer Approach

In composites, the alignment of the fibrous direction is important and the constitutive relations are always prescribed in that direction. This direction being in the local coordinate (1 and 2) system whereas the global coordinate (x and y) system is what is analysed (seen in Figure 3.4).In order to transform the coordinates from the local into the global a transformation matrix is needed.

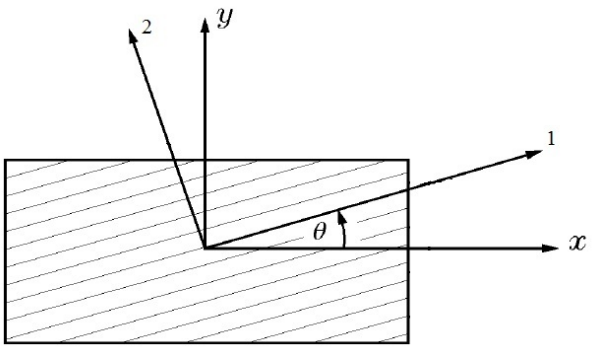

Figure 3.4: Coordinate configurations of a single ply composite [3]

It is defined as

$$\mathbf{T}_{CLT} = \begin{bmatrix} c^2 & s^2 & -2sc \\ s^2 & c^2 & 2sc \\ sc & -sc & c^2 - s^2 \end{bmatrix}, \tag{3.123}$$

where

$$c = \cos(\theta) \text{ and } s = \sin(\theta). \tag{3.124}$$

This transformation matrix can then be used to transform the constitutive relation in the following way

$$\boldsymbol{\sigma}_{xy} = [\mathbf{T}_{CLT}^{-1}\mathbf{C}_E\mathbf{R}_{CLT}\mathbf{T}_{CLT}\mathbf{R}_{CLT}^{-1}]\boldsymbol{\epsilon}_{xy}, \tag{3.125}$$

where

$$\mathbf{R}_{CLT} = \begin{bmatrix} 1 & 0 & 0 \\ 0 & 1 & 0 \\ 0 & 0 & 2 \end{bmatrix}. \tag{3.126}$$

Here $\mathbf{R}_{CLT}$ is the Reuter matrix used to accommodate engineering strain. This means that the new constitutive relation for a single ply is

$$\overline{\mathbf{Q}} = \overline{\mathbf{C}}_E = \mathbf{T}_{CLT}^{-1}\mathbf{C}_E\mathbf{R}_{CLT}\mathbf{T}_{CLT}\mathbf{R}_{CLT}^{-1}, \tag{3.127}$$

where $\overline{\mathbf{C}}_E$ is the constitutive relation in global coordinates. However, for the multi-layered system this term $\overline{\mathbf{C}}_E$ is termed as $\overline{\mathbf{Q}}$ for the specified material constants [3].

3.3.3 Multi-Layer Approach

A means of clarifying the multi-layer approach, is to assume that the laminate is thin enough that the stresses in each ply can be grouped into an averaged total. This total is relative to the plies individual thickness's and properties. The prior assumption is valid if a plain stress assumption is made that assumes the out of plane stresses to be zero. Considering these two assumptions and realising that bending might play an effect on the outcome, strain can be redefined as

$$\boldsymbol{\epsilon} = \boldsymbol{\epsilon}_0 + z\boldsymbol{\kappa}, \tag{3.128}$$

where

$$\boldsymbol{\epsilon}_0 = \begin{bmatrix} \dfrac{\partial u_0}{\partial x} \\ \dfrac{\partial v_0}{\partial y} \\ \dfrac{\partial u_0}{\partial y} + \dfrac{\partial v_0}{\partial x} \end{bmatrix} \tag{3.129}$$

and

$$\boldsymbol{\kappa} = \begin{bmatrix} \dfrac{\partial^2 w_0}{\partial x^2} \\ \dfrac{\partial^2 w_0}{\partial y^2} \\ -2\dfrac{\partial w_0}{\partial x \partial y} \end{bmatrix}, \tag{3.130}$$

where u_0, v_0 and w_0 are the displacements along the neutral axis in the x, y and z directions respectively [3]. Noting the new strain term the relation for the stress strain relation changes to

$$\boldsymbol{\sigma} = \overline{\mathbf{Q}}\boldsymbol{\epsilon}_0 + z\overline{\mathbf{Q}}\boldsymbol{\kappa}, \tag{3.131}$$

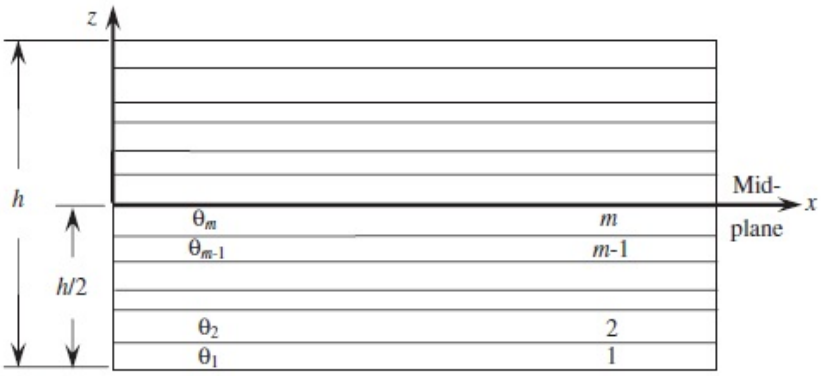

Figure 3.5: A laminate [4], showing numbering scheme.

where $\overline{\mathbf{Q}}$ was defined in Equation (3.127).

Figure 3.5 shows the classical set-up for a perfect laminate with $2m$ ply-layers. The first thing to note from the figure is that all the layers have different orientations of the ply. This means that the $\overline{\mathbf{Q}}$ matrix has to be computed for each layer of the ply. A second thing to note is that the laminate has all its layer thickness coordinates from $-h/2$ to $h/2$. This means that the positions of the top and bottom layer of each ply can be found relatively easily as long as the thickness(t_k) of each ply is known. Following this information, the mid-plane forces and moments per unit length of the laminate can be worked out as

$$\mathbf{N}_{xy} = \int_{-\frac{h}{2}}^{\frac{h}{2}} \boldsymbol{\sigma}_{xy}\, dz \text{ and } \mathbf{M}_{xy} = \int_{-\frac{h}{2}}^{\frac{h}{2}} z\boldsymbol{\sigma}_{xy}\, dz \tag{3.132}$$

and implimenting the new stress strain relation of Equation (3.131)

$$\begin{bmatrix} \mathbf{N}_{xy} \\ \mathbf{M}_{xy} \end{bmatrix} = \begin{bmatrix} \mathbf{A}_{CLT} & \mathbf{B}_{CLT} \\ \mathbf{B}_{CLT} & \mathbf{D}_{CLT} \end{bmatrix} \begin{bmatrix} \boldsymbol{\epsilon}_0 \\ \boldsymbol{\kappa} \end{bmatrix}, \tag{3.133}$$

where

$$\mathbf{A}_{CLT} = \sum_{k=1}^{2m} \overline{\mathbf{Q}}_k (z_k - z_{k-1}), \tag{3.134}$$

$$\mathbf{B}_{CLT} = \frac{1}{2} \sum_{k=1}^{2m} \overline{\mathbf{Q}}_k (z_k^2 - z_{k-1}^2), \tag{3.135}$$

$$\mathbf{D}_{CLT} = \frac{1}{3} \sum_{k=1}^{2m} \overline{\mathbf{Q}}_k (z_k^3 - z_{k-1}^3) \tag{3.136}$$

and z_k is the position of the top of the ply whilst z_{k-1} is the bottom [3]. This ABBD matrix can now be used in the FE methods that follow and are essential in piezoelectric plate and shell analysis.

3.4 The Plate Elements

The main difference between plate and shell elements is the co-ordinate systems [1]. Plate elements are described in a rectilinear system, while shells are described in a curvilinear system. This allows plates to be altered into shells using a transformation matrix. Formulation of the plate is a necessity before this transformation can take place and therefore needs to be explained.

In most plate theories the Kirchhoff plate theory is the simplest [23]. It does not however allow for a very good element formulation as it does not take transverse shear into account [12]. A sounder approach takes into account the shear stresses and is called the Mindlin plate elements and is based on the first order shear deformation theory (FSDT) [22]. Although the Mindlin approach to solving plate element systems is widely used, the method only allows for shear stress to take into account a single point integration scheme. This can prove inadequate in the cases of extreme shear differences. To overcome this problem E.N. Devorkin and K.-J. Bathe published an assumed shear element for non-linear analysis in 1984 and expanded it further in 1985 [5; 6]. This assumed shear element based on the Mindlin/Reissner assumption takes into account an altered four point integration scheme that will be elaborated upon in Section 3.4.1.2.

Although these plate theories are indeed important, they are only building blocks to the piezo-electric element and only parts will be used.

3.4.1 The General Plate

A plate is a flat sheet of material where the thickness is very small, in comparison to it's length and width, which means that it is easier to represent as a 2-D element than a 3-D body. Using Figure 3.3 as reference it is analogous that these bodies are represented by 4-noded elements. The degrees of freedom for each node differ for the Kirchoff and Mindlin element types. In each case however the membrane displacements are not taken into account. To implement these displacements the membrane is imposed on the plate and the form is described in the subsection that follows.

3.4.1.1 The Mindlin Approach

For a Mindlin plate there are 3 primary degrees of freedom. They are: one displacement in the z and two rotations about the x and y axis. Further expansion to include the membrane allows for the x and y displacements as well. The primary strains are

$$\epsilon_x = z\frac{\delta\theta_x}{\delta x}, \tag{3.137}$$

$$\epsilon_y = z\frac{\delta\theta_y}{\delta y}, \tag{3.138}$$

$$\gamma_{xy} = z\left(\frac{\delta\theta_y}{\delta x} + \frac{\delta\theta_x}{\delta y}\right), \tag{3.139}$$

$$\gamma_{xz} = \frac{\delta w}{\delta x} + \theta_x \tag{3.140}$$

and

$$\gamma_{yz} = \frac{\delta w}{\delta y} + \theta_y \tag{3.141}$$

here, θ is the angular deformation around each respective axis. These strains can be used in much the same way as the finite element formulation in Section 3.1.2. Formulation of the kinematic matrices are a point of difference and are constructed using the derivative matrices. The derivative matrices are

$$\boldsymbol{\nabla}_b = \begin{bmatrix} 0 & \frac{\partial}{\partial \xi} & 0 \\ 0 & 0 & \frac{\partial}{\partial \eta} \\ 0 & \frac{\partial}{\partial \eta} & \frac{\partial}{\partial \xi} \end{bmatrix} \tag{3.142}$$

and

$$\boldsymbol{\nabla}_s = \begin{bmatrix} \frac{\partial}{\partial \xi} & N & 0 \\ \frac{\partial}{\partial \eta} & 0 & N \end{bmatrix}, \tag{3.143}$$

where the subscripts b and s are used for bending and shear, respectively. These are formulated using the potential energy form

$$U = \frac{1}{2}\mathbf{q}^T \int_\Gamma \int_z (\boldsymbol{\nabla}_b \mathbf{N})^T \mathbf{C}_{Eb} (\boldsymbol{\nabla}_b \mathbf{N})\, dz\, d\Gamma\, \mathbf{q} + \frac{\alpha}{2}\mathbf{q}^T \int_\Gamma \int_z (\boldsymbol{\nabla}_s \mathbf{N})^T \mathbf{C}_{Eb} (\boldsymbol{\nabla}_s \mathbf{N})\, dz\, d\Gamma\, \mathbf{q}. \tag{3.144}$$

Thus for a single isotropic layer the stiffness matrix is

$$K = \frac{h^3}{12} \int_{-1}^{1} \int_{-1}^{1} (\boldsymbol{\nabla}_b \mathbf{N})^T \mathbf{C}_{Es} (\boldsymbol{\nabla}_b \mathbf{N}) \det \mathbf{J}\, d\xi\, d\eta + \alpha h \int_{-1}^{1} \int_{-1}^{1} (\boldsymbol{\nabla}_s \mathbf{N})^T \mathbf{C}_{Es} (\boldsymbol{\nabla}_s \mathbf{N}) \det \mathbf{J}\, d\xi\, d\eta, \tag{3.145}$$

where $\mathbf{C}_{Eb}$ is the 3x3 normal plain stress material matrix, $\mathbf{C}_{Es}$ is the 2x2 shear stress material matrix, $\mathbf{N}$ is the shape function matrix, α is a shear correction factor of 5/6 and h is the thickness of the plate.

A further expansion of this form is to include the information of Section 3.3 that allows for laminated plates. To do this normal and bending stresses must be taken into account. Thus the

differentiation matrices change to

$$\boldsymbol{\nabla}_n = \begin{bmatrix} \frac{\partial}{\partial \xi} & 0 & 0 & 0 & 0 \\ 0 & \frac{\partial}{\partial \eta} & 0 & 0 & 0 \\ \frac{\partial}{\partial \eta} & \frac{\partial}{\partial \xi} & 0 & 0 & 0 \\ 0 & 0 & 0 & 0 & 0 \\ 0 & 0 & 0 & 0 & 0 \end{bmatrix}, \tag{3.146}$$

$$\boldsymbol{\nabla}_b = \begin{bmatrix} 0 & 0 & 0 & \frac{\partial}{\partial \xi} & 0 \\ 0 & 0 & 0 & 0 & \frac{\partial}{\partial \eta} \\ 0 & 0 & 0 & \frac{\partial}{\partial \eta} & \frac{\partial}{\partial \xi} \\ 0 & 0 & 0 & 0 & 0 \\ 0 & 0 & 0 & 0 & 0 \end{bmatrix} \tag{3.147}$$

and

$$\boldsymbol{\nabla}_s = \begin{bmatrix} 0 & 0 & \frac{\partial}{\partial \xi} & N & 0 \\ 0 & 0 & \frac{\partial}{\partial \eta} & 0 & N \end{bmatrix} \tag{3.148}$$

This changes the final form to

$$\begin{aligned} U = &\frac{1}{2} \int_{\Gamma} \mathbf{q}^T \int_z \Big[(\boldsymbol{\nabla}_n \mathbf{N})^T \mathbf{A}_{CLT} (\boldsymbol{\nabla}_n \mathbf{N}) + (\boldsymbol{\nabla}_n \mathbf{N})^T \mathbf{B}_{CLT} (\boldsymbol{\nabla}_b \mathbf{N}) + (\boldsymbol{\nabla}_b \mathbf{N})^T \mathbf{B}_{CLT} (\boldsymbol{\nabla}_n \mathbf{N}) \\ &+ (\boldsymbol{\nabla}_b \mathbf{N})^T \mathbf{D}_{CLT} (\boldsymbol{\nabla}_b \mathbf{N}) \Big] dz\, \mathbf{q}\, d\Gamma + \frac{1}{2} \int_{\Gamma} \mathbf{q}^T \int_z \Big[(\boldsymbol{\nabla}_s \mathbf{N})^T \mathbf{A}_{CLTs} (\boldsymbol{\nabla}_s \mathbf{N}) \Big] dz\, \mathbf{q}\, d\Gamma, \end{aligned} \tag{3.149}$$

where $\mathbf{A}_{CLT}$, $\mathbf{B}_{CLT}$ and $\mathbf{D}_{CLT}$ are from the Equations 3.134 to 3.136 and $\mathbf{A}_{CLTs}$ is the shear component of Equation (3.134). Where the full stiffness matrices are the sum of all of the smaller components. To obtain the shear component, the layer approach of Section 3.3.3 needs to be expanded to three dimensions. The forth and fifth rows and columns of the $\overline{\mathbf{Q}}$ matrix are used to obtain $\mathbf{A}_{CLTs}$ in much the same way as in obtaining $\mathbf{A}_{CLT}$. The full transformation matrix and Reuter matrix are seen below:

$$\mathbf{T}_{CLT} = \begin{bmatrix} c^2 & s^2 & 0 & 0 & 0 & -2sc \\ s^2 & c^2 & 0 & 0 & 0 & 2sc \\ 0 & 0 & 1 & 0 & 0 & 0 \\ 0 & 0 & 0 & c & -s & 0 \\ 0 & 0 & 0 & s & c & 0 \\ sc & -sc & 0 & 0 & 0 & c^2 - s^2 \end{bmatrix} \tag{3.150}$$

and

$$\mathbf{R}_{CLT} = \begin{bmatrix} 1 & 0 & 0 & 0 & 0 & 0 \\ 0 & 1 & 0 & 0 & 0 & 0 \\ 0 & 0 & 1 & 0 & 0 & 0 \\ 0 & 0 & 0 & 2 & 0 & 0 \\ 0 & 0 & 0 & 0 & 2 & 0 \\ 0 & 0 & 0 & 0 & 0 & 2 \end{bmatrix} \tag{3.151}$$

In the preceding stiffness matrices of Equation (3.149) the shear component is integrated with a one point Gaussian rule. This shear component will be replaced by a higher order assumed shear that is explained in the next section.

3.4.1.2 A Higher Order Assumed Shear Stress

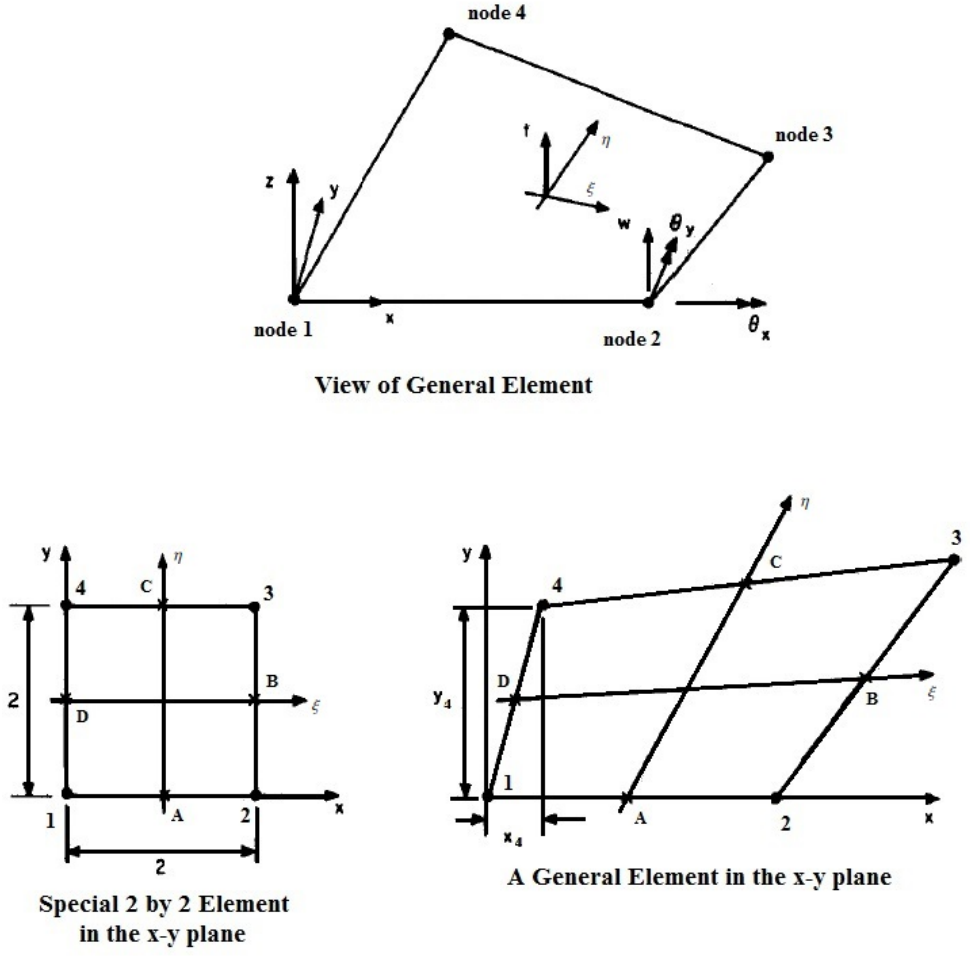

Figure 3.6: The isoparametric element shown for the assumed shear plate [5]

Bathe and Dvorkin wrote 2 papers about the assumed shear element in 1984-5 in which they formulate the element in its entirety [5; 6]. After their pioneering work on the element Groenwold went into a little more detail on the element in 1993 [8]. The element uses the same interpolations as the normal plate as seen in Figure 3.6. Although the figure also shows new integration points at 'A', 'B', 'C' and 'D'. The degrees of freedom are also shown in the same figure and are the same as a regular plate. The difference is in the way in which the element is created.

Figure 3.7 shows the wedges that form the shear stress instead of the FSDT where it would be a flat square. These wedges show the form of the shear stress and emphasize what occurs when the integration points 'A' to 'D' are used. They are used in the form

$$\gamma_{\eta\xi} = \frac{1}{2}(1-\xi)\gamma^A_{\eta z} + \frac{1}{2}(1+\xi)\gamma^C_{\eta z} \tag{3.152}$$

and

$$\gamma_{\xi z} = \frac{1}{2}(1+\eta)\gamma^B_{\xi z} + \frac{1}{2}(1-\eta)\gamma^D_{\xi z} \tag{3.153}$$

where, the subscripts ξ, η and z refer to the coordinate system.

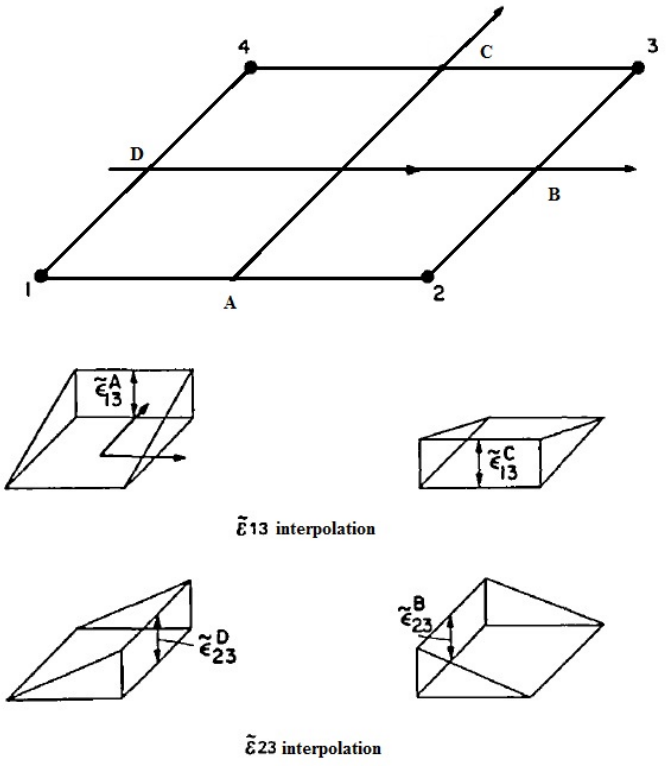

Figure 3.7: Transverse shear interpolation for a plate [6]

When implementing these equations into the finite element code it involves an initial integration step to obtain the strains at points 'A' to 'D' and then a 2×2 Gaussian integration to compile the equations.

3.4.2 The Piezoelectric Plate

There are many theories for piezoelectric plates and in most the Mindlin approach is used as in Section 3.4.1. This is generally used in conjunction with the CLT of Section 3.3.3, as piezoelectric plates are seldom homogeneous and are usually a composite layup combined with one or more piezoelectric layers.

There were multiple methods for the formulation of the finite element solution. Carrera, Brischetto and Nali proposed the use of CLT when compiling the piezoelectric and permeability material constants [1]. They took into account piezoelectric normal, bending and shear movements. To date this is one of the more complicated theories to implement. Another author, Ho-Jun Lee, completed a report for NASA on thermopiezoelectrics which is a slightly expanded theory that can be simplified to only implement the piezoelectrics [35]. Although both these references are theoretically sound, the implementation was found to be relatively complex. A simpler implementation was proposed by Piefort which uses a single piezoelectric degree of freedom per element per piezoelectric layer [13].

3.4.2.1 The Polarization of Piezoelectric Plates

Polarization (Polling) is the process whereby the intermolecular bonds of a piezoelectric material are aligned along a specified axis [13]. More specifically the ferroelectric domains of a piezoceramic material are aligned creating a piezoelectric material [67]. This process is conducted by the application of voltage in the respective axis's direction [67]. The degree to which the polling effects the piezoceramic material is based on the magnitude of the voltage, the temperature and the length of application [67].

When looking at the programming of the polling trait, the axes are important. Using the values 1-6 for the axes as are represented in the complete material matrices $\mathbf{C}_E$, $\mathbf{e}$ and $\boldsymbol{\gamma}_\epsilon$ which are 6×6, 3×6 and 3×3 respectively, which are seen in Equation (3.57). With the axis numbering being standard and referring to

1. X-axis
2. Y-axis
3. Z-axis
4. Shear around the X-axis
5. Shear around the Y-axis
6. Shear around the Z-axis

where the X, Y and Z are as seen in Figure 3.2 [67]. The material constants of respective rows and columns for the piezoelectric coupling, **e**, can now be changed to negative or positive in order to control the polling direction [13; 67]. Note however that in the coupling matrix the major side is the mechanical polling and the minor is the electrical polling [67].

3.4.2.2 The Piezoelectric Plate Formulation

All of the formulation for piezoelectrics depart with the Equation (3.57) in their extended matrix form. It is known from the prior formulations that strain is a function of displacement. This is also relevant to the electric conditions [1]. Formulating the displacements in finite element form gives:

$$u(x,y,z,t) = N_i q_{u_\Theta i} + zN_i q_{\theta_x i}, \tag{3.154}$$
$$v(x,y,z,t) = N_i q_{v_\Theta i} + zN_i q_{\theta_y i}, \tag{3.155}$$
$$w(x,y,z,t) = N_i q_{w_\Theta i}, \tag{3.156}$$

and

$$\phi^k(x,y,z,t) = N_i q^k_{\phi_0 i} + (z - \bar{z}_k) N_i q^k_{\phi_1 i} \tag{3.157}$$

And using these displacements to define the strains gives [1]:

$$\epsilon_x = \frac{\partial u}{\partial x} = \frac{\partial u_\Theta}{\partial x} + z\frac{\partial \theta_x}{\partial x} = \epsilon_x + \kappa_x, \tag{3.158}$$
$$\epsilon_y = \frac{\partial v}{\partial y} = \frac{\partial v_\Theta}{\partial y} + z\frac{\partial \theta_y}{\partial y} = \epsilon_y + \kappa_y, \tag{3.159}$$
$$\gamma_{xy} = \frac{\partial u}{\partial y} + \frac{\partial v}{\partial x} = \frac{\partial u_\Theta}{\partial y} + z\frac{\partial \theta_x}{\partial y} + \frac{\partial v_\Theta}{\partial x} + z\frac{\partial \theta_y}{\partial x} = \epsilon_{xy} + \kappa_{xy}, \tag{3.160}$$
$$\gamma_{xz} = \frac{\partial u}{\partial z} + \frac{\partial w}{\partial x} = \frac{\partial w_\Theta}{\partial x} + \theta_x = \epsilon_{xz}, \tag{3.161}$$
$$\gamma_{yz} = \frac{\partial v}{\partial z} + \frac{\partial w}{\partial y} = \frac{\partial w_\Theta}{\partial y} + \theta_y = \epsilon_{yz}, \tag{3.162}$$
$$E^k_x = -\frac{\partial \phi^k}{\partial x} = -(\frac{\partial \phi^k_0}{\partial x} - \bar{z}_k \frac{\partial \phi^k_1}{\partial x}) - z\frac{\partial \phi^k_1}{\partial x} = E^{k(0)}_x + zE^{k(1)}_x, \tag{3.163}$$
$$E^k_y = -\frac{\partial \phi^k}{\partial y} = -(\frac{\partial \phi^k_0}{\partial y} - \bar{z}_k \frac{\partial \phi^k_1}{\partial y}) - z\frac{\partial \phi^k_1}{\partial y} = E^{k(0)}_y + zE^{k(1)}_y \tag{3.164}$$

and

$$E^k_z = -\frac{\partial \phi^k}{\partial z} = -\phi^k_1 = E^{k(0)}_z \tag{3.165}$$

Section 3.2.1 uses the Hamiltonian Principle for the method of formulation, here however it begins with the principle of virtual work. Initially internal energy is broken up into its mechanical and electrical components and expanded into the integral over the structure [34].

$$\delta U = \delta U_m + \delta U_e = \int_{\Omega} (\delta U_{0m} + \delta U_{0e})\, d\Omega. \tag{3.166}$$

Assuming that the structure is multi-layered the volume integral can change to include separate integrals over the thickness and the surface area.

$$= \int_{\Gamma} \Big(\int_{-h/2}^{h/2} [\boldsymbol{\sigma}^k \delta\boldsymbol{\epsilon} - \mathbf{D}^k \delta \mathbf{E}^k]\, dz \Big) d\Gamma, \tag{3.167}$$

$$= \int_{\Gamma} \Big(\int_{-h/2}^{h/2} [\boldsymbol{\sigma}^k \delta(\boldsymbol{\epsilon} + \boldsymbol{\kappa}) - \mathbf{D}^k (\delta \mathbf{E}^{k(0)} + z\delta \mathbf{E}^{k(1)})]\, dz \Big) d\Gamma. \tag{3.168}$$

This resulting equation can once again be expanded by replacing the respective stress variables using the coupling Equation (3.57) [1].

$$\delta U = \int_{\Gamma} \Big(\sum_{k=1}^{N_l} \int_{-h_k/2}^{h_k/2} [(\overline{\mathbf{Q}}^k \boldsymbol{\epsilon} - \mathbf{e}^k \boldsymbol{E}^k)\delta(\boldsymbol{\epsilon} + \boldsymbol{\kappa}) - (\mathbf{e}^k \boldsymbol{\epsilon} + \boldsymbol{\gamma}_{\epsilon}^k \mathbf{E}^k)(\delta \mathbf{E}^{k(0)} + z\delta \mathbf{E}^{k(1)})]\, dz \Big) d\Gamma. \tag{3.169}$$

Expanding the strains into their sub-components gives

$$\begin{aligned} = \int_{\Gamma} \Big(\sum_{k=1}^{N_l} \int_{-h_k/2}^{h_k/2} & [\delta(\boldsymbol{\epsilon} + \boldsymbol{\kappa})\overline{\mathbf{Q}}^k (\boldsymbol{\epsilon} + \boldsymbol{\kappa}) - \delta(\boldsymbol{\epsilon} + \boldsymbol{\kappa})\mathbf{e}^k (\mathbf{E}^{k(0)} + z\mathbf{E}^{k(1)}) \\ & - \delta(\mathbf{E}^{k(0)} + z\mathbf{E}^{k(1)})\mathbf{e}^k (\boldsymbol{\epsilon} + \boldsymbol{\kappa}) + \delta(\mathbf{E}^{k(0)} + z\mathbf{E}^{k(1)})\boldsymbol{\gamma}_{\epsilon}^k (\mathbf{E}^{k(0)} + z\mathbf{E}^{k(1)})]\, dz \Big) d\Gamma \end{aligned} \tag{3.170}$$

and

$$\begin{aligned} = \int_{\Gamma} \Big(\sum_{k=1}^{N_l} \int_{-h_k/2}^{h_k/2} & [\delta\boldsymbol{\epsilon}\overline{\mathbf{Q}}^k \boldsymbol{\epsilon} + \delta\boldsymbol{\epsilon}\overline{\mathbf{Q}}^k \boldsymbol{\kappa} + \delta\boldsymbol{\kappa}\overline{\mathbf{Q}}^k \boldsymbol{\epsilon} + \delta\boldsymbol{\kappa}\overline{\mathbf{Q}}^k \boldsymbol{\epsilon} \\ & - \delta\boldsymbol{\epsilon}\mathbf{e}^k \mathbf{E}^{k(0)} - \delta\boldsymbol{\kappa}\mathbf{e}^k \mathbf{E}^{k(0)} - z\delta\boldsymbol{\epsilon}\mathbf{e}^k \mathbf{E}^{k(1)} - z\delta\boldsymbol{\kappa}\mathbf{e}^k \mathbf{E}^{k(1)} \\ & - \delta\mathbf{E}^{k(0)}\mathbf{e}^k \boldsymbol{\epsilon} - z\delta\mathbf{E}^{k(1)}\mathbf{e}^k \boldsymbol{\epsilon} - \delta\mathbf{E}^{k(0)}\mathbf{e}^k \boldsymbol{\kappa} - z\delta\mathbf{E}^{k(1)}\mathbf{e}^k \boldsymbol{\kappa} \\ & - \delta\mathbf{E}^{k(0)}\boldsymbol{\gamma}_{\epsilon}^k \mathbf{E}^{k(0)} - z\delta\mathbf{E}^{k(0)}\boldsymbol{\gamma}_{\epsilon}^k \mathbf{E}^{k(1)} - z\delta\mathbf{E}^{k(1)}\boldsymbol{\gamma}_{\epsilon}^k \mathbf{E}^{k(0)} - z^2\delta\mathbf{E}^{k(1)}\boldsymbol{\gamma}_{\epsilon}^k \mathbf{E}^{k(1)}]\, dz \Big) d\Gamma. \end{aligned} \tag{3.171}$$

Replacing the strains with their displacement definitions gives

$$
\begin{aligned}
&= \int_{\Gamma} \Bigg(\sum_{k=1}^{N_l} \int_{-h_k/2}^{h_k/2} [(\delta\nabla_m \mathbf{Nq})^T \overline{\mathbf{Q}}^k (\nabla_m \mathbf{Nq}) + (\delta\nabla_m \mathbf{Nq})^T \overline{\mathbf{Q}}^k (z\nabla_{mb} \mathbf{Nq}) \\
&+ \delta(z\nabla_{mb} \mathbf{Nq})^T \overline{\mathbf{Q}}^k (\nabla_m \mathbf{Nq}) + \delta(z\nabla_{mb} \mathbf{Nq})^T \overline{\mathbf{Q}}^k (z\nabla_{mb} \mathbf{Nq}) - (\delta\nabla_m \mathbf{Nq})^T \mathbf{e}^k (\nabla_e^k \mathbf{N}\phi^k) \\
&- \delta(z\nabla_{mb} \mathbf{Nq})^T \mathbf{e}^k (\nabla_e^k \mathbf{N}\phi^k) - (\delta\nabla_m \mathbf{Nq})^T \mathbf{e}^k (z\nabla_{eb} \mathbf{N}\phi^k) - \delta(z\nabla_{mb} \mathbf{Nq})^T \mathbf{e}^k (z\nabla_{eb} \mathbf{N}\phi^k) \\
&- \delta(\nabla_e^k \mathbf{N}\phi^k)^T \mathbf{e}^k (\nabla_m \mathbf{Nq}) - \delta(z\nabla_{eb} \mathbf{N}\phi^k)^T \mathbf{e}^k (\nabla_m \mathbf{Nq}) - \delta(\nabla_e^k \mathbf{N}\phi^k)^T \mathbf{e}^k (z\nabla_{mb} \mathbf{Nq}) \\
&- \delta(z\nabla_{eb} \mathbf{N}\phi^k)^T \mathbf{e}^k (z\nabla_{mb} \mathbf{Nq}) - \delta(\nabla_e^k \mathbf{N}\phi^k)^T \gamma_\epsilon^k (\nabla_e^k \mathbf{N}\phi^k) - \delta(\nabla_e^k \mathbf{N}\phi^k)^T \gamma_\epsilon^k (z\nabla_{eb} \mathbf{N}\phi^k) \\
&- \delta(z\nabla_{eb} \mathbf{N}\phi^k)^T \gamma_\epsilon^k (\nabla_e^k \mathbf{N}\phi^k) - \delta(z\nabla_{eb} \mathbf{N}\phi^k)^T \gamma_\epsilon^k (z\nabla_{eb} \mathbf{N}\phi^k)] \, dz \Bigg) d\Gamma. \qquad (3.172)
\end{aligned}
$$

Using CLT to complete the ABBD matrices from Equations 3.134 to 3.136 results in

$$
\begin{aligned}
\delta U = &\int_{\Gamma} \Big((\delta\nabla_m \mathbf{Nq})^T \mathbf{A}_{CLT} (\nabla_m \mathbf{Nq}) + (\delta\nabla_m \mathbf{Nq})^T \mathbf{B}_{CLT} (\nabla_{mb} \mathbf{Nq}) + \delta(\nabla_{mb} \mathbf{Nq})^T \mathbf{B}_{CLT} (\nabla_m \mathbf{Nq}) \\
&+ \delta(\nabla_{mb} \mathbf{Nq})^T \mathbf{D}_{CLT} (\nabla_{mb} \mathbf{Nq}) + \sum_{k=1}^{N_l} \int_{-h_k/2}^{h_k/2} [-(\delta\nabla_m \mathbf{Nq})^T \mathbf{e}^k (\nabla_e^k \mathbf{N}\phi^k) \\
&- \delta(z\nabla_{mb} \mathbf{Nq})^T \mathbf{e}^k (\nabla_e^k \mathbf{N}\phi^k) - (\delta\nabla_m \mathbf{Nq})^T \mathbf{e}^k (z\nabla_{eb} \mathbf{N}\phi^k) - \delta(z\nabla_{mb} \mathbf{Nq})^T \mathbf{e}^k (z\nabla_{eb} \mathbf{N}\phi^k) \\
&- \delta(\nabla_e^k \mathbf{N}\phi^k)^T \mathbf{e}^k (\nabla_m \mathbf{Nq}) - \delta(z\nabla_{eb} \mathbf{N}\phi^k)^T \mathbf{e}^k (\nabla_m \mathbf{Nq}) - \delta(\nabla_e^k \mathbf{N}\phi^k)^T \mathbf{e}^k (z\nabla_{mb} \mathbf{Nq}) \\
&- \delta(z\nabla_{eb} \mathbf{N}\phi^k)^T \mathbf{e}^k (z\nabla_{mb} \mathbf{Nq}) - \delta(\nabla_e^k \mathbf{N}\phi^k)^T \gamma_\epsilon^k (\nabla_e^k \mathbf{N}\phi^k) - \delta(\nabla_e^k \mathbf{N}\phi^k)^T \gamma_\epsilon^k (z\nabla_{eb} \mathbf{N}\phi^k) \\
&- \delta(z\nabla_{eb} \mathbf{N}\phi^k)^T \gamma_\epsilon^k (\nabla_e^k \mathbf{N}\phi^k) - \delta(z\nabla_{eb} \mathbf{N}\phi^k)^T \gamma_\epsilon^k (z\nabla_{eb} \mathbf{N}\phi^k)] \, dz \Big) d\Gamma. \qquad (3.173)
\end{aligned}
$$

Assuming that shear plays a role in the theorem and that the theory used is FSDT for both the electric and the mechanical conditions, the result is [1]

$$
\begin{aligned}
\delta U = &\int_{\Gamma} \Big((\delta\nabla_m \mathbf{Nq})^T \mathbf{A}_{CLT} (\nabla_m \mathbf{Nq}) + (\delta\nabla_m \mathbf{Nq})^T \mathbf{B}_{CLT} (\nabla_{mb} \mathbf{Nq}) + \delta(\nabla_{mb} \mathbf{Nq})^T \mathbf{B}_{CLT} (\nabla_m \mathbf{Nq}) \\
&+ \delta(\nabla_{mb} \mathbf{Nq})^T \mathbf{D}_{CLT} (\nabla_{mb} \mathbf{Nq}) + (\delta\nabla_{ms} \mathbf{Nq})^T \mathbf{A}_{CLTs} (\nabla_{ms} \mathbf{Nq}) + \sum_{k=1}^{N_l} \int_{-h_k/2}^{h_k/2} [\\
&- (\delta\nabla_m \mathbf{Nq})^T \mathbf{e}^k (\nabla_e^k \mathbf{N}\phi^k) - \delta(z\nabla_{mb} \mathbf{Nq})^T \mathbf{e}^k (\nabla_e^k \mathbf{N}\phi^k) - (\delta\nabla_m \mathbf{Nq})^T \mathbf{e}^k (z\nabla_{eb} \mathbf{N}\phi^k) \\
&- \delta(z\nabla_{mb} \mathbf{Nq})^T \mathbf{e}^k (z\nabla_{eb} \mathbf{N}\phi^k) - \delta(\nabla_e^k \mathbf{N}\phi^k)^T \mathbf{e}^k (\nabla_m \mathbf{Nq}) - \delta(z\nabla_{eb} \mathbf{N}\phi^k)^T \mathbf{e}^k (\nabla_m \mathbf{Nq}) \\
&- \delta(\nabla_e^k \mathbf{N}\phi^k)^T \mathbf{e}^k (z\nabla_{mb} \mathbf{Nq}) - \delta(z\nabla_{eb} \mathbf{N}\phi^k)^T \mathbf{e}^k (z\nabla_{mb} \mathbf{Nq}) - \delta(\nabla_e^k \mathbf{N}\phi^k)^T \gamma_\epsilon^k (\nabla_e^k \mathbf{N}\phi^k) \\
&- \delta(\nabla_e^k \mathbf{N}\phi^k)^T \gamma_\epsilon^k (z\nabla_{eb} \mathbf{N}\phi^k) - \delta(z\nabla_{eb} \mathbf{N}\phi^k)^T \gamma_\epsilon^k (\nabla_e^k \mathbf{N}\phi^k) - \delta(z\nabla_{eb} \mathbf{N}\phi^k)^T \gamma_\epsilon^k (z\nabla_{eb} \mathbf{N}\phi^k) \\
&- (\delta\nabla_{ms} \mathbf{Nq})^T \mathbf{e}_s^k (\nabla_e^k \mathbf{N}\phi^k) - \delta(\nabla_{ms} \mathbf{Nq})^T \mathbf{e}_s^k (z\nabla_{eb}^k \mathbf{N}\phi^k) - \delta(\nabla_e^k \mathbf{N}\phi^k)^T \mathbf{e}_s^k (\nabla_{ms} \mathbf{Nq}) \\
&- \delta(z\nabla_{eb} \mathbf{N}\phi^k)^T \mathbf{e}_s^k (\nabla_{ms} \mathbf{Nq})] \, dz \Big) d\Gamma. \qquad (3.174)
\end{aligned}
$$

Using a variation of the CLT for the piezoelectric and electric conditions the preceding equation can be simplified into the form

$$\delta U = \int_{\Gamma} \begin{bmatrix} \dfrac{\delta \mathbf{q}}{\delta \phi^k} \\ \vdots \end{bmatrix}^T \begin{bmatrix} \nabla_m \mathbf{N} \\ \nabla_{ms} \mathbf{N} \\ \nabla_{mb} \mathbf{N} \\ \hline \nabla_e^k \mathbf{N} \\ \nabla_{eb} \mathbf{N} \\ \vdots \end{bmatrix}^T \left[\begin{array}{cc|c} \mathbf{C}_E & & \mathbf{e}_E \quad \cdots \\ & & \\ \hline \mathbf{e}_E^T & & \gamma_\epsilon \\ \vdots & & \ddots \end{array}\right] \begin{bmatrix} \nabla_m \mathbf{N} \\ \nabla_{ms} \mathbf{N} \\ \nabla_{mb} \mathbf{N} \\ \hline \nabla_e^k \mathbf{N} \\ \nabla_{eb} \mathbf{N} \\ \vdots \end{bmatrix} \begin{bmatrix} \dfrac{\mathbf{q}}{\phi^k} \\ \vdots \end{bmatrix} d\Gamma, \tag{3.175}$$

where

$$\mathbf{C}_E = \begin{bmatrix} \mathbf{A}_{CLT} & 0 & \mathbf{B}_{CLT} \\ 0 & \mathbf{A}_{CLTs} & 0 \\ \mathbf{B}_{CLT} & 0 & \mathbf{D}_{CLT} \end{bmatrix}, \tag{3.176}$$

$$\mathbf{e}_E = \begin{bmatrix} -\mathbf{E}_{CLT}^k & -\mathbf{F}_{CLT}^k \\ -\mathbf{E}_{CLTs}^k & -\mathbf{F}_{CLTs}^k \\ -\mathbf{F}_{CLT}^k & -\mathbf{G}_{CLT}^k \end{bmatrix}, \tag{3.177}$$

$$\gamma_\epsilon = \begin{bmatrix} \mathbf{R}_{CLT}^k & \mathbf{S}_{CLT}^k \\ \mathbf{S}_{CLT}^k & \mathbf{T}_{CLT}^k \end{bmatrix}, \tag{3.178}$$

and

$$(\mathbf{E}_{CLT}^k, \mathbf{F}_{CLT}^k, \mathbf{G}_{CLT}^k) = \int_{z_k}^{z_{k+1}} \mathbf{e}_{1,2,6;1,2,6}^k (1, z, z^2) dz \quad \text{for } k = 1 \ldots n, \tag{3.179}$$

$$(\mathbf{R}_{CLT}^k, \mathbf{S}_{CLT}^k, \mathbf{T}_{CLT}^k) = \int_{z_k}^{z_{k+1}} \gamma_{\epsilon_{1,2,6;1,2,6}}^k (1, z, z^2) dz \quad \text{for } k = 1 \ldots n, \tag{3.180}$$

$$(\mathbf{E}_{CLTs}^k, \mathbf{F}_{CLTs}^k) = \int_{z_k}^{z_{k+1}} \mathbf{e}_{4,5;4,5}^k (1, z) dz \quad \text{for } k = 1 \ldots n, \tag{3.181}$$

where n is the number of layers. Equation (3.175) provides the extended theory for piezoelectric plates however a less complicated theory was proposed by Piefort, 2001, where instead of assessing each node for the piezoelectric voltage a single point per-layer per-element is used [13]. The formula is an abbreviation of Equation (3.175) and is as follows

$$K = \sum_{i=1}^{g} g_i \begin{bmatrix} [B]_{(i)}^T & 0 \\ 0 & I_n \end{bmatrix} \left[\begin{array}{ccc|ccc} \mathbf{A}_{CLT} & \mathbf{B}_{CLT} & 0 & & \varepsilon_k^T & \\ \mathbf{B}_{CLT} & \mathbf{D}_{CLT} & 0 & \cdots & \varepsilon_k^T z_{mk} & \cdots \\ 0 & 0 & \mathbf{A}_{CLTs} & & 0 & \\ \hline & \vdots & & \ddots & & 0 \\ \varepsilon_k^T & \varepsilon_k z_{mk} & 0 & & -\gamma_{\epsilon(3,3)}/h_k & \\ & \vdots & & 0 & & \ddots \end{array}\right] \begin{bmatrix} [B]_{(i)}^T & 0 \\ 0 & I_n \end{bmatrix}, \tag{3.182}$$

where

$$\varepsilon_k = \begin{bmatrix} e_{13} & e_{23} & 0 \end{bmatrix}_k [\mathbf{T}_{CLT}^{-1}]_k \tag{3.183}$$

and $\mathbf{T}_{CLT}$ is the transformation matrix from Equation (3.123) [13]. Carrara *et.al.* proposed Equations 3.175 to 3.181 where n refers to the total number of layers, thereby assuming that all materials have some permittivity and piezoelectric coupling. Pieforts theory assumes n is only for the number of piezoelectric layers thereby implying that the values of permittivity and piezoelectric coupling for non piezoelectric materials are negligible. This assumption greatly reduces the size of the stiffness matrix and the number of material specifications that need to be stored.

3.4.2.3 The Programming Procedure

Algorithm 3: FEM basic structure for displacement solution of P4 plate element

begin
  Declaration of Control Parameters;
  Declaration of General Constitutive Relation;
  Implementation of CLT to the Constitutive Relation;
  Declaration of Mesh;
  Declaration of Force Inputs;
  Initialization of Total Matrices;
  Declaration of Gaussian Integration Scheme;
  for *1⟶element total* **do**
    for *1⟶nodes per element* **do**
      Extract Element Nodal Data;
    end
    Initialization of Sub-Matrix Structures;
    for *first dimensional integration* **do**
      Extract x Sampling Points and Weights;
      for *second dimensional integration* **do**
        Extract y Sampling Points and Weights;
        Solve for $\mathbf{K}$ using Math of Equation (3.182);
        i.e. $\mathbf{K}_m = \mathbf{K}_m + math(\mathbf{K}_A)$;
        i.e. $\mathbf{K}_m = \mathbf{K}_m + math(\mathbf{K}_B)$;
        i.e. $\mathbf{K}_m = \mathbf{K}_m + math(\mathbf{K}_B^T)$;
        i.e. $\mathbf{K}_m = \mathbf{K}_m + math(\mathbf{K}_D)$;
        i.e. $\mathbf{K}_p = \mathbf{K}_p + math(\mathbf{K}_E)$;
        i.e. $\mathbf{K}_p = \mathbf{K}_p + math(\mathbf{K}_F)$;
        i.e. $\mathbf{K}_e = \mathbf{K}_e + math$;
      end
    end
    Assemble 3 Large Stiffness Matrices Using Indexing($\mathbf{K}_m$, $\mathbf{K}_p$ and $\mathbf{K}_e$);
  end
  repeat loop for shear only using shear Gaussian points($\mathbf{K}_{As}$);
  Assemble Stiffness Matrix as in Equation (3.94);
  Solve for Displacements using Equation (3.50) Noting that the Matrix Definitions Differ from Algorithm 1;
end

Unlike the previous algorithms where the material specifications were fairly ordinary, the specifications for the plate have to take into account multiple layered materials and on occasion, multiple materials. This adds a new degree of complexity.

One complexity is that in order to obtain the stresses at the post-processing step the materials need to be passed along in their entirety. Another, is that in piezoelectric materials the polling needs to be specified for each piezoelectric layer in each coordinate. This means that the material

can be poled in any of the x, y or z directions for each layer.

Once the specifications are made the mechanical properties for the element need to be compiled using the classical laminate theory step. The piezoelectric and permittivity properties need to be compiled in a manner that caters for the number of piezoelectric layers in the structure. When compiling these properties care must be taken to assemble them correctly as they also need to conform to classical lamination theory.

In the stiffness composition the only relevant point is that the base stiffness matrices, shown in Algorithm 2, are expanded. This expansion is done to incorporate the classical lamination theory alterations. The general principle is shown in Algorithm 3. A CD of the code is provided in Appendix B to further illustrate the programming procedure.

3.5 Results

There are generally a large number of test problems that can be used for the analysis of new elements. Each case has its own ideal analytical solution that the test problem should converge upon. The convergence patterns for each test problem generally differ based on the degrees of freedom being tested and the element used. In this section the test problems will include multiple elements based on the definitions of the above sections as well as the degrees of freedom associated with the membrane and the plate element types.

3.5.1 Membrane Results

The test problems for this section derive mostly from papers by Long and Sze *et. al* [7; 65]. As a point of reference, results of the above formulations for the membrane element will be compared to those obtained from Long's Ph.D [2]. Further, as a point of clarity, the comparison will be in relative percentage error and absolute error, which are defined as

$$\%error = \frac{obtained\,result - accepted\,value}{accepted\,value} \times 100\% \tag{3.184}$$

and

$$\Delta e = |obtained\,result - accepted\,value| \tag{3.185}$$

respectively.

The initial step in all element proofs is the patch test as it shows the validity of the element in its refinement to an exact solution [12]. Following this, a 2 element beam is analysed with distorted elements which shows how stiffness affects the element formulation [2]. The same beam is then discretized into 4 elements to see the effects of simple mesh refinement on the stiffness [2]. A 10 element beam of the same outer geometry is analysed next, this is done to test the validity of the hybrid elements [2]. Lastly, Cooks membrane is analysed in multiple forms of discretization to show the effects of shear on the element and that the convergence path is stable.

In all of these tests the analytical solutions need to be known. For simplicity in solving the analytical solution, the material type for each test is restricted to PZT-4, however other materials can be used, they are shown in Appendix A.

The material constants used for these tests are laid out as

$$\begin{bmatrix} \sigma_{xx} \\ \sigma_{yy} \\ \sigma_{xy} \\ D_x \\ D_y \end{bmatrix} = \begin{bmatrix} c_{11} & c_{13} & 0 & 0 & -e_{31} \\ c_{13} & c_{33} & 0 & 0 & -e_{33} \\ 0 & 0 & c_{55} & -e_{15} & 0 \\ 0 & 0 & e_{15} & \gamma_{11} & 0 \\ e_{31} & e_{33} & 0 & 0 & \gamma_{33} \end{bmatrix} \begin{bmatrix} \epsilon_{xx} \\ \epsilon_{yy} \\ \epsilon_{xy} \\ E_x \\ E_y \end{bmatrix} \tag{3.186}$$

following the PZT-4 structure and the constants

$$\begin{bmatrix} s_{11} & s_{13} & g_{31} \\ s_{13} & s_{33} & g_{33} \\ -g_{31} & -g_{33} & \beta_{33} \end{bmatrix} = \begin{bmatrix} c_{11} & c_{13} & -e_{31} \\ c_{13} & c_{33} & -e_{33} \\ e_{31} & e_{33} & \gamma_{33} \end{bmatrix}^{-1} \tag{3.187}$$

are used for the analytical solutions, where

$$\begin{aligned} &c_{11} = 139 \times 10^3, \quad c_{13} = 74.3 \times 10^3, \quad c_{33} = 113 \times 10^3, \; c_{55} = 25.6 \times 10^3 \text{ N/mm}^2 \\ &e_{31} = -6.98 \times 10^6, \; e_{33} = 13.84 \times 10^6, \; e_{15} = 13.44 \times 10^6 \text{ pC/mm}^2 \\ &\gamma_{11} = 6.00 \times 10^9, \quad \gamma_{33} = 5.47 \times 10^9 \text{ pC/(GVmm)}. \end{aligned} \tag{3.188}$$

Thickness needs to be specified for each test for the membrane and is 1 mm unless otherwise stated. Consequently, from the units shown thus far, all dimensions for the test cases are in mm.

The last details that need to be mentioned are the boundary conditions. In general, a structure needs to be restricted at some points to stop translation. This also applies to the potential, ϕ, variable. This value needs to be grounded at one point (at the very least) in the structure as it would in the case of an electrical system.

3.5.1.1 The Patch Test

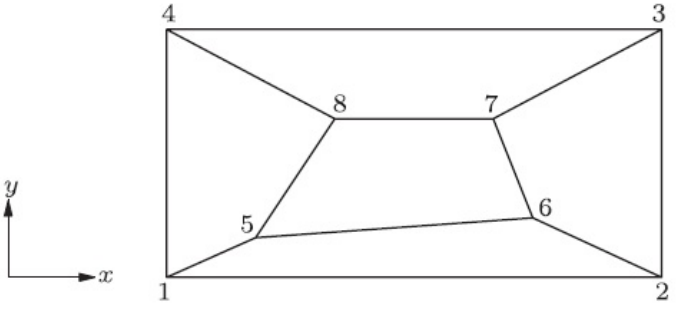

Coordinates:

Vertex	x	y
1	0.20	0.00
2	0.44	0.00
3	0.44	0.12
4	0.20	0.12
5	0.24	0.02
6	0.38	0.03
7	0.36	0.08
8	0.28	0.08

Figure 3.8: The patch test for a piezoelectric element [7]

The dimensions of the patch test are laid out in Figure 3.8 [28; 65]. The piezoelectric patch test differs from the regular one in that the potential has to be taken into account. Taking into account the nodal numbers, the fixed degrees of freedom are at node 1, 2 and 4. Node 1 is fully constrained for x and y displacements and for the grounded potential. Node 2 is constrained for potential only as this means the bottom surface is grounded. Lastly, node 4 is constrained in the x-displacement.

In the definition of the patch test by Macneal and Harder (1985) a stress is applied to both sides of the structure [28]. Taking into account the constrained conditions, the stress is only applied to the one side and this caters for the opposing stress at the constraints. This stress condition can be broken up numerically into 2 forces applied to node 2 and 3. Using a force at each of these nodes of 0.06 N, the total stress is 1 Pa. This makes the analytical solutions simpler to process from the equations

$$u_x = s_{11}\sigma_0 x, \quad u_y = s_{13}\sigma_0 y, \quad \phi = g_{31}\sigma_0 y \tag{3.189}$$

where σ_0 is the total stress. The resulting analytical solution is shown in Table 3.2, taking into account that the x co-ordinates of Figure 3.8 must be altered by 0.2 to have a base of 0.

Table 3.2: The analytical solution to the patch test

Node	u_x	u_y	ϕ
1	0	0	0
2	1.9012×10^{-6}	0	0
3	1.9012×10^{-6}	-0.36376×10^{-6}	-2.1334×10^{-9}
4	0	-0.36376×10^{-6}	-2.1334×10^{-9}
5	0.31687×10^{-6}	-0.060626×10^{-6}	-0.35557×10^{-9}
6	1.4259×10^{-6}	-0.090939×10^{-6}	-0.53335×10^{-9}
7	1.2675×10^{-6}	-0.24251×10^{-6}	-1.4223×10^{-9}
8	0.63375×10^{-6}	-0.24251×10^{-6}	-1.4223×10^{-9}

Comparison to these values was made and proven for all of the numerically constructed elements, showing that they pass the patch test. Which is a necessary and sufficient condition for proving convergence.

3.5.1.2 The 2 Element Beam

The 2 element beam is shown in Figure 3.9. Here, e in the figure is the common distortion that is applied to the elements, the node of interest for the numerical results is situated at point A and the forces F are 1 N in their respective directions. The bottom nodes of the structure are prescribed at the coordinate $y = -1$ and the potential at these nodes is grounded to 0.

Using this information the analytical solution at point A for u_y is $1.18827 \times 10^{-3}$and for ϕ is 0 based on the formulae

$$u_x = -s_{11}\sigma_0 xy, \; u_y = \frac{s_{13}\sigma_0}{2}\left(\frac{h^2}{4} - y^2\right) + \frac{s_{11}}{2}\sigma_0 x^2 \text{ and } \phi = \frac{g_{31}\sigma_0}{2}\left(\frac{h^2}{4} - y^2\right) \tag{3.190}$$

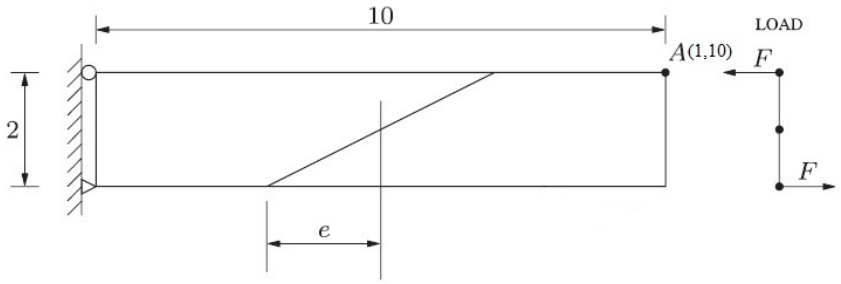

Figure 3.9: A 2 element beam with distortion [7]

subject to

$$\sigma_x = -\sigma_0 y,\ \sigma_y = \sigma_{xy} = D_x = D_y = 0 \text{ and } M = \int_{h/2}^{h/2} y\sigma_x\, dy = -\frac{h^3\sigma_0}{12} = -hF, \tag{3.191}$$

where h is the total height of the structure and, x and y are nodal point co-ordinates.

Analysing the structure numerically for the 4 piezoelectric membrane elements (with, P for piezoelectric, 4 for the number of nodes and further D and T being the relative hybrid formulation for D and σ, respectively) in terms of u_y and ϕ, and comparing to the analytical solution, the results can be plotted for the point A as in Figure 3.10. The results are in relative error for the deformation, u_y, and absolute error for the potential, ϕ. These results show increased stiffening that occurs with the increasing distortion.

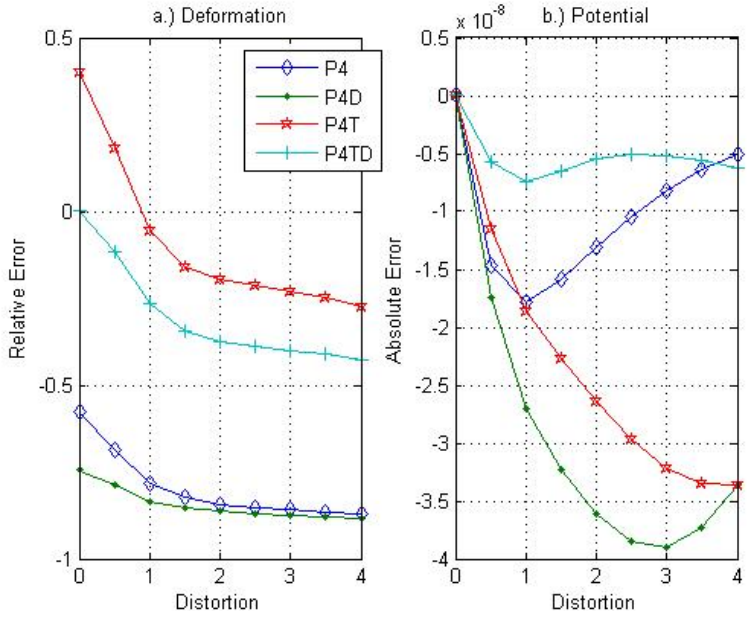

Figure 3.10: The 2 element beam results at A for the u_y and ϕ

Discretising this structure further into 4 elements by splitting the beam at $y = 0$ results in a smoother solution but with the same profiles (As seen in Figure 3.11) and only a marginally better result.

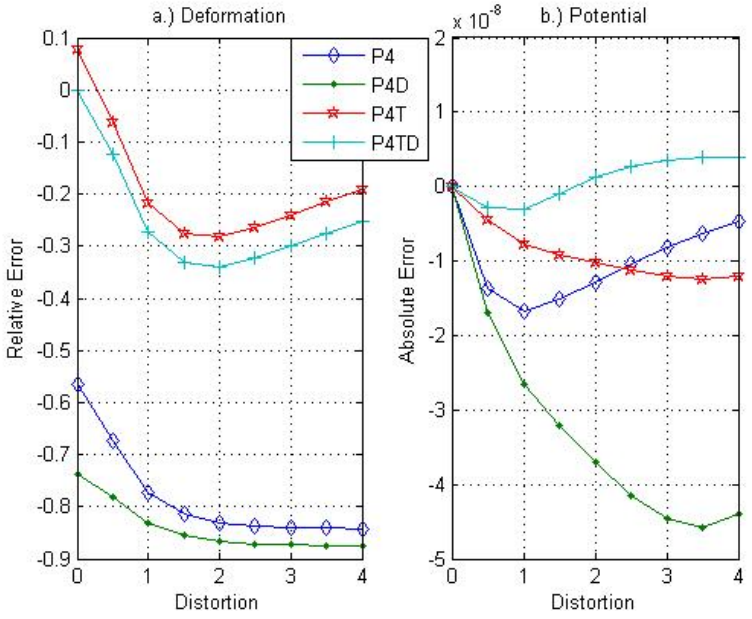

Figure 3.11: The 4 element beam results at A for the u_y and ϕ

3.5.1.3 The 10 Element Beam

The 10 element beam is an expansion of the prior test problem. It uses the same outside geometry with arbitrarily shaped elements and again, the same fixed degrees of freedom are used. The node B, seen in Figure 3.12, is used for the displacements and the node C is used for the potential.

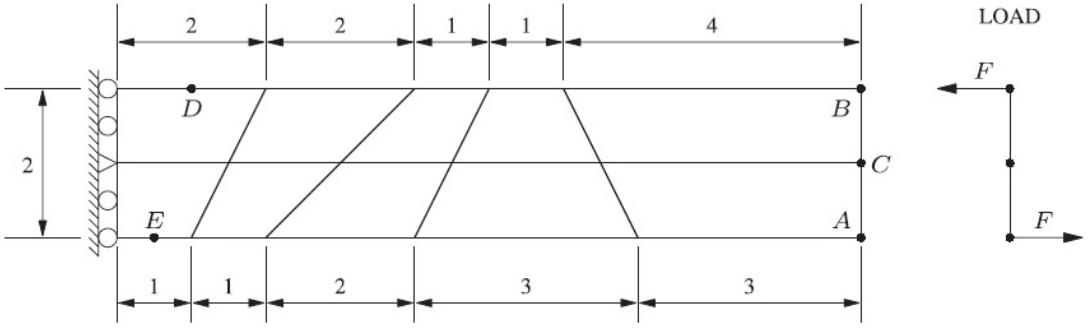

Figure 3.12: A 10 element beam [7]

The results displayed in Table 3.3 and correspond directly to Long's (2007) work in his PhD [2].

Table 3.3: The 10 element beam results

Element	Relative % Error		
	u_{xB}	u_{yB}	ϕ_C
$P4$	−40.417	−36.107	−48.118
$P4_D$	−50.158	−44.432	−68.754
$P4_\sigma$	1.0325	2.9906	7.5772
$P4_{\sigma D}$	−5.7882	−4.0459	1.7143

3.5.1.4 Cook's Membrane

Cook's membrane, shown in Figure 3.13, is used to test the convergence profile that the elements produce under mesh refinement. In the model the fixed degrees of freedom are prescribed as zero displacement at the wall in both the x and y directions and a zero potential along the bottom of the structure. The force at the tip is divided up amongst the nodal points and analysis of the node at C is then used to produce the y-displacement and potential results.

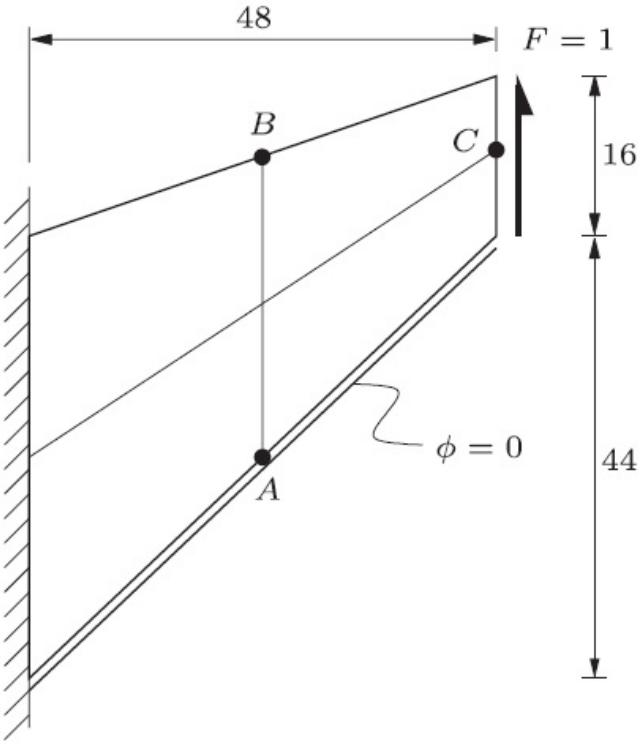

Figure 3.13: Cooks membrane for piezoelectric analysis [7]

The structure is analysed for discretizations of 2×2, 4×4, 8×8, 16×16 and 32×32 elements. This effects a doubling of x and y element numbers at each stage and the resulting solution should be of log linear form. For comparison, the best known solution is 0.2109×10^{-3} and 0.1732×10^{-9} for displacement and potential, respectively. Figure 3.14 shows the convergence results in terms of the relative error where it is observed that all the elements converge at a steady rate with respect to the log scale. This conforms with what is expected and with Long's results [2].

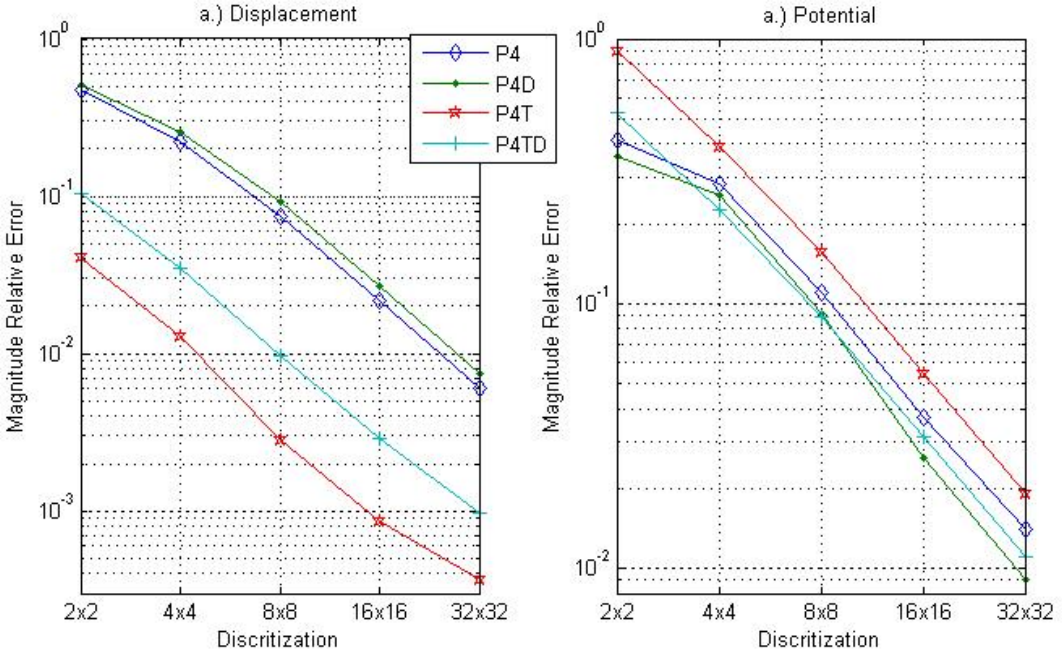

Figure 3.14: Cooks membrane of relative error results on a log scale[7]

3.5.2 Plate Results

3.5.2.1 General Plate Results

In the case of plates there are 5 patch tests to be conducted. They are the elongation, in-plane-shear, shear, bending and twisting. They are conducted using the same co-ordinates as in Figure 3.8 however, the constrained degrees of freedom at every node change for each case. Figure 3.15 shows the tests and each one has been confirmed for both the FSDT and the assumed shear element.

In addition to these patch tests there are 2 moment bending tests in the papers by Bathe and Dvorkin and a shear bending test in Groenwold's thesis [5; 8; 6]. All 3 of these tests (as seen in Figure 3.16) have been completed with satisfactory results that coincide with the literature. This confirms the validity of the constructed element.

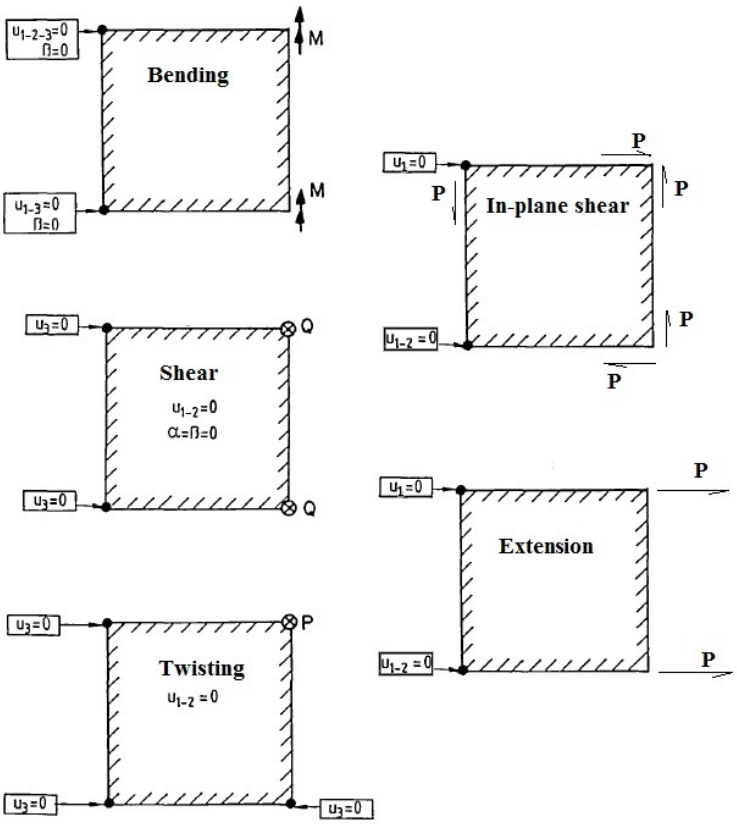

Figure 3.15: Plate shear tests [8]

3.5.2.2 Static Piezoelectric Bi-morph Results

Initially the patch test is conducted following the same procedure as in Section 3.5.1.1. The outcome of the test has been verified as correct. The Patch Test for piezoelectrics only tests the element in the membrane sense, other tests need to be conducted to verify the bending due to enforced conditions. Thus, no piezoelectrically extended Patch Test as in Figure 3.15 was verified.

One static test to check the piezoelectric relation was conducted, based on the work done by Hwang and Park in 1993 [9]. The test enforces bending in a bi-morph based on two sets of enforced conditions. The first set is a constantly applied unit voltage through the thickness, thereby inducing an expected tip displacement of 330 *nm* [13]. This tip displacement is obtained in the first part of the program as only the displacement solution needs to be obtained. This

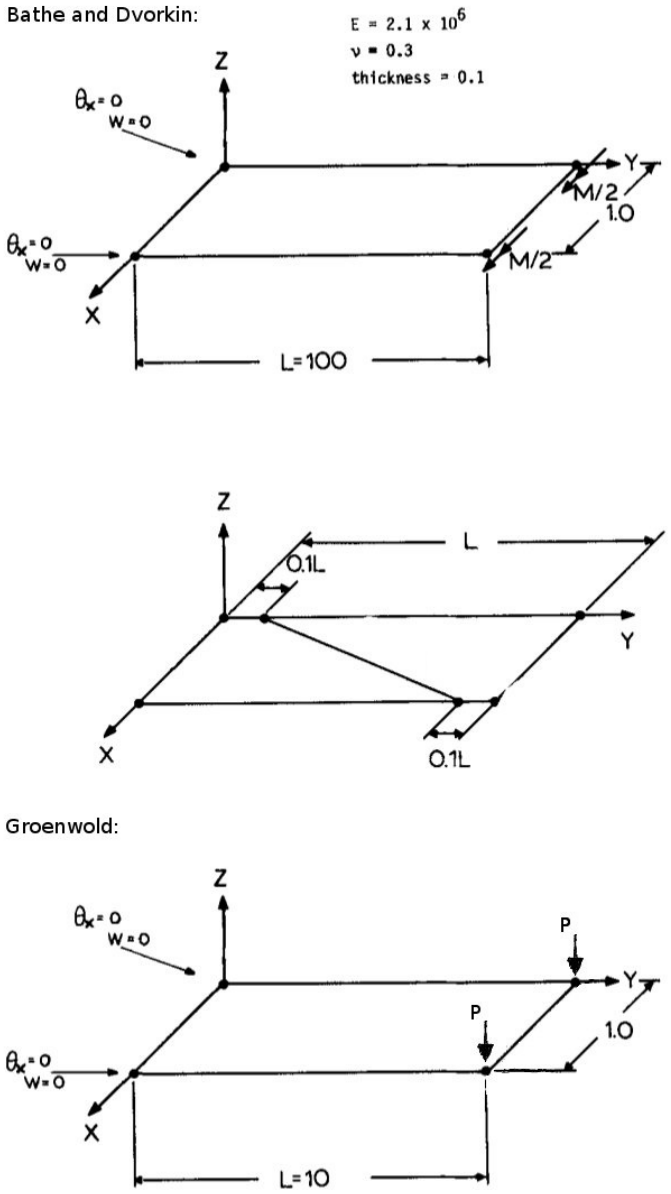

Figure 3.16: The plate models for the tests [5]

solution is confirmed through the use of the analytical formula

$$\frac{\partial^2 z}{\partial x^2} = -\frac{M}{YI}, \tag{3.192}$$

$$z(x) = -\frac{Mx^2}{2YI}, \tag{3.193}$$

$$= -\frac{3d_{13}\phi x^2}{2h^2}.$$

The second set is an enforced tip displacement of 10 mm, thereby inducing an open-circuit Voltage. To obtain this voltage the post processing of the model needs to be conducted in

order to obtain the dielectric displacements at the mid-planes of each layer [9]. These dielectric displacements are at the Gaussian points and are summed for each layer (This being relative to integration over area). Due to the electric polling of the material the sum, rather than the difference across the layers, is used to obtain the open total charge (these can be left separate in the case of different layer materials or thickness's). This charge is then used in the formula

$$V_{el}^{k} = q^{k}/C^{k} \tag{3.194}$$

with

$$C^{k} = \frac{\gamma_{\epsilon_0}\Gamma}{t^{k}} \tag{3.195}$$

and V_{el}^{k} the elemental layer-wise voltage, q^{k} the layer-wise charge and γ_{ϵ_0} the absolute permittivity [9].

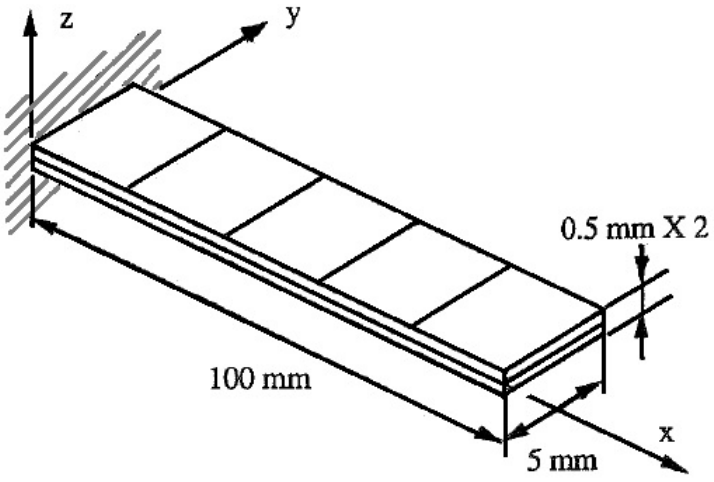

Figure 3.17: A piezoelectric bi-morph plate model [9]

The model used is shown in Figure 3.17 with the wall boundary condition being constrained for all mechanical degrees of freedom. In the case of the applied voltage all the electrical boundary condition are constrained and are set to 0 at the bottom layer and 1 at the top. In the case of the enforced tip displacement the electrical boundary conditions are unconstrained and the tip is constrained in the z to -10 mm. The output displacement obtained for the enforced voltage matches perfectly with the expected analytical output and can be seen in Figure 3.18.

The voltage output after subjecting the model to the enforced tip displacement, also closely matched that obtained in Pieforts Thesis [13].

As a point of interest the elements were distorted from 0 to 8 mm in a parallel and trapezoidal manner and the relative voltage errors were mapped. This shows the shear locking that is experienced under element distortion. These errors are displayed in Table's 3.4 and 3.5, where the differing voltage lines are generally close to linear in descent. It is relevant to note that this

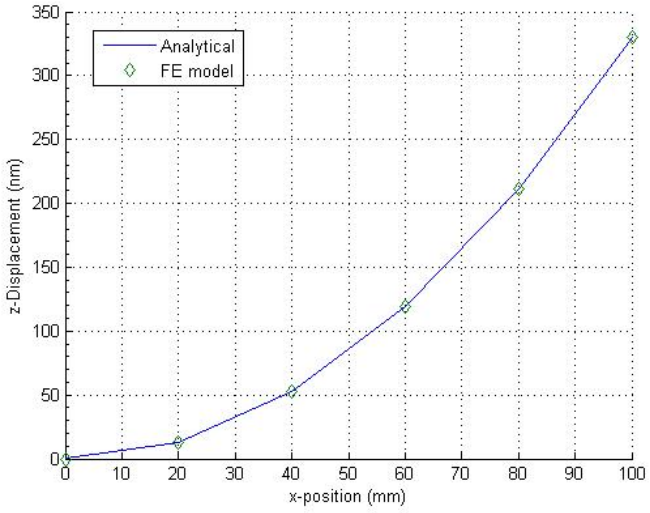

Figure 3.18: A piezoelectric bi-morph z-displacement results

is not necessary for the enforced voltage as the tip-displacement will remain unchanged due to the similar through thickness elements.

In Table 3.4 the first distortion, 0 mm*, refers to the case where the boundary constraints do not include the rotation in the y-plane. As already stated, these results are extremely close to the results produced by Hwang and Park in 1993 and separately by Piefort in 2001 [13; 9]. When the rotation constraint is included the values change to those referred to by the 0 mm distortion. There are two probable reasons for this difference, firstly in the Hwang and Park results there was no coupling with the x and y displacements as they used standard plate theory. Secondly, in Piefort's thesis, the exact criterion on the numerical experiment is somewhat lacking so the particulars are assumed to be the same as in the Hwang and Park paper. This, however, creates a contradiction as the Piefort element clearly has cross coupling, thus when the boundary conditions are altered, as stated above, the output closely matches the results Piefort presented.

The distortions in Table 3.4 and 3.5 go up to 8 mm which is a highly unrealistic distortion. Though unrealistic, it is useful to emphasise the errors that each element is subjected to. The elements, with element 1 starting at the wall, initially have high voltage as the charge is relative to the mechanical strains and then trail off to a lower voltage at the tip. The percentage error however increases as a relative error is larger at the end of the beam. In all cases the errors are calculated using Equation (3.184) with reference to the actual value as the 0 mm distortion.

Table 3.4: The parallel element bi-morph

Distortion	Element 1		Element 2		Element 3		Element 4		Element 5	
	Voltage	*%error*	Voltage	*%error*	Voltage	*%error*	Voltage	*%error*	Voltage	*%error*
0 *mm**	296.87	N/A	230.90	N/A	164.93	N/A	98.955	N/A	32.985	N/A
0 *mm*	305.52	N/A	237.63	N/A	169.73	N/A	101.84	N/A	33.947	N/A
1 *mm*	305.89	0.121	236.24	−0.584	170.25	0.306	101.99	0.147	34.093	0.430
3 *mm*	306.68	0.379	232.4	−2.20	171.45	1.01	101.79	−0.049	37.486	10.4
5 *mm*	305.29	−0.0752	231.65	−2.51	171.78	1.20	103.38	1.51	44.449	30.9
8 *mm*	299.82	−1.86	231.18	−2.71	174.23	2.65	112.23	10.2	61.19	80.2

Table 3.5: The trapezoidal element bi-morph

Distortion	Element 1		Element 2		Element 3		Element 4		Element 5	
	Voltage	*%error*	Voltage	*%error*	Voltage	*%error*	Voltage	*%error*	Voltage	*%error*
0 *mm*	305.52	N/A	237.63	N/A	169.73	N/A	101.84	N/A	33.947	N/A
1 *mm*	305.91	0.127	237.18	−0.189	168.8	−0.547	101.85	0.0098	33.405	−1.59
3 *mm*	310.3	1.56	233.55	−1.71	167.2	−1.49	100.25	−1.56	35.436	4.38
5 *mm*	317.86	4.039	228.01	−4.04	166.6	−1.84	98.819	−2.96	42.227	24.3
8 *mm*	329.23	7.76	221.79	−6.66	166.23	−2.06	98.403	−3.37	55.052	62.17

3.5.2.3 Static Piezoelectric Plate Results

Typically, a plate is not presented as in the case of the above bimorph. A test problem for a plate is usually presented as n by n simply supported elements. The bimorph is not without merit though, as it shows that the element works under cantilever bending situations and that the inter-ply relations are correct. A further test is a static simply supported case by Carrera *et al.* (2011). In this situation a bi-sinusoidal force/voltage is applied to the surface of the simply supported plate as seen in Figure 3.19.

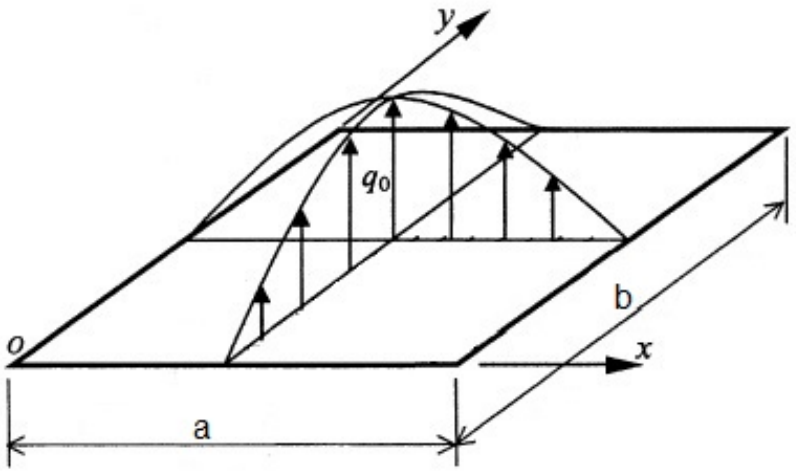

Figure 3.19: The Carrera piezoelectric plate set-up[10]

The plate consists of 4 layers, 2 being piezoelectric which sandwich a 0/90 Graphite/Epoxy layup. The dimensions are specified as $a \times b \times h$ with $a = b = 0.04$ m and $h = 0.01$ m or 0.0008 m giving a/h a ratio of 4 or 50. The situation is best presented in Table 3.6 with the material properties available in Table A.2. The boundary conditions for the plate are important. Here, simply supported means that the plate is supported around all the edges in the z-displacement, at the first corner the x-displacement and y-displacement are constrained and at one other adjacent corner the normal displacement is constrained. On top of this, for the sensor case, both sets of piezoelectric layers are set to 0 V and in the case of the actuator the bottom layer is grounded. The last bit of information needed is the force and voltage applications which are seen in the equations below:

$$f(x,y) = f \sin(\frac{\pi x}{a}) \sin(\frac{\pi y}{b}) \text{ and } \phi(x,y) = \phi \sin(\frac{\pi x}{a}) \sin(\frac{\pi y}{b}), \tag{3.196}$$

with f and ϕ as unit values of force and voltage respectively and x and y spatial coordinates.

Two types of results were obtained using this example. Firstly, a convergence study (Figure 3.20) to confirm the element viability to the problem stated by Carrera *et al.* while using a different element and secondly, a comparison of a/h to confirm the viability of the plate itself. In both 'a' and 'b' the figures should be comparable such that there is no thickness interaction. The figures represents the displacements and surface forces for the two separate situations that are identical baring their overall thicknesses.

Table 3.6: The piezoelectric plate set-up

Layer	Type	Orientation	Thickness
1	PZT-4	0	$0.1h$
2	Graphite/Epoxy	0	$0.4h$
3	Graphite/Epoxy	90	$0.4h$
4	PZT-4	0	$0.1h$

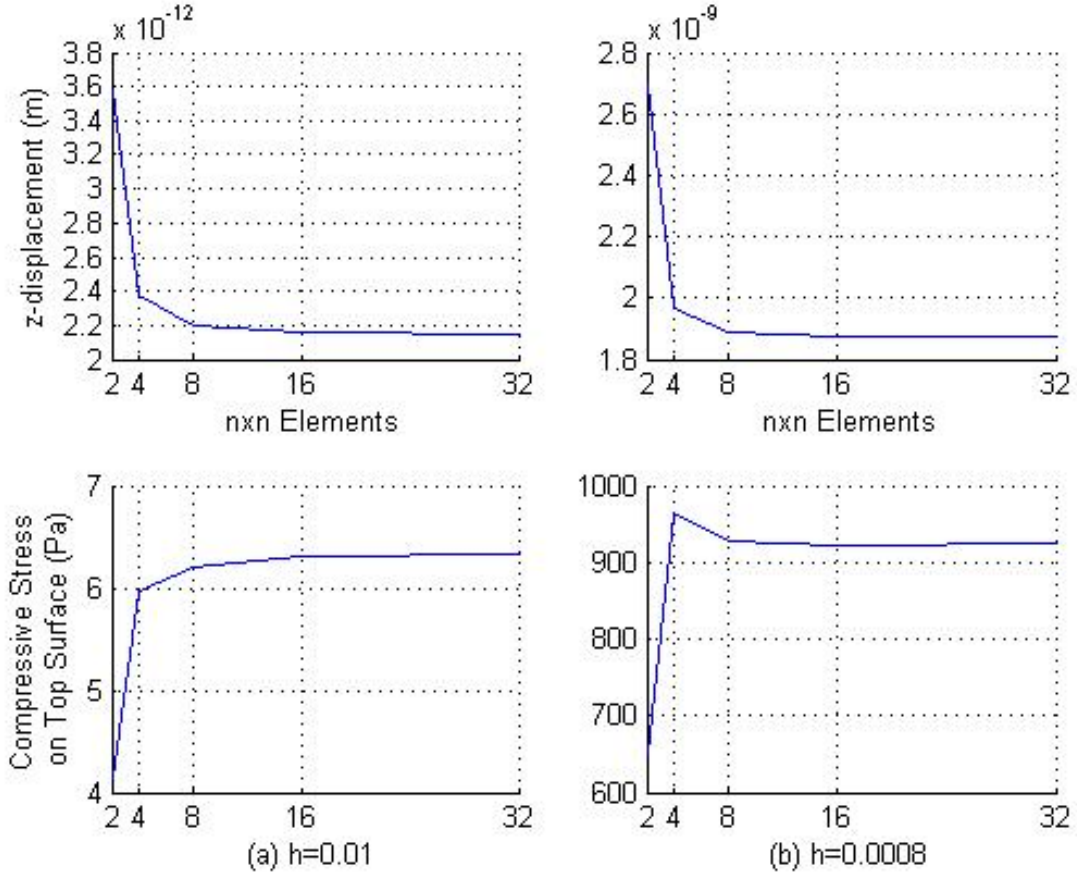

Figure 3.20: Convergence study for the Carrera piezoelectric plate

By comparison, an $a/h = 50$ yields results that are very closely attuned to the FSDT element in the literature at the limit of convergence.

Chapter 4

Optimisation

Optimisation is a process humans have engaged in consistently throughout their existence. A form of optimisation was the birth of the wheel in order to improve movement of heavy objects rather than carrying them. In more recent times and in everyday activities, humans optimise everything from their budget, to their schedules, or to just getting ready to go out of the house. Optimisation is in everything man does and in most cases is exceptionally difficult to describe mathematically. This mathematical description, which can be called engineering optimisation, is the focus of this chapter.

The founding mathematical description for an optimisation problem is

$$\text{Find } \mathbf{x} = \begin{bmatrix} x_1 \\ x_2 \\ \vdots \\ x_n \end{bmatrix} \text{ which minimise } f(\mathbf{x})$$

subject to

$$\begin{aligned} g_i(\mathbf{x}) &\leq 0, \quad i = 1, 2, \ldots, m \\ h_j(\mathbf{x}) &= 0, \quad j = 1, 2, \ldots, p \end{aligned} \tag{4.1}$$

where $\mathbf{x}$ is a vector of unknown variables $(x_1, \ldots, x_n)$, $f(\mathbf{x})$ is the objective function, $g(\mathbf{x})$ is a set of inequality constraints and $h(\mathbf{x})$ is a set of equality constraints [36].

This mathematical description of optimisation is extremely general and can be altered and adapted to the situation at hand. Three broad distinctions can be made, firstly the classification of the type of optimisation problem, be it linear or non-linear, single or multi-modal etc. This pertains to the general type of optimisation that will be used. Secondly, whether the optimisation is an unconstrained or constrained problem and lastly the option of a bounded range for each of the x_i variables. Within these distinctions there are a variety of optimisation schemes that can be used based on the objective function that is to be solved.

S.S. Rao wrote a book on the various optimisation methods used in engineering [36]. Although not all existing methods are described in the book, it does give a reasonable description of the traditional methods and their uses. For the purpose of optimisation of a finite element problem,

methods that cater for the objective function (typically being multi-modal) are used. Most modern methods allow for this type of problem. For FEA the traditionally used modern methods are the genetic algorithm and the particle swarm optimisation, although others have also been used successfully.

In this chapter the particle swarm optimisation will be used together with the finite element analysis of the preceding chapter. A number of heuristics will be explained and test cases will be used to prove the validity of the optimiser and any heuristics that were implemented.

4.1 The Particle Swarm Optimizer (PSO)

The PSO was originally developed by Eberhart and Kennedy in 1995. The formulation was based on the movements of swarm based organisms such as fish and birds. By maintaining a known best position, the rest of the swarm moves around until a new best position is found. For fish and birds this mainly applies to the search food. In the mathematical sense it means that no gradient information is required due to the search type methodology.

The PSO falls under the category of 'modern methods' and is constantly being developed. The developments mostly lie in the areas of boundary, velocity and variation heuristics. The algorithm is as follows:

$$\begin{aligned} \mathbf{v}_i^{k+1} &= \mathbf{v}_i^k + c_1 \times r_1 \times (\mathbf{x}_{BL} - \mathbf{x}_i^k) + c_2 \times r_2 \times (\mathbf{x}_{BG} - \mathbf{x}_i^k), \\ \mathbf{x}_i^{k+1} &= \mathbf{x}_i^k + \mathbf{v}_i^{k+1}, \end{aligned} \tag{4.2}$$

where $\mathbf{v}$ is called the velocity and is used to update a vector of unknowns $\mathbf{x}$. c_1 and c_2 are constant multipliers usually of the value 2 and more specifically referred to as the cognitive and social learning rates. r_1 and r_2 are vectors of random numbers of equivalent size to the unknowns. $\mathbf{x}_{BL}$ and $\mathbf{x}_{BG}$ are vectors of the stored local and global best known positions, respectively. The indices k and i are the iteration and particle number respectively.

4.1.1 PSO Types

There are two major types of PSO's. The first is the linear type, which is distinguished by the fact that its r_1 and r_2 variables are not vectors but scalars. The linear type is referred to as the linear velocity update rule and is not used without consideration of many heuristics as it generally collapses to a line search without them.

The second case is the classical velocity update rule which is a more robust version of the linear with its r_1 and r_2 variables being vectors. By using vectors the algorithm maintains its randomness and does not generally collapse. There are still many heuristics that improve upon the classical type, however they are not normally as essential as in the linear case.

As this field of optimisation is a fairly recent one and is constantly expanding, new optimisation methods and heuristics are introduced regularly though not all are an improvement upon the originals. One improvement that shows promise is the momentum based PSO developed by Liu and Lin in 2006 [37]. The algorithm differed in comparison to Equation (4.2) in order to take

advantage of the previous and current positions thereby creating a momentum. The momentum based algorithm is as follows:

$$\begin{aligned} \triangle \mathbf{v}_i^{k-1} &= \mathbf{v}_i^k - \mathbf{v}_i^{k-1}, \\ \mathbf{v}_i^{k+1} &= \beta \times \triangle \mathbf{v}_i^{k-1} + c_1 \times r_1 \times (\mathbf{x}_{BL} - \mathbf{x}_i^k) + c_2 \times r_2 \times (\mathbf{x}_{BG} - \mathbf{x}_i^k), \\ \mathbf{x}_i^{k+1} &= \mathbf{x}_i^k + \alpha \times \mathbf{v}_i^{k+1}, \end{aligned} \tag{4.3}$$

where α is the velocity multipliers and is set to 1 for true velocity, β is the momentum constant and is set to 0.1 and the rest of the variables are the same as in Equation (4.2) [37]. Although only a couple of papers have been published on this work it shows promise in certain areas.

4.1.2 Constraint Handling

For PSO's constraints are set up by use of the penalty method, though there are other methods. The idea behind the penalty method is to penalise the objective function if the constraints are not satisfied. So, for example, in the case of minimisation of an objective function, if a constraint is not satisfied a very large value will be added on to the calculated function value at the present $\mathbf{x}$ co-ordinates. The basic penalty method looks like

$$\text{Find } \mathbf{x} \text{ which minimises } F(\mathbf{x})$$

subject to

$$g_i(\mathbf{x}) \leq 0, \quad i = 1, 2, \ldots, m$$

where

$$F(\mathbf{x}) = f(\mathbf{x}) + p_k \sum_{i=1}^{m} G_i[g_i(\mathbf{x})] \tag{4.4}$$

and p_k is a penalty constant. The $G_i[g_i(\mathbf{x})]$ term is problem dependent. For a problem using the interior method where the solution is approached from inside the feasible solution area, the G_i could look like

$$G_i = -\frac{1}{g_i(\mathbf{x})} \tag{4.5}$$

or

$$G_i = \log\left(-g_i(\mathbf{x})\right), \tag{4.6}$$

whereas for exterior method where the problem is approached from outside of the feasible solution area, it could look like

$$G_i = \max 0, g_i(\mathbf{x}) \tag{4.7}$$

or

$$G_i = \{\max 0, g_i(\mathbf{x})\}^2. \tag{4.8}$$

However, these are problem specific.

A new penalty type approach was developed specifically for the PSO by Liu and Lin in 2006 [37]. It is based on the non-stationary approach where the penalty changes based on the iteration unlike the above cases. The consequence of this change is a subtly improved outputted result and thus the literature recommends this type of constraint handling for the PSO [37]. The non-stationary penalty method is implemented by

$$F(\mathbf{x}) = f(\mathbf{x}) + C(k)H(\mathbf{x}), \tag{4.9}$$

where

$$\begin{aligned} C(k) &= (c \times k)^{\lambda} \\ H(\mathbf{x}) &= \sum_{i=1}^{m} [\theta(g_i(\mathbf{x})) \times g_i(\mathbf{x})^{\varrho(g_i(\mathbf{x}))}] \\ \theta(g_i(\mathbf{x})) &= a \times \left(1 - \frac{1}{e^{g_i(\mathbf{x})}}\right) + b, \end{aligned} \tag{4.10}$$

where $C(k)$ represents a dynamically modified penalty function wherein $\lambda = 2$ and $c = 0.5$, and $H(\mathbf{x})$ denotes the penalty factor. The penalty factor is subject to the $g_i(\mathbf{x})$ term being the same as in Equation (4.7), and the $\varrho(g_i(\mathbf{x}))$ term yielding 1 if $g_i(\mathbf{x}) \leq 1$, or 2 otherwise. Lastly, the $\theta(g_i(\mathbf{x}))$ term is subject to the constants $a = 150$ and $b = 10$ which can change if needed.

4.1.3 Boundary Handling Mechanisms

In the situation that constraints are present it is usually the case that all of the co-ordinates should lie within some greater bounds. In such a situation using a randomly generated update rule, as in the case of the of the PSO, the updated variables should still lie within the predefined bounds. This is not always the case and an added measure needs to be implemented to enforce this compliance. Padhye and Deb prescribed the typical boundary handling mechanisms for optimisation into the formats: *random, periodic, set on boundary, shrink and exponential distribution* [40]. Of these five methods the more useful are the periodic, set on boundary and exponential distribution where each functions better under different constraint types. Apart from these five prescribed formats Padhye and Deb proposed two original mechanisms for the PSO which include the *adaptive spread distribution and the adaptive confined distribution* [40]. Padhye and Deb concluded that of the seven total mechanisms the most robust were the *exponential distribution and the adaptive spread distribution* mechanisms [40].

In this work, the experimental distribution method will be used, due to ease of application.

$$\mathbf{x}_{new} = \mathbf{x}_{not} \pm d,$$

where

$$d = \log\left[1 + r(e^{U-\mathbf{x}_{not}} - 1)\right] \text{ for the plus and}$$
$$d = \log\left[1 + r(e^{\mathbf{x}_{not}-L} - 1)\right] \text{ for the minus} \tag{4.11}$$

for the cases where the upper and lower bound are violated, respectively. In these equations X_{not} is the previous, not viable, co-ordinates set, U is the upper bound, L is the lower bound and r is a uniformly distributed random number between 0 and 1.

4.1.4 Heuristics

Excluding the momentum based velocity update rule, the velocity update rules can be influenced by heuristics to improve the output or speed up the convergence to solution. There are many heuristics that have been developed for the algorithms and only a few will be covered. Some work well together and should almost always be used, others are problem dependent and clash if used together. Therefore it is important to understand the implications and effects that a heuristic will have on the program and the already in place heuristics.

Some useful heuristics include the *inertial decay, elitism, greedy criteria and elite velocities*. Inertia, w, is a coefficient of the prior velocity i.e.

$$\mathbf{v}_i^{k+1} = w\mathbf{v}_i^k + c_1 \times r_1 \times (\mathbf{x}_{BL} - \mathbf{x}_i^k) + c_2 \times r_2 \times (\mathbf{x}_{BG} - \mathbf{x}_i^k) \tag{4.12}$$

in the velocity update rule. It is used to weight the velocity of the previous iteration in such a way that it doesn't overpower the position terms. The heuristic inertial decay is an update rule for the inertia, w, and can be stated as

$$w = w_{max} - \frac{w_{max} - w_{min}}{k_{max}} \times k, \tag{4.13}$$

where all the w variables are inertias with the min at 0.4 and the max at 0.9. The k_{max} variable is the total iterations which means that the inertia will be reduced as the algorithm converges on a solution. The elitism and elite velocities are similar as they deal with the retention of the best solution over the next iteration, in the case of elitism the best particle position is kept and in the elite velocities the best particle velocity is retained. Lastly greedy criteria is a heuristic that is sometimes used and when it is, it is applied after the algorithm has been proven. It is used in speeding up the algorithm but reducing the accuracy and hence will not be used in this thesis.

4.2 The PSO Algorithm

The PSO algorithm in itself is a simple one (see Algorithm 4). This is due to the fact that most of the complexities lie in the formulation of the objective function. The function is usually a

lengthy program or formula. It becomes even more lengthy when penalty functions are added.

Algorithm 4: The basic particle swarm algorithm

```
1  begin
2      Input to algorithm: Total Runs, Amount of Particles, Function to Evaluate ;
3      Declaration of Internal and bounded variables;
4      for 1⟶total individual runs do
5          Initialization of position and velocity variables;
6          for 1⟶total iterations (k) do
7              Velocity and position updates;
8              for 1⟶total particles (n) do
9                  Check for global and local bests and store if valid;
10             end
11         end
12         Sum up the function value for the current run to total;
13     end
14     Average summed total over runs;
15     return time taken, average, function, and constraint violation data;
16 end
```

When considering this algorithm one point of note, especially for the FEM algorithm in the next chapter, is that when comparing the objective functions the minimum possible calls is the particle total. This reduces time spent on recalling large objective functions.

4.3 Test Cases and Results

From the work of Lin and Liu eleven test cases were documented and are as follows [37]:

Problem 1: In this test case the best known function value is $f(\mathbf{x}) = 3.00$ at the position $\mathbf{x} = [0; -1]$

$$\begin{aligned} \text{Minimize } f(\mathbf{x}) =& [1 + (x_1 + x_2 + 1)^2 \times (19 - 14x_1 + 3x_1^2 - 14x_2 + 6x_1x_2 + 3x_2^2)] \\ & \times [30 + (2x_1 - 3x_2)^2(18 - 32x_1 + 12x_1^2 + 48x_2 - 36x_1x_2 + 27x_2^2)] \\ \text{subject to} \quad & -2 \leq x_i \leq 2 \, for \, i = 1, 2. \end{aligned} \tag{4.14}$$

Problem 2: In this test case the best known function value is $f(\mathbf{x}) = -186.73$ at any one of 18 positions as this is a true multi-modal problem

$$\begin{aligned} \text{Minimize } f(\mathbf{x}) &= \sum_{i=1}^{5} i \cos[(i+1)x_1 + i] \times \sum_{i=1}^{5} i \cos[(i+1)x_2 + i] \\ \text{subject to} \quad & -10 \leq x_j \leq 10 \, for \, j = 1, 2. \end{aligned} \tag{4.15}$$

Problem 3: In this test case the best known function value is $f(\mathbf{x}) = -1.216N_{dim}$ which when using 50 dimensions is said to be 60.8

$$\begin{aligned} &\text{Minimize } f(\mathbf{x}) = \sum_{i=1}^{N_{dim}} \left[\sin(x_i) + \sin\frac{2x_i}{3} \right] \\ &\text{subject to} \qquad 3 \leq x_i \leq 13 \; for \; i = 1, \ldots, N_{dim}. \end{aligned} \tag{4.16}$$

Problem 4: In this test case the best known function value is $f(\mathbf{x}) = 680.6300573$

$$\begin{aligned} \text{Minimize} \quad f(\mathbf{x}) &= (x_1 - 10)^2 + 5(x_2 - 12)^2 + x_3^4 + 3(x_4 - 11)^2 + 10x_5^6 + 7x_6^2 \\ &\quad + x_7^4 - 4x_6x_7 - 10x_6 - 8x_7 \\ \text{subject to } g_1(\mathbf{x}) &\Rightarrow -127 + 2x_1^2 + 3x_2^4 + x_3 + 4x_4^2 + 5x_5 \leq 0, \\ g_2(\mathbf{x}) &\Rightarrow -282 + 7x_1 + 3x_2 + 10x_3^2 + x_4 - x_5 \leq 0, \\ g_3(\mathbf{x}) &\Rightarrow -196 + 23x_1 + x_2^2 + 6x_6^2 - 8x_7 \leq 0, \\ g_4(\mathbf{x}) &\Rightarrow 4x_1^2 + x_2^2 - 3x_1x_2 + 2x_3^2 + 5x_6 - 11x_7 \leq 0, \\ &\quad -2 \leq x_i \leq 2 \; for \; i = 1, 2. \end{aligned} \tag{4.17}$$

Problem 5: In this test case the best known function value is $f(\mathbf{x}) = -6961.81388$

$$\begin{aligned} \text{Minimize} \quad f(\mathbf{x}) &= (x_1 - 10)^3 + (x_2 - 20)^3 \\ \text{subject to } g_1(\mathbf{x}) &\Rightarrow -(x_1 - 5)^2 - (x_2 - 5)^2 + 100 \leq 0, \\ g_2(\mathbf{x}) &\Rightarrow (x_1 - 6)^2 - +(x_2 - 5)^2 - 82.81 \leq 0, \\ &\quad 13 \leq x_1 \leq 100 \; and \; 0 \leq x_2 \leq 100. \end{aligned} \tag{4.18}$$

Problem 6: In this test case the best known function value is $f(\mathbf{x}) = -31025.56142$

$$\begin{aligned} \text{Minimize} \quad f(\mathbf{x}) &= 5.3578547x_3^2 + 0.8356891x_1x_5 + 37.2932239x_1 - 40792.141 \\ \text{subject to } g_1(\mathbf{x}) &\Rightarrow 0 \leq 85.334407 + 0.0056858x_2x_5 + 0.00026x_1x_4 \\ &\quad - 0.0022053x_3x_5 \leq 92, \\ g_2(\mathbf{x}) &\Rightarrow 90 \leq 80.51249 + 0.0071317x_2x_5 + 0.0029955x_1x_2 \\ &\quad + 0.0021813x_3^2 \leq 110, \\ g_3(\mathbf{x}) &\Rightarrow 20 \leq 9.300961 + 0.0047026x_3x_5 + 0.0012547x_1x_3 \\ &\quad + 0.0019085x_3x_4 \leq 25, \\ &\quad 78 \leq x_1 \leq 102, \;\; 33 \leq x_2 \leq 45, \;\; 27 \leq x_i \leq 45 \; for \; i = 3, \ldots, 5. \end{aligned} \tag{4.19}$$

Problem 7: In this test case the best known function value is $f(\mathbf{x}) = -11$

$$\begin{aligned}
\text{Minimize} \quad & f(\mathbf{x}) = 6.5x - 0.5x^2 - y_1 - 2y_2 - 3y_3 - 2y_4 - y_5 \\
\text{subject to } & g_1(\mathbf{x}) \Rightarrow x + 2y_1 + 8y_2 + y_3 + 3y_4 + 5y_5 \leq 16, \\
& g_2(\mathbf{x}) \Rightarrow -8x - 4y_1 - 2y_2 + 2y_3 + 4y_4 - y_5 \leq -1, \\
& g_3(\mathbf{x}) \Rightarrow 2x + 0.5y_1 + 0.2y_2 - 3y_3 - y_4 - 4y_5 \leq 24, \\
& g_4(\mathbf{x}) \Rightarrow 0.2x + 2y_1 + 0.1y_2 - 4y_3 + 2y_4 + 2y_5 \leq 12, \\
& g_5(\mathbf{x}) \Rightarrow -0.1x - 0.5y_1 + 2y_2 + 5y_3 - 5y_4 + 3y_5 \leq 3, \\
& x \geq 0, \quad y_3 \leq 1, \quad y_4 \leq 1, \quad y_5 \leq 2, \quad y_i \geq 0 \; for \; i = 1, \ldots, 5.
\end{aligned} \tag{4.20}$$

Problem 8: In this test case the best known function value is $f(\mathbf{x}) = -213$

$$\begin{aligned}
\text{Minimize} \quad & f(\mathbf{x}) = -10.5x_1 - 7.5x_2 - 3.5x_3 - 2.5x_4 - 1.5x_5 - 10y \\
& \qquad - 0.5 \sum_{i=1}^{5} x_{i^2} \\
\text{subject to } & g_1(\mathbf{x}) \Rightarrow 6x_1 + 3x_2 + 3x_3 + 2x_4 + x_5 - 6.5 \leq 0, \\
& g_2(\mathbf{x}) \Rightarrow 10x_1 + 10x_3 + y - 20 \leq 0, \\
& -2 \leq x_i \leq 2 \; for \; i = 1, \ldots, 5.
\end{aligned} \tag{4.21}$$

Problem 9: In this test case the best known function value is $f(\mathbf{x}) = -47.707579$

$$\begin{aligned}
\text{Minimize} \quad & f(\mathbf{x}) = \sum_{j=1}^{10} x_j \left(c_j + \ln \frac{x_j}{\sum_{i=1}^{10} x_i} \right) \\
\text{where} \quad & c_1 = -6.089, \quad c_2 = -17.164, \quad c_3 = -34.054, \\
& c_4 = -5.914, \quad c_5 = -24.721, \quad c_6 = -14.986, \\
& c_7 = -24.100, \quad c_8 = -10.708, \quad c_9 = -26.662, \\
& c_{10} = -22.179, \\
\text{subject to } & h_1(\mathbf{x}) \Rightarrow x_1 + 2x_2 + 2x_3 + x_6 + x_{10} = 2, \\
& h_2(\mathbf{x}) \Rightarrow x_4 + 2x_5 + x_6 + x_7 = 1, \\
& h_3(\mathbf{x}) \Rightarrow x_3 + x_7 + x_8 + 2x_9 + x_{10} = 1, \\
& x_i \geq 0.000001 \; for \; i = 1, \ldots, 10.
\end{aligned} \tag{4.22}$$

Problem 10: In this test case the best known function value is $f(\mathbf{x}) = -0.803619$

$$\begin{aligned}
\text{Minimize} \quad & f(\mathbf{x}) = \left| \frac{\sum_{i=1}^{N_{dim}} \cos^4(x_i) - 2 \sum_{i=1}^{N_{dim}} \cos^2(x_i)}{\sqrt{\sum_{i=1}^{N_{dim}} i x_i^2}} \right| \\
\text{subject to } & g_1(\mathbf{x}) \Rightarrow 0.75 - \prod_{i=1}^{N_{dim}} x_i < 0, \\
& g_2(\mathbf{x}) \Rightarrow \sum_{i=1}^{N_{dim}} x_i - 7.5N_{dim} < 0, \\
& 0 \leq x_i \leq 10 \; for \; i = 1, \ldots, N_{dim}.
\end{aligned} \tag{4.23}$$

Problem 11: In this test case the best known function value is $f(\mathbf{x}) = 6059.715$

$$\begin{aligned}
\text{Minimize} \quad & f(\mathbf{x}) = 0.6224x_1x_3x_4 + 1.7781x_2x_3^2 + 3.1661x_1^2x_4 + 19.84x_1^2x_3 \\
\text{subject to} \quad & g_1(\mathbf{x}) \Rightarrow -x_1 + 0.0193x_3 \leq 0, \\
& g_2(\mathbf{x}) \Rightarrow -x_2 + 0.00954x_3 \leq 0, \\
& g_3(\mathbf{x}) \Rightarrow -\pi x_3^2 x_4 - \frac{4}{3}\pi x_3^3 + 1296000 \leq 0, \\
& g_4(\mathbf{x}) \Rightarrow x_4 - 240 \leq 0, \\
& 1 \leq x_{1,2} \leq 99 \textit{ and } 10 \leq x_{3,4} \leq 200.
\end{aligned} \tag{4.24}$$

The results obtained from the above test cases and its extensions can be seen in Table 4.1. In the Table the headings are explained as; 'Prob' is for Test Case, 'Iter' is for the number of iterations in each run, 'Part' is for number of particles used in the test case, 'Average' is for the function value averaged over the 100 runs, 'Best' is for the overall best function value in all the runs and 'Time' is for the time per run in seconds.

When analysing the results, it is seen that the 'Best' and 'Average' for most of the test cases directly match the literature. However, there were differences in the results for problem 5, 6 and 11 which can be attributed to errors/differences made in the coded process of the bounds or constraints (for a better description of these problem see the literature) [37]. The solutions in these cases are still sufficiently close to the true result. Otherwise the code functioned correctly with the momentum based PSO slightly outdoing the standard PSO.

Table 4.1: The results of problem 1 - 11 over 100 runs

			Momentum Based			Standard PSO		
Prob	Iter	Part	Average	Best	Time[s]	Average	Best	Time[s]
1	150	100	3.0	3.0	4.62	3.0	3.0	4.57
2	1000	20	−186.73	−186.73	8.57	−1816.73	−186.73	8.51
3	5000	100	−60.789	−60.799	379.97	−60.49	−59.80	379.42
4	2000	20	680.73	680.73	24.76	680.70	680.67	24.78
5	1000	20	−6961.727	−6961.5591	6.81	−6961.808	−6961.809	6.83
6	1000	20	−31025.560	−31025.561	13.35	−31025.42	−31025.56	13.49
7	1000	20	−10.9810	−11	12.83	−10.87	−11	13.15
8	1000	20	−213	−213	9.45	−213	−213	10.12
9	1000	20	−44.699	−45.419	3.13	−44.77	−44.59	3.21
10	1000	100	−0.7323	−0.7858	16.79	−0.6981	−0.6093	16.26
11	1000	20	5797.646	5204.699	2.39	4324.85	110450.65	2.26

Chapter 5

Combining of Piezoelectric FEM and the PSO

In this chapter the combination of the piezoelectric FEM and the PSO optimisation will be described and the results shown. To achieve this outcome the generalised objective function is stated below.

Find $\mathbf{x}$ which minimises

$$F(\mathbf{x}) = -\mathbf{q}^T\mathbf{f} \tag{5.1}$$

subject to

$g(\mathbf{x})_i$: FEM Post-Processor Max Principle Stress Criterion,
$g(\mathbf{x})_j$: FEM Post-Processor Tsai-Wu/Hill Criterion,

where $\mathbf{x}$ is the vector of layer orientations from bottom to top, $\mathbf{f}$ is the vector of forces that influence the structure, $\mathbf{q}$ is the vector of displacements obtained through the FEA, and the constraints are based on relevant breaking criterion.

The focal point of this chapter is on the optimisation of the layer orientation of a piezo-composite layup. This is usually not done as it would be a fairly difficult and expensive process to achieve. It is however an interesting problem to see if the posed poled piezoelectric material alignment can influence the compliance of the structure. This has potential applications if mass production of smart materials were to occur.

5.1 The Criterion Constraints

For any material there are a set of yield or breaking criteria which an engineer keeps in mind through the design process. The constraints take those criteria and input them into the optimisation loop in order to improve the overall structure. Here certain criterion are used which have been designed to take into account the material differences.

Piezoelectrics are essentially isotropic piezo-ceramic materials which have been poled. This means that in breaking they can be treated as isotropic materials and the maximum principle stress criterion can be used. This criterion assesses whether or not the stress lies between the maximum compressive and tensile range. When considering a piezoelectric material one must consider that the material loses its polarization at 20 to 30% of the maximum tensile stress and thus there is an altered stress range that must be likewise considered and is material dependent.

In the case of the composite materials, termed orthotropic, the maximum stress criterion is a poor estimate of their actual breaking properties[3]. It is better to use the Tsai-Hill or Tsai-Wu criterion's. These criteria are rather arbitrary and were created as rules of thumb that work by analysing the experimental data based on underlying isotropic failure theories. In the case of Tsai-Hill the failure theory was the distortion energy failure theory of Von-Mises' distortional energy yield criterion, and in the Tsai-Wu case it was the total strain energy theory of Beltrami [3]. The Tsai-Hill criterion is defined in tensor form by

$$G_{ij}\sigma_i\sigma_j \leq 1 \tag{5.2}$$

and can be expanded to

$$\begin{aligned}&(G_2+G_3)\sigma_1^2+(G_1+G_3)\sigma_2^2+(G_1+G_2)\sigma_3^2-2G_3\sigma_1\sigma_2\\&-2G_2\sigma_1\sigma_3-2G_1\sigma_2\sigma_3+2G_4\tau_{23}^2+2G_5\tau_{13}^2+2G_6\tau_{12}^2\leq 1,\end{aligned} \tag{5.3}$$

where

$$\begin{aligned}G_1&=\frac{1}{2}\left(\frac{2}{[(\sigma_2^T)_{ult}]^2}-\frac{1}{[(\sigma_1^T)_{ult}]^2}\right),\\G_2&=\frac{1}{2}\left(\frac{1}{[(\sigma_1^T)_{ult}]^2}\right),\\G_3&=\frac{1}{2}\left(\frac{1}{[(\sigma_1^T)_{ult}]^2}\right),\\G_4&=\frac{1}{2}\left(\frac{1}{[(\tau_{23}^T)_{ult}]^2}\right),\\G_5&=\frac{1}{2}\left(\frac{1}{[(\tau_{13}^T)_{ult}]^2}\right),\end{aligned}$$

and

$$G_6=\frac{1}{2}\left(\frac{1}{[(\tau_{12}^T)_{ult}]^2}\right). \tag{5.4}$$

The Tsai-Wu criterion was developed after the Tsai-Hill and is even more general as it distinguishes between compression and tension. The Tsai-Wu criterion is defined in tensor form by

$$H_i\sigma_i+H_{ij}\sigma_i\sigma_j\leq 1 \tag{5.5}$$

and can be expanded to

$$\begin{aligned} &H_1\sigma_1 + H_2\sigma_2 + H_3\sigma_3 + H_4\tau_{23} + H_5\tau_{13} + H_6\tau_{12} + H_{11}\sigma_1^2 + \\ &H_{22}\sigma_2^2 + H_3\sigma_{33}^2 + H_{44}\tau_{23}^2 + H_{55}\tau_{13}^2 + H_{66}\tau_{12}^2 + \\ &H_{12}\sigma_1\sigma_2 + H_{13}\sigma_1\sigma_3 + H_{23}\sigma_2\sigma_3 \leq 1, \end{aligned} \tag{5.6}$$

where as $\sigma_3 = 0$ only the following are needed

$$\begin{aligned} H_1 &= \frac{1}{(\sigma_1^T)_{ult}} - \frac{1}{(\sigma_1^C)_{ult}}, \\ H_2 &= \frac{1}{(\sigma_2^T)_{ult}} - \frac{1}{(\sigma_2^C)_{ult}}, \\ H_4 &= 0, \\ H_5 &= 0, \\ H_6 &= 0, \\ H_{11} &= \frac{1}{(\sigma_1^T)_{ult}(\sigma_1^C)_{ult}}, \\ H_{22} &= \frac{1}{(\sigma_2^T)_{ult}(\sigma_2^C)_{ult}}, \\ H_{44} &= \frac{1}{(\tau_{23})_{ult}^2}, \\ H_{55} &= \frac{1}{(\tau_{13})_{ult}^2}, \\ H_{66} &= \frac{1}{(\tau_{12})_{ult}^2}, \end{aligned}$$

and

$$H_{12} = -\frac{1}{2}\sqrt{\frac{1}{(\sigma_1^T)_{ult}(\sigma_1^C)_{ult}(\sigma_2^T)_{ult}(\sigma_2^C)_{ult}}} \tag{5.7}$$

and here H_{12} is per the Mises-Hencky criterion [3].

These three criterion gave the constraints where necessary for the PSO optimiser in the cases that follow.

5.2 Program Alterations

Originally, the program was going to consist of MATLAB only, however due to speed considerations all of the code was translated into FORTRAN 95. The reason for this is that the PSO needs to run the FEA once per particle. The average run of this PSO is thus particle multiplied by iterations multiplied by runs being $20 \times 1000 \times 100 = 2000000$ FEA calls. When applying so many FEA calls, a small change in the speed of the FEA influences the overall time substantially. Other initiatives to improve computational speed are detailed below.

5.2.1 Basic Linear Algebra Subroutines (BLAS) and the Linear Algebra Package (LAPACK)

The BLAS and LAPACK were implemented to lower the time taken when inverting the **K** stiffness matrix [50]. To do this, a subroutine to calculate the LU decomposition of the stiffness matrix was used (DGETRF). After the calculation of this decomposition another subroutine (DGETRS) is used to solve the FEM $\mathbf{Kq} = \mathbf{f}$, here the DGE refers to double precision general solver and the last three letters refer to the type of solver used in the LAPACK library. This was implemented after a profile on the program showed that most of the time was spent on the inversion. This by no means completes the BLAS implementation in the code as the BLAS library is huge and time consuming to implement, however the speed improvement from the changes made were significant.

5.2.2 OpenMP Implementation

An improvement step that is being seen in large systems is that of parallel processing. There are four major types of parallel implementation. The first is a pseudo-type parallel step that uses multiple threads in a single core to do many things at once. The next step up is the use of all the cores on the processor at once. This is usually done through the use of OpenMP. The last processor type is that of OpenMPI which allows multiple processors to be used. Finally the fourth type is the implementation of CUDA which uses the parallel capabilities of one or more graphics cards. Of all of these the first two steps are the easiest to implement as the others generally require specific and expensive hardware and software. The one which this program uses is OpenMP.

Although using OpenMP does not necessarily mean a speed up in time (based on the parallel initialisation overheads required), it usually gives one. The reason for this uncertainty is that there are overheads involved in the memory allocation of the program. For very small 1 element FEM problems, usually the application of OpenMP slows the program down, however as the structure increases in size the time taken reduces significantly when OpenMP is in use.

5.2.3 Regression

A PSO is generally an easy to implement but slow optimiser that specializes in extremely multimodal problems. When coupled with FEA this proves to be extremely onerous in the time spent to obtain a solution. A method of sidestepping most of the FEA computations is to use a limited number of random FEA computations within the search space to create a regression model. This regression procedure will be elaborated on in the next section.

5.3 General Regression Neural Networks (GRNN)

Regression, as stated above, is the creation of a simplified curve based on some known data that is used in order to predict future data. There are many types of regression that can be

implemented each based on the primary assumption to the order of the system that is to be dealt with. For a simple system, a polynomial (linear) regression can be used. Note that the linear does not refer to the function but to the functions' constant terms. For more complex systems with interaction between the processes a non-linear regression could be used, although many more types are available. Each type has its place and in most cases a simple linear regression is implemented first and then expanded if needed. This type of regression is generally based on a statistical approach and has lead to the field of machine learning.

Machine learning is a field that has sprung up in computer systems in order to train programs to the adapting needs of the user [42]. The concept is much the same as with regression where some known data is used to build a function. However in the case of machine learning the algorithms used have been tailored to the process of learning and adapting. Although the fundamental theory of machine learning is beyond the scope of this report, the regression machine used comes from this line of research.

The regression machine used is the GRNN based on the work by Specht in 1991 [11]. The theory is stated:

$$\text{Given } \mathbf{X}, \mathbf{Z} \text{ and } \mathbf{Q} \text{ for } i = 1, \ldots, m \text{ and } j = 1, \ldots, o$$

$$\mathbf{D2}_j = (\mathbf{X}_i - \mathbf{Q}_j)(\mathbf{X}_i - \mathbf{Q}_j)^T, \tag{5.8}$$

$$\mathbf{K}_j = e^{\left(\frac{-\mathbf{D2}_j}{2\sigma^2}\right)}, \tag{5.9}$$

$$\mathbf{Y}_j = \frac{\sum_{i=1}^{m}(\mathbf{K}_j \mathbf{Z}_j)}{(\sum_{i=1}^{m} \mathbf{K}_{i,j})}, \tag{5.10}$$

where, $\mathbf{X}$ and $\mathbf{Z}$ are a set of training data with $\mathbf{X}$ being the array of $m \times n$ variables and $\mathbf{t}$ the array of $m \times o$ function values. $\mathbf{Q}$ is a set of $1 \times n$ query variables, $\mathbf{D2}$ is a $1 \times m$ instance pairwise squared distances array, σ is a smoothing scalar usually ranging in value from 0.09 to 1.0 and finally $\mathbf{Y}$ is the predicted function value from the query input. This method is based on the Gaussian statistical structure and the process is to place a Gaussian at each training data point and then to map the structure using these Gaussians.

At this point no further information on the regression will be given apart form the proof of application testing data provided later in this section. For more information on this topic consult the literature provided in Chapter 2.

5.4 Testing of the Final Program

As with all stages of the process so far, this stage will need simple iterative testing of each new part and then the whole, in order to confirm the results. The new additions of this chapter have been the constraints, the OpenMP and the GRNN Regression. Of these the OpenMP has been confirmed to be operative by running many analyses with and without the paralising and the results are comparative. The other two however need to be elaborated upon further.

5.4.1 Testing of the Regression

The easiest means of testing the regression is to extract it from the program and apply a simple curve of training data. A SinC curve was used, as defined by the following equation:

$$f(x) = \begin{cases} \dfrac{\sin(x)}{x} & \text{if } x \neq 0 \\ 1 & \text{if } x = 0 \end{cases} \tag{5.11}$$

After such a curve has been trained, prediction points can be assigned randomly and then plotted. The plotted points should coincide as seen in Figure 5.1. Further a 2-dimensional curve can be attempted in the same manner with $f(\mathbf{X}) = f(X_1)f(X_2)$ (Figure 5.2).

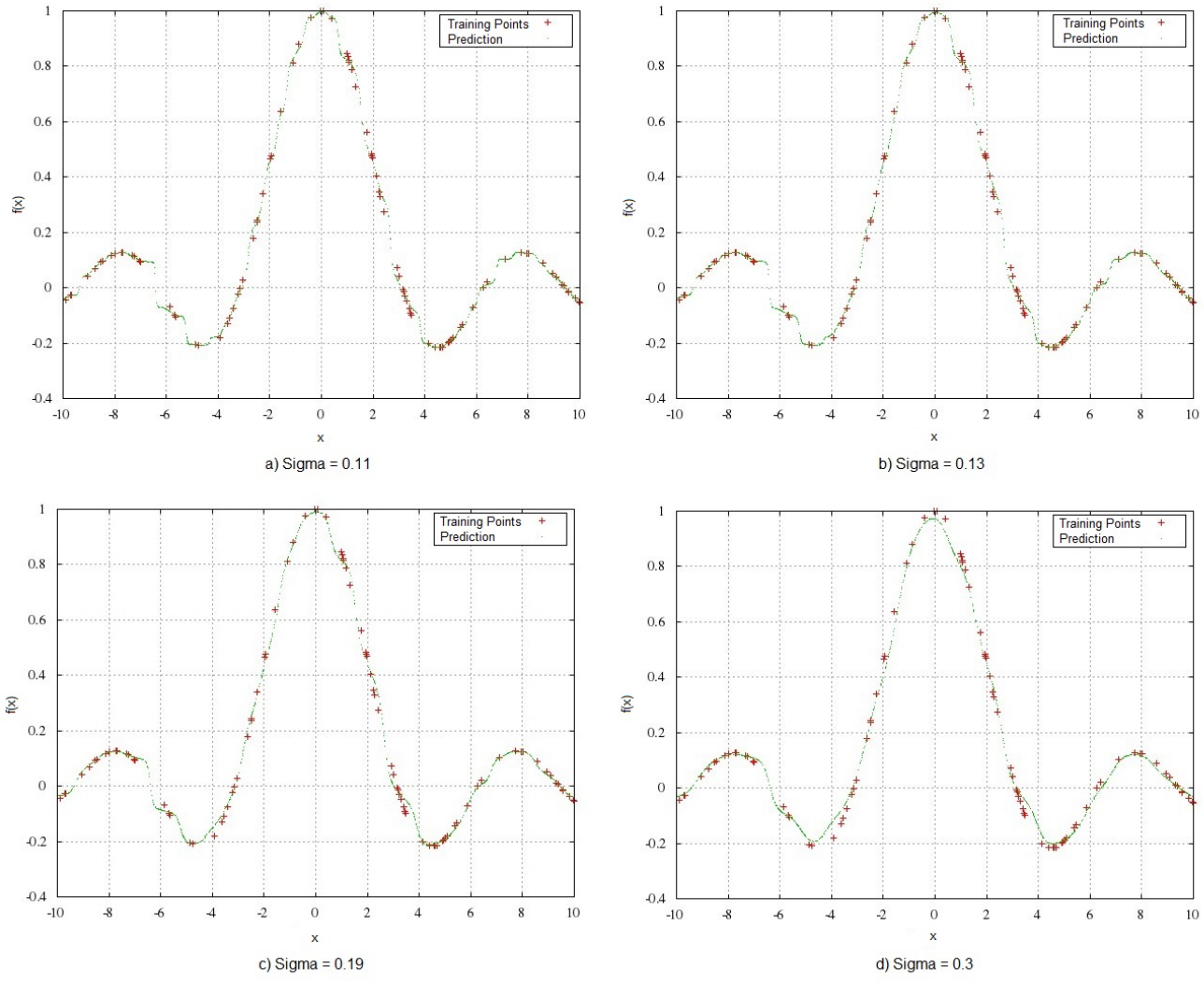

Figure 5.1: A sinC curve with 1 dependent variable

In Figure 5.1 a SinC curve is utilised to assess the effect of the smoothing factor on the results of a GRNN regression. The SinC curve, proposed by Hwang, is a relatively standard introductory

test case for regression and here it is seen clearly that good results require a trained smoothing factor [68]. a further expansion of this test case is to expand its dimensionality to that of a volume plot as seen in Figure 5.2. The two diagrams, although not to clear, coincide indicating a relatively accurate prediction in 'b'. The final test case, proposed by Specht, was a plant model [11].

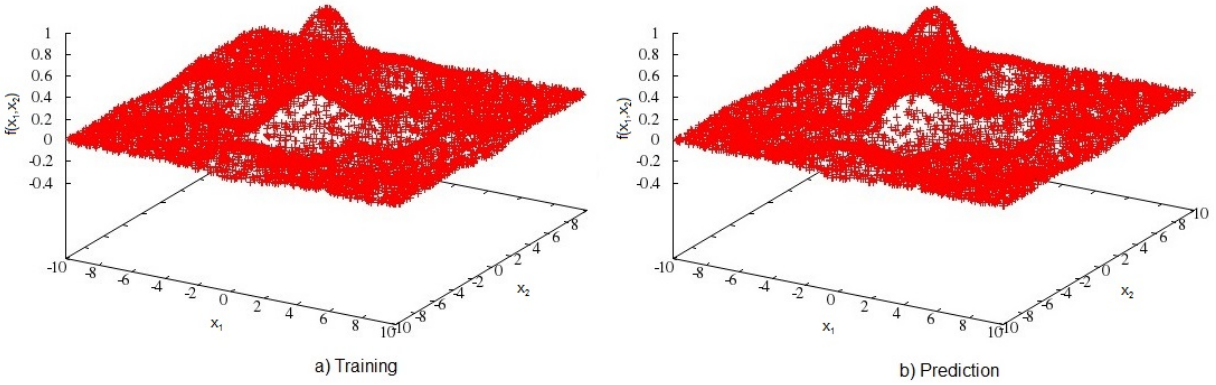

Figure 5.2: A sinC curve with 2 dependent variables

Specht proposed a plant model where

$$f(x) = \begin{cases} -1 & \text{if } x < -1 \\ x - 1 & \text{if } x = [-1, 1] \\ 1 & \text{if } x > 1. \end{cases} \tag{5.12}$$

This model is in the shape of a sigmoid and the GRNN adapts to the discontinuities fairly well as seen in Figure 5.3.

5.4.2 Testing of the Constraints

The testing of the constraints was conducted by a numerical comparison to the documented results in the work by Kaw [3, p139-160]. No further testing was conducted. The reason for this section is to elaborate upon a few points of interest rather than the testing itself.

The first point is that although the constraints on the objective function are very necessary in a real world model, in the initial stages of the program development they are tedious and fairly pointless. Expanding upon this statement, they complicate debugging and show results other than what would be expected in an unconstrained case. Also, they are by no means complete as would be seen in a real world model. The constraints in general are a section that could definitely be improved upon but that will be left for future work.

5.4.3 A Complete Testing of the FEM and PSO Set-up with Regression

The last phase of testing took into account the FEM and PSO with regression and attempted to produce models based on the expected outcome of a composite material of 1 and 2 layers. For

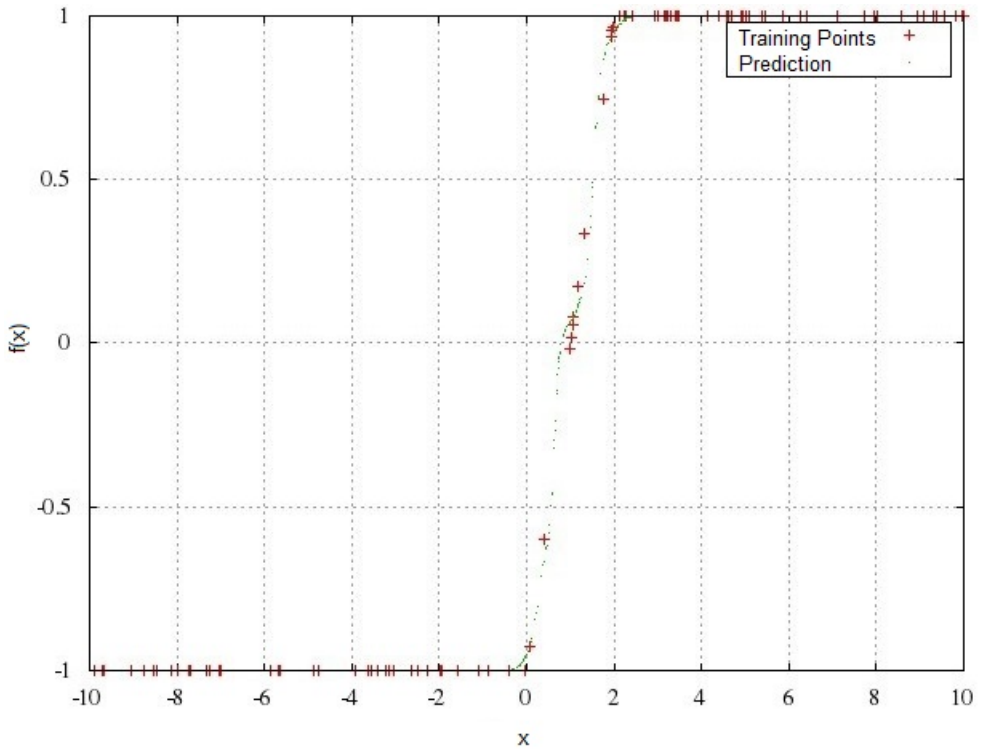

Figure 5.3: A plant model proposed by Specht [11]

this problem a finite element model based on the patch test seen in Figure 3.15 for in-plane shear is used. The model uses a 5×5 element mesh. In Figure 5.4 the 1 layer graph of compliance vs degrees is modelled for the situation of maximum stiffness/minimum compliance. This is due to the abundance of data on this type of optimisation. In this plot the *a* shows the finite element solution of 1 run, *b* shows that over 100 runs and *c* shows 10 runs of the regression. The variance of *c* shows the approximation of the solution using the regression and although the results are similar, each time there is a subtle loss in accuracy.

Figure 5.5 shows surface plot of the model for 2 layers. For the cases of *a* to *c* which use the regression system the testing data is increased from 200 to 500 to 2000 samples and in *d* the finite element solution is seen. This clearly shows that with increasing samples the accuracy of the regression improves. This accuracy must however be weighted against the necessary speed-up expected. The speed-up when using the regression is of extreme significance and Table 1 shows the time gain when using the various methods. The accuracy of the regression reduces as more layers are added. In essence there should be more training data for more layers. Keep in mind that at this point only the composite layups are tested.

5.4.4 Testing of the FEM and PSO Set-up with Regression for Piezoelectric materials

In a similar manner, as with the previous subsection, the program will now be tested for the piezoelectric material. At this point the optimisation will remain as a minimisation of the

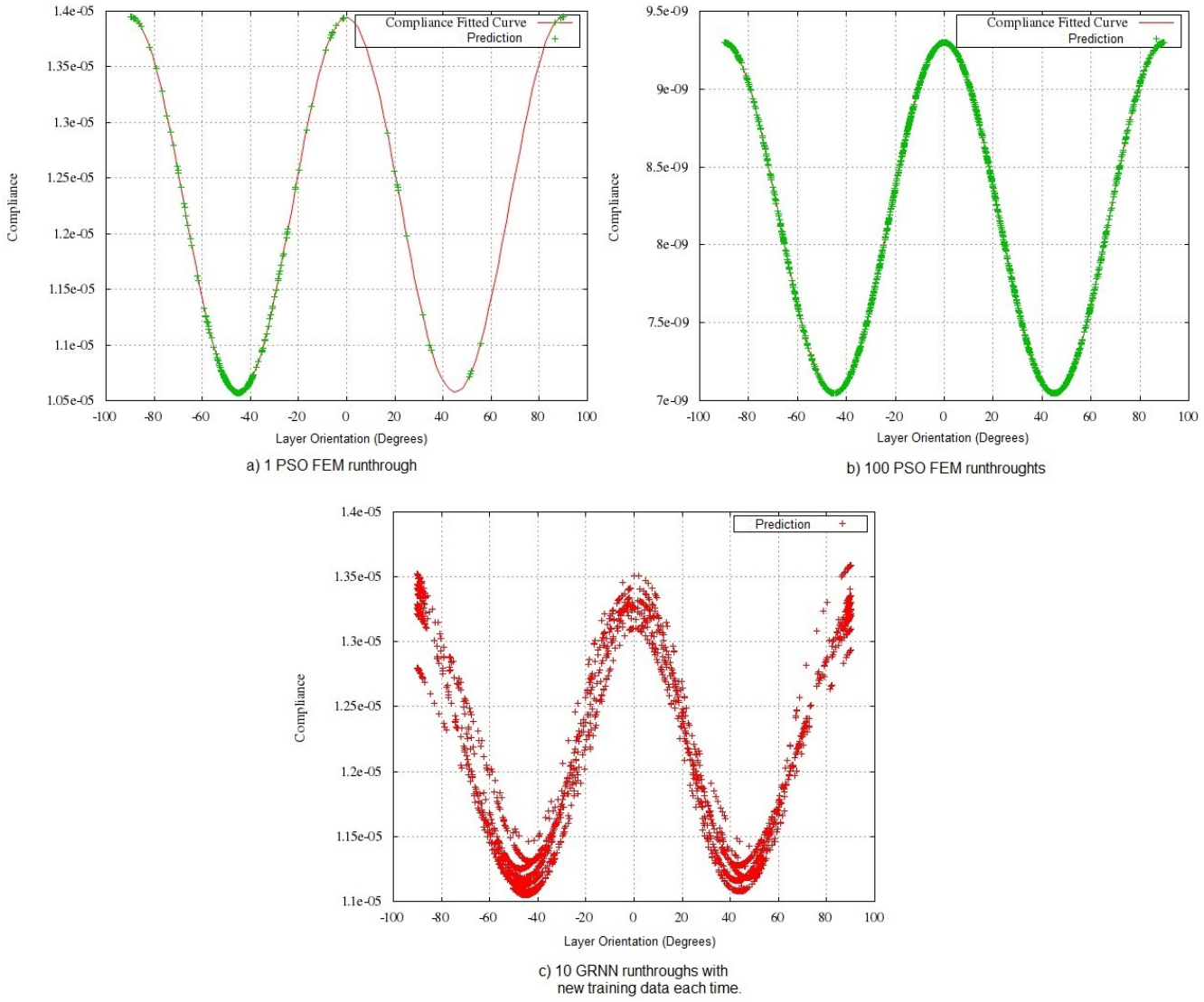

Figure 5.4: A GRNN single layer shear analysis

Table 5.1: A time comparison of 100 runs of the FEA PSO using openMP and regression

Layers	Normal		OpenMP	
	FEM [s]	Regression [s]	FEM [s]	Regression [s]
1	14909	247	4320	1255
2	17813	565	5120	256
4	29198	1449	6746	476

compliance. From the resulting data a curve of the compliance vs. the angle can once again be produced as seen in Figure 5.6. This curve however, shows that the compliance change is very small in magnitude compared to the compliance change in the composite. Furthermore, it shows a curve that is flipped around the x-axis. These small changes are inherited from the material properties and when the material changes or the polarisation direction is different

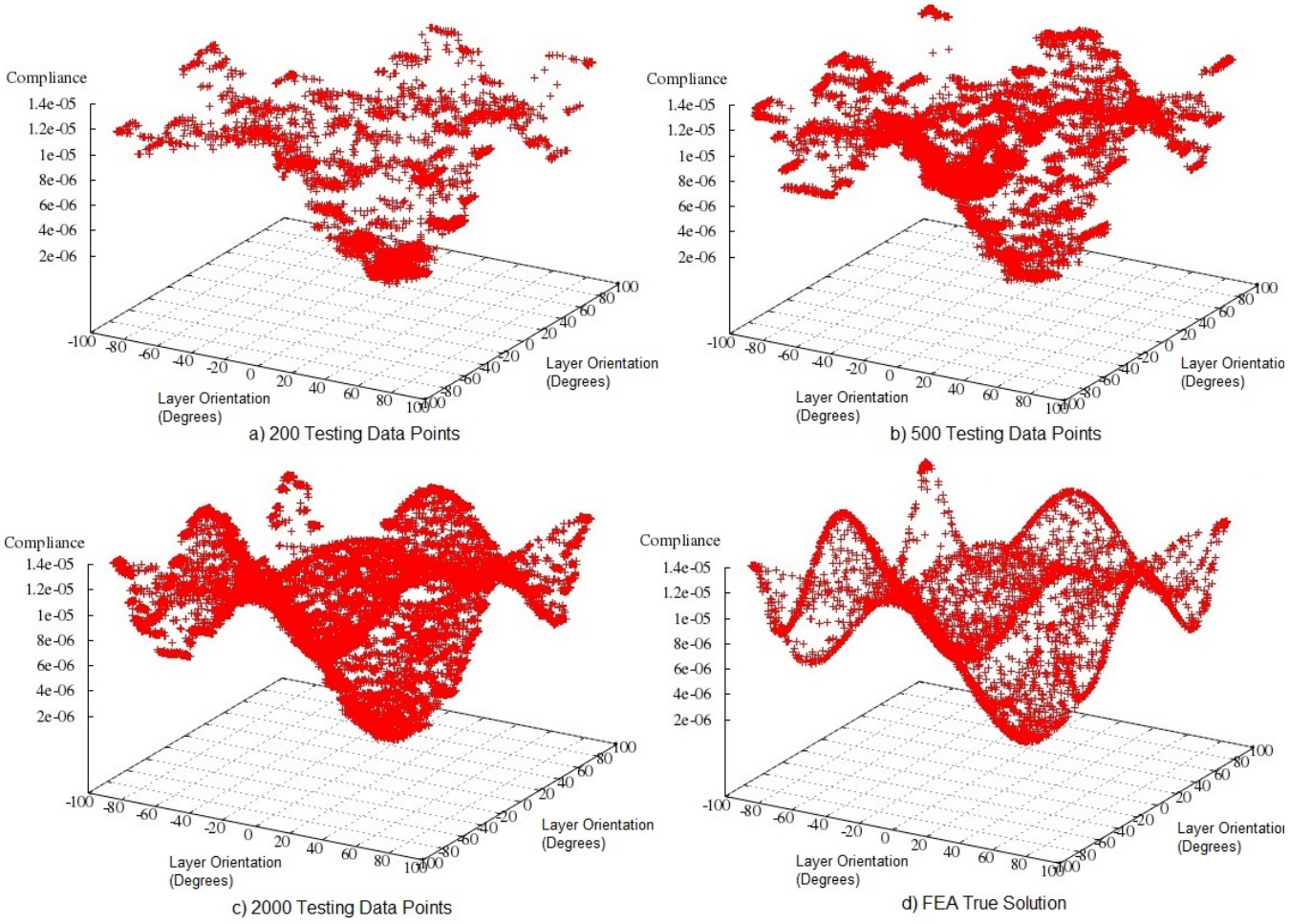

Figure 5.5: A 2-layer GRNN testing point analysis of an in-plane-shear model

the curve will produce different results. These changes in polarisation may be understood by referring to Figure 5.7.

Here the concept shows proof that the material can be aligned although this is highly dependent on the polarization direction. From here onwards, the examples will attempt the maximisation of compliance as was stated in the introduction to this chapter.

5.5 Simulations for the Piezoelectric Optimisation

In this section the program will be tested on a number of examples from the literature and classical testing schemes. The first test is that of a classical testing scheme where patch test membrane problems are analysed for increasingly computationally expensive problem types. The latter tests attempt to improve upon the test cases proposed by Carrera and Piefort that were used in Section 3.5.2.

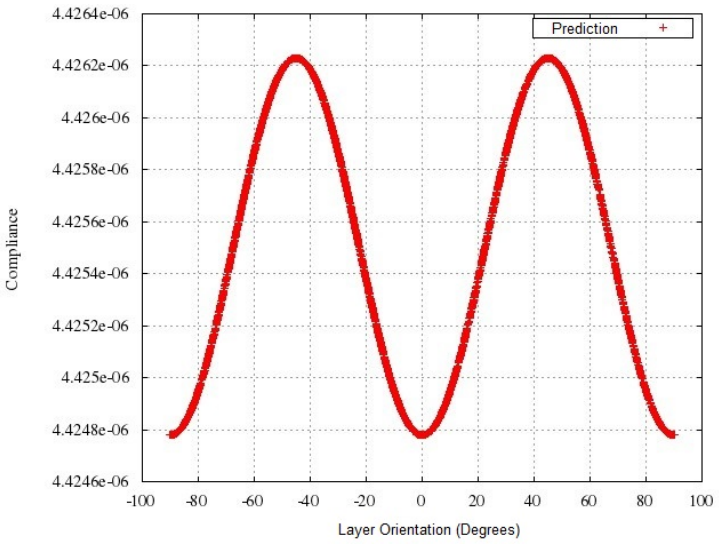

Figure 5.6: The compliance of a piezoelectric layer polled through the thickness

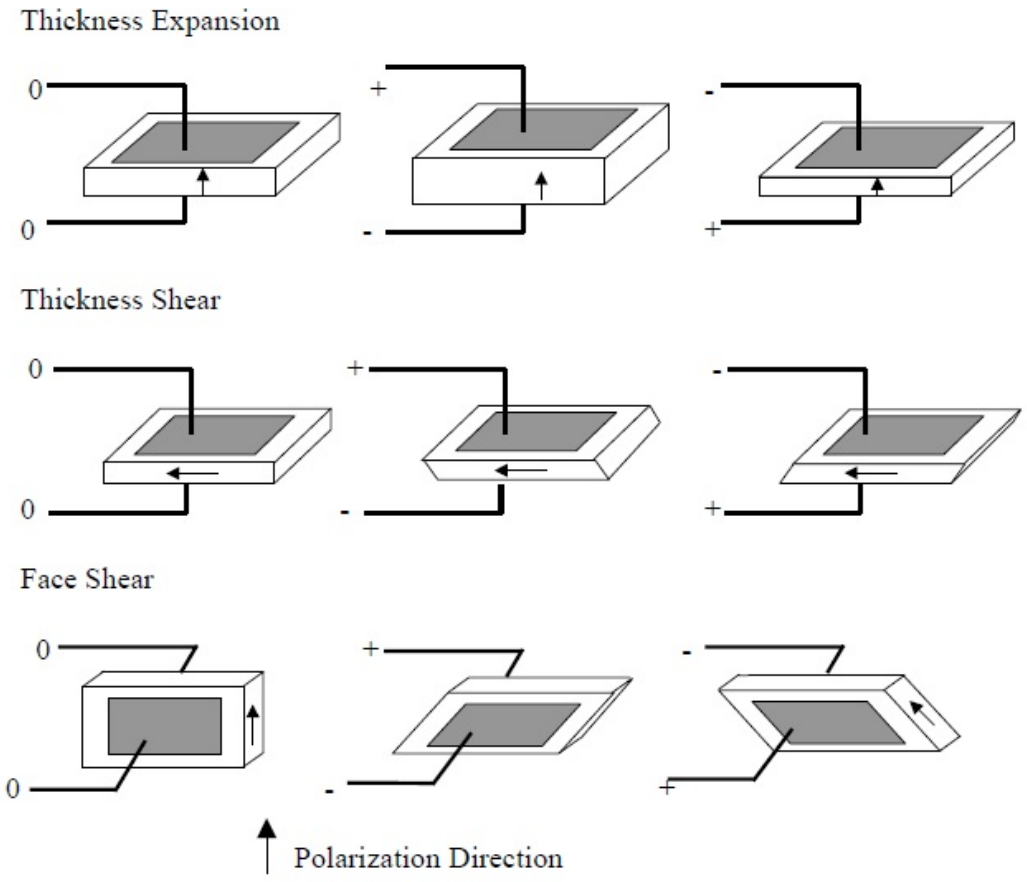

Figure 5.7: The polarization types for piezoelectric materials

5.5.1 Test 1: A Membrane Critical Analysis of the Optimiser

In this section the membrane applicable patch test models seen in Figure 3.15 will be used to test the optimiser under different conditions. These conditions will be the mesh density and the layer total. In order to expedite this process only 10 true FEM-PSO runs will be conducted in each test for the comparison to the regression. The meshing types will include a 4×4, 8×8 and 16×16 mesh size. The layer total will be 4, 8 and 16 layers with the orientations being symmetric. This problem will be conducted using a 10×10 mm patch with a thickness of 0.1 mm.

Considering the information in the previous section the result for the optimised stacking sequence, can be predicted for each test. In the test of in-plane-shear, as seen in Figure 3.15, one would expect a $[p/90_{n-2}/p]$ layup. For the Extension test the expected result would also be $[p/90_{n-2}/p]$, here the p represents a quasi-isotropic in-plane piezoelectric material and the angles can vary. Here the 90 can be + or - 90 and in the test of the in-plane-shear a 0 is also satisfactory. The results for the optimised tests are reported in Table 5.2 and 5.3. It would be expected that the results should be closely comparable if not the same.

Table 5.2: A 10 run optimisation of the FEA PSO under elongation

Layers	Mesh		
	4	8	16
4(FEA)	$[59.5/-64.4]_S$	$[-11.6/-64.4]_S$	$[58.6/-64.4]_S$
(Reg)	$[-8.5/60.7]_S$	$[-4.5/66.2]_S$	$[-8.3/60.8]_S$
8(FEA)	$[-89.1/-67.4/-67.4/-67.4]_S$	$[-89.1/-67.5/-67.5/-67.5]_S$	$[87.2/67.5/-67.5/-67.5]_S$
(Reg)	$[56.1/-61.6/62.6/69.2]_S$	$[64.8/-61.8/62.9/64.7]_S$	$[68.0/-63.4/66.5/69.3]_S$
16(FEA)	$[-78.9/-74.3/-74.4/-74.4\ /-74.4/-74.3/-74.3/-74.3]_S$	$[-78.9/-74.3/-74.4/-74.4\ /-74.3/-74.4/-74.3/-74.3]_S$	$[-66.0/-73.9/-73.9/-73.9\ /-73.9/-73.8/-73.9/-73.9]_S$
(Reg)	$[-26.4/-58.7/-89.6/-88.6\ /71.8/-89.9/-89.6/88.3]_S$	$[-89.9/-89.7/-89.9/3.0\ /64.1/-84.3/-79.3/89.5]_S$	$[-89.8/39.9/-89.6/-70.2\ /-64.4/84.6/89.8/-20.3]_S$

Table 5.3: A 10 run optimisation of the FEA PSO under in-plane shear

Layers	Mesh		
	4	8	16
4(FEA)	$[67.6/90.0]_S$	$[88.8/90.0]_S$	$[90.0/90.0]_S$
(Reg)	$[-2.1/-98.3]_S$	$[-2.0/-87.9]_S$	$[-52.9/-88.5]_S$
8(FEA)	$[52.6/90.0/90.0/-90.0]_S$	$[-87.2/-90.0/-90.0/-90.0]_S$	$[48.1/90.0/90.0/-90.0]_S$
(Reg)	$[-88.1/85.7/-0.5/-12.5]_S$	$[-89.9/-88.6/12.6/1.7]_S$	$[-90/-85.4/-5.9/1.02]_S$
16(FEA)	$[90.0/90.0/90.0/90.0\ /90.0/90.0/90.0/90.0]_S$	$[25.8/-90.0/-90.0/-90.0\ /-90.0/-90.0/-90.0/-90.0]_S$	$[-28.0/-90.0/-90.0/-90.0/-90.0/-90.0/-90.0/-90.0]_S$
(Reg)	$[32.7/-14.2/-6.8/-11.2\ /89.7/-89.9/-89.4/-89.4]_S$	$[48.3/89.7/79.5/89.3\ /52.7/26.6/81.1/81.4]_S$	$[51.6/87.0/89.0/87.9\ /87.3/45.8/41.2/53.1]_S$

5.5.2 Test 2: Piefort Bi-morph Displacement Optimisation

Section 3.5.2.2 shows the finite element analysis of the Piefort Bi-morph for which this optimisation pertains. The problem specifically refers to the bi-morph where the tip is free and there is a voltage application along the top surface of the structure.

The optimisation will attempt to improve the tip displacement when changing the angles of the piezoelectric material while maintaining the material within stress limits. All of the dimensions and problem specifics are defined in Section 3.5.2.2 and will remain the same except for the angle of each layer. This change in layer angle will effect the piezoelectric properties of the material and theoretically produce small change in the objective function.

Before this problem could run the objective function of the optimiser needed to be altered, as in this test there were electric boundary conditions that required mechanical outputs. To facilitate this change the compliance was altered to

$$f = \mathbf{q}_m^T \mathbf{I} \mathbf{q}_m, \tag{5.13}$$

where the subscript m refers to the mechanical displacements only, I is the identity matrix and q remains the displacements. The only requirement is that the displacements are pre-scaled to be greater than 1. This can be achieved by inputting bigger boundary conditions, forces or post scaling of the displacements.

The results obtained for this problem were not random, this was expected due to the 3D orthotropic material set-up. The results showed optima at [0/0], [0/90] and [0/ − 90] with the final best at [0/ − 0.7]. As a last note, it has also been confirmed that the optimiser complied with the FEM results from the Piefort thesis [13].

5.5.3 Test 3: Simply Supported Plate Displacement Optimisation

The Carrera plate displacement optimisation deals with the problem from Section 3.5.2.3. A more detailed explanation of this and other problems were obtained from the paper by Cen *et al.* [10]. An alternate problem from this paper was used. The problem had 5 layers with the centre 3 being composite unidirectional materials of a 3 mm thickness and the outer 2 being piezoelectric of 40 μm in thickness. The problem layout is much the same as the Carrera problem of Section 3.5.2.3 although the material properties are altered. They can be seen in Appendix A. For this problem the results were compared to the literature and the results obtained were similar for a single FEM run.

Due to the small outer thickness of the piezoelectric layer the aspect ratio ignores these two layers and uses the composite layers for the determination of the problem dimensions. Here, the aspect ratio used was 10. The problem ran through 1000 iterations and takes a 100 run average.

The results showed that the optimum is obtained at [−90/37.9/90/−37.9/85.2] and was -5.452×10^{-16} by comparison to the -2.22×10^{-16} given by the layup from Cen *et al.* [10].

5.6 Discussion

So far in this thesis, FEM has been validated and following this, optimisation has been conducted. In each test the results have been shown and discussed. Here it is no different and this section will comment on the results obtained in the tests above.

In test 1, Table 5.2 shows a deviation from the expected results that converges on 90 degrees as the layers are increased. This is in an unexpected result and proves interesting. The problem will converge on 90 degrees in two situations, the first is as the outer piezoelectric layers material properties are reduced in magnitude, the second is when the thickness is reduced. It appears that the quasi-isotropic material changes the unidirectional balance in the CLT/FSDT. Essentially this imposes an averaging system with the quasi-isotropic material dominating the system resulting in the non-conformity seen in the table.

The next interesting point to note is the accuracy of the regression. The accuracy for 4 and 8 layers is acceptable when compared to Figure 5.4 c but this fails in the 16 layer regime. This is as a result of the testing points and can be improved upon with the adaptation of the algorithm used for the determination of these points. This, however, will not be conducted in this thesis and is left for future work. Inclusive in this future work, should be an attempt to assess other schemes such as latern hypercubes, elm or any of the many other regression schemes. This could promote a much improved optimisation approach in terms of processing speed.

The second set of results for test 1 are the in-plane shear results of Table 5.3. Here the results are as expected and the regression remains the same as stated above. The completion of this test shows that the optimiser can handle membrane problems.

Test 2 shows the Piefort bending of a bi-morph under electric boundary conditions. This was conducted to not only check the effects of the piezoelectric coupling but also as an initial test case for the plate bending situation. The material was handled as a 3-dimensional-orthotropic material and therefore shows optima at the stated positions. This proves that numerically the piezoelectric materials can be optimised based on the material type and profile. It also shows the ability of the optimiser to handle simple piezoelectric plate problems.

Test 3 shows the optimiser under a 2 material 5 layer plate bending case. Here, the results clearly show an optimised result mostly due to the composites, as the piezoelectric material is taken as an isotropic material. The term ‘mostly’ is used as the piezoelectric effects do have very small influences based on the effects of the expansion.

At this point no in-plane orthotropic piezoelectric materials were used as no documented problem with results were found. However, the results show that should such a material be used then an optima would be found for this material type. The reduction of the compliance clearly influenced the induced voltage of the piezoelectric materials. Further investigation into this problem type can be conducted in the future where enhanced elements, optimisation techniques and regression could be used. At this time however, the optimiser has improved the composite-piezoelectric layer interaction as can be seen in all the tests above.

Chapter 6

Conclusion

This research was conducted with a major objective in mind. It has been achieved as follows:

Optimising the piezoelectric-composite layer interaction to improve the overall compliance of the structure.

The procedure for completing this objective was broken up into a number of stages. These stages allowed for the growth of the objective in manageable pieces. In Chapter 3 the author proved his understanding of the finite element method. He showed the development of the finite element from the variational formulation through to the set up of the piezoelectric plate that was used to analyse the structures obtained from the literature. This method was used in the creation of a program that allowed for the solving of piezoelectric membranes and plates using the finite element method. The program was then tested by using problems taken from various literature sources. The results obtained from the author's program were compared to the literature sources and the results were comparative. This showed the author had a comprehensive understanding of piezoelectric finite elements with regards to plate and membrane modelling, as well as a more general view of the whole procedure.

In Chapter 4 the author detailed a general explanation of mathematical optimisation. Enhancing this explanation, the particle swarm algorithm was explained in depth. Once again, a program was created that could solve the researched principles. The literature was perused for problems pertaining to the particle swarm and the problems were run in the created program. The results obtained were compared to the literature and the results were equivalent. This proved his understanding of optimisation methods by use of comparable modelling of the particle swarm optimisation.

Chapter 5 detailed the procedure whereby the coded optimiser of Chapter 4 was linked to the coded finite element analysis of Chapter 3. Here the optimiser was specifically tuned to optimise the layer orientation with regards to the compliance taken from the finite element analysis. In addition to this, constraints were included based on the maximum principle stress, Tsai-Hill and Tsai-Wu criterion. Three sets of tests were conducted where the results showed that the piezoelectric-composite layer interaction improved the overall compliance.

The first was a finite element type refinement test that compared the mesh and layer amount. From this test it was deemed that the optimiser correlated correctly to the membrane type

problems although there were some interesting and unexpected results due to the use of multiple materials. The second and third showed the optimiser under the effects of bending for a bi-morph cantilever and a 5 layer simply supported plate. Again the results showed an improvement in the overall compliance of the structure.

In conclusion, the stated objectives have been achieved.

Chapter 7

Future Work

Due to time constraints many areas of interest have been left for future work and are listed here.

- Enhancement of the element in the FE model
- Incorporation of an improved optimisation method
- Improvement of the regression
- Further numerical testing and application to experimental models
- Improvement of the program to use sparsity or other memory saving techniques
- Further OpenMP improvements for speed and memory handling

The listed improvements are some of the more important ones but there are many others that can be achieved. For instance a graphical input system or an auto-meshing system. Although these would be beneficial to the usability of the program they require an enormous amount of time to implement correctly.

List of References

[1] Carrera, E., Brischetto, S. and Nali, P.: *Plates and Shells for Smart Structures - Classical and Advanced Theories for Modeling and Analysis*. 1st edn. John Wiley and Sons, Ltd, Chichester, 2011.

[2] Long, C.S.: *Finite Element Developments and Applications in Structural Topology Optimization*. Ph.D. thesis, University of Pretoria, 2007.

[3] Kaw, A.K.: *Mechanics of Composite Materials*. 2nd edn. Taylor and Francis Group, USA, 2006.

[4] Akbulut, M. and Sonmez, F.O.: Design Optimization of Laminated Composites Using a New Variant of Simulated Annealing. *Computers & Structures*, vol. 89, pp. 1712–1724, September 2011.

[5] Bathe, K.J. and Dvorkin, E.N.: Short Communication A Four-Node Plate Bending Element Based On Mindlin/Reissner Plate Theory And A Mixed Interpolation. *international Journal for Numerical Methods in Engineering*, vol. 21, pp. 367–383, 1985.

[6] Dvorkin, E.N. and Bathe, K.J.: A continuum mechanics based four-node shell element for general non-linear analysis. *Engineering Computations*, vol. 1, pp. 77–88, 1984.

[7] Long, C.S., Loveday, P.W. and Groenwold, A.a.: Planar four node piezoelectric elements with drilling degrees of freedom. *International Journal for Numerical Methods in Engineering*, vol. 65, pp. 1802–1830, 2006.

[8] Groenwold, A.A.: *Finite Element Analysis of Composite Plates and Shells*. Doctorate Thesis, University of Pretoria, 1993.

[9] Hwang, W.S. and Park, H.C.: Finite Element Modeling of Piezoelectric Sensors and Actuators. *AIAA Journal*, vol. 31, pp. 930–937, 1993.

[10] Cen, S., Soh, A.-K., Long, Y.-Q. and Yao, Z.-H.: A New 4-node Quadrilateral FE Model with Variable Electrical Degrees of Freedom for the Analysis of Piezoelectric Laminated Composite Plates. *Composite Structures*, vol. 58, pp. 583–599, 2002.

[11] Specht, F.D.: A General Regression Neural Network. *IEEE transactions on neural networks*, vol. 2, no. 6, 1991.

[12] Cook, R.D., Malkus, D.S., Plesha, M.E. and Witt, R.J.: *Concepts and Applications of Finite Element Analaysis*. 2nd edn. John Wiley & Sons, New York, 2002.

[13] Piefort, V.: *Finite Element Modelling of Piezoelectric Active Structures*. Ph.D. thesis, Université libre de Bruxelles, Brussels, 2001.

[14] eex: Improve Aircraft Aerodynamics.
Available at: `http://eex.gov.au/opportunity/improve-aircraft-aerodynamics/`

[15] Reneaux, J.: Overview on Drag Reduction Technologies for Civil Tranport Aircraft. *European Congress on Computational Methods in Applied Sciences and Engineering*, 2004.

[16] Green Car Congress: Adaptive Wings Could Improve Aircraft Fuel Consumption 5% to 15%.
Available at: `http://www.greencarcongress.com/2006/11/adaptive_wings_.html`

[17] Jani, J.M., Leary, M., Subic, A. and Gibson, M.A.: A Review of Shape Memory Alloy Research, Applications and Opportunities. *Materials and Design*, 2014.
Available at: `http://dx.doi.org/10.1016/j.matdes.2013.11.084`

[18] Grainger, D.W.: Connecting Drug Delivery Reality to Smart Materials Design. *International Journal of Pharmaceutics*, vol. 454, pp. 521–524, 2013.

[19] Morgan Ceramics: A Piezoelectric Explanation.
Available at: `http://www.morgantechnicalceramics.com/resources/piezoelectric-ceramics-properties-and-applications/`

[20] Chen, Q., Natale, D., Neese, B., Ren, K., Lin, M., Zhang, Q.M., Pattom, M., Wang, K.W., Fang, H. and Im, E.: Piezoelectric Polymers Actuators for Precise Shape Control of Large Scale Space Antennas. *International Journal for Numerical Methods in Engineering*.

[21] Cook, R.D.: *Finite Element Modeling for Stress Analysis*. John Wiley & Sons, New York, 1995.

[22] Reddy, J.N.: *Energy and Variational Methods in Applied Mechanics*. 1st edn. John Wiley & Sons, Verginia, 1984.

[23] Reddy, J.N.: *Mechanics of Laminated Composite Plates*. 1st edn. CRC Press, Inc., Florida, 1997.

[24] Reddy, J.N.: *Theory and Analysis of Elastic Plates and Shells*. 2nd edn. CRC Press, Inc., Florida, 2007.

[25] Solin, P., Segeth, K. and Dolezel., I.: *Higher-Order Finite Element Methods*. CRC Press LLC, Florida, 2004.

[26] Zienkiewicz, O.C. and Taylor, R.L.: *The Finite Element Method for Solid and Structural Mechanics*. 6th edn. Elsevier Butterworth-Heinemann, Oxford, 2005.

[27] Dlowinski, R., Rodin, E.Y. and Zienkiewicz, O.C.: *Energy Methods in Finite Element Analysis*. John Wiley & Sons, New York, 1979.

[28] Macneal, R.H. and Harder, R.L.: A Proposed Standard Set of Problems to Test Finite Element Accuracy. *Finite Elements in Analysis and Design*, vol. 1, pp. 3–20, 1985.

[29] Di, S. and Ramm, E.: On Alternative Hybrid Stress 2-D and 3-D Elements. *Engineering Computiations*, vol. 11, pp. 49–68, 1994.

[30] Benjeddou, A.: Advances in Piezoelectric Finite Element Modeling of Adaptive Structural Elements: A Survey. *Computers & Structures*, vol. 76, pp. 347–363, 2000.

[31] Allik, H. and Hughes, T.J.R.: Finite element method for piezoelectric vibration. *International Journal of Numerical Methods in Engineering*, vol. 2, pp. 151–157, 1970.

[32] Brischetto, S.: *Classical and Mixed Multilayered Plate/Shell Models for Multifield Problems Analysis*. Ph.D. thesis, Paris West University Nanterre La Défense, 2009.

[33] Maxwell, K.S.: *Finite Element Analysis of Three-Phase Piezoelectric Nanocomposites*. Ph.D. thesis, Texas A&M University, 2009.

[34] Carrera, E. and Brischetto, S.: Reissner Mixed Theorem Applied to Static Analysis of Piezoelectric Shell Systems. *Journal of Intelligent Material Systems and Structures*, vol. 18, pp. 1083–1107, 2007.

[35] Lee, H.-J.: Finite Element Analysis of Active and Sensory Thermopiezoelectric Composite Materials. Tech. Rep. May, NASA, Hanover, 2001.

[36] Rao, S.S.: *Engineering Optimisation - Theory and Practice*. 4th edn. John Wiley & Sons, New Jersey, 2009.

[37] Liu, J.L. and Lin, J.H.: Evolutionary computation of unconstrained and constrained problems using a novel momentum-type particle swarm optimization. *Engineering Optimization*, vol. 39, pp. 287–305, 2007.

[38] Wilke, D.N., Kok, S. and Groenwold, A.A.: Comparison of Linear and Classical Velocity Update Rules in Particle Swarm Optimization : Notes on Diversity. *International Journal for Numerical Methods in Engineering*, vol. 70, pp. 985–1008, 2007.

[39] Wilke, D.N., Kok, S. and Groenwold, A.A.: Comparison of Linear and Classical Velocity Update Rules in Particle Swarm Optimization : Notes on Scale and Frame Invariance. *International Journal for Numerical Methods in Engineering*, vol. 70, pp. 985–1008, 2007.

[40] Padhye, N. and Deb, K.: Boundary Handling Approaches in Particle Swarm Optimization.

[41] Myers, R.H., Montgomery, D.C. and Anderson-Cook, C.M.: *Response Surface Methodology - Process and Product Optimisation Using Design Experiments*. Third edit edn. John Wiley & Sons, Inc., New Jersey, 2009.

[42] Alpaydin, E.: *Introduction to Machine Learning*. 2nd edn. Massachusetts Institute of Technology, USA, 2010.

[43] Smola, A. and Vishwanathan, S.V.N.: *Introduction to Machine Learning*. Cambridge University Press, Cambridge, 2008.

[44] Huang, G.B. and Babri, H.A.: Upper Bounds on the Number of Hidden Neurons in Feedforward Networks with Arbitrary Bounded Nonlinear Activation Functions. *IEEE transactions on neural networks*, vol. 9, pp. 224–229, 1998.

[45] Huang, G.B., Zhu, Q.Y. and Chee, C.K.: Extreme learning machine: Theory and applications. *Neurocomputing*, vol. 70, pp. 489–501, 2006.

[46] Lu, J. and Bai, Y.: Applications of GRNN Based on Particle Swarm Algorithm Forecasting Stock Prices. *International Conference on Information, Business and Education Technology*, vol. 2, pp. 1–4, 2013.

[47] Ferreira, A.J.M.: *MATLAB Codes for Finite Element Analysis*. Springer Science & Business Media, Porto, 2009.

[48] Ellis, T.M.R., Philips, I.R. and Lahey, T.M.: *Fortran Programming 90*. 1st edn. Addison-Wesley Publishing Company, Inc., 1994.

[49] Centre for High Performance Computing: An intorduction to parallel programming. Available at: `http://www.chpc.ac.za`

[50] LAPACK - Linear Algebra PACKage. Available at: `http://www.netlib.org/lapack/`

[51] Desai, C.S. and Abel, J.F.: *Introduction to the Finite Element Method: a Numerical Method for Engineering Analysis*. Litton Educational Publising, New York, 1972.

[52] Kulakowski, B.T., Gardner, J.F. and Shearer, J.L.: *Dynamic Modeling and Control of Engineering Systems*. 3rd edn. Cambridge University Press, New York, 2007.

[53] Zill, D.G.. and Cullen, M.R.: *Advanced Engineering Mathematics*. 3rd edn. Jones and Bartlett Publishers, Sudbury, 2006.

[54] Sadd, M.H.: *Elasticity - Theory, Applications and Numerics*. Elsevier, Inc, Oxford, 2005.

[55] Saouma, V.E.: *Lecture Notes - Introduction to Continuum Mechanics and Elemetns of Elasticity/Structural Mechanics*, vol. 56. 1998.

[56] Timoshenko, S. and Goodier, J.N.: Theory of Elasticity. 1951.

[57] Kwon, Y.W. and Bang, H.: *The Finite Element Method using MATLAB*. CRC Press LLC, Florida, 1997.

[58] Hilton, E. and Owen, J.D.R.: *Finite Element Programming*. Academic Press, Inc, London, 1977.

[59] Chapra, S.C.: *Applied Numerical Methods with MATLAB for Engineers and Scientists*. 2nd edn. McGraw-Hill, New York, 2008.

[60] Piezoelectric Materials. 2007.
Available at: `http://www.piezomaterials.com/`

[61] Sze, K. and Pan, Y.: Hybrid Finite Element Models for Piezoelectric Materials. *Journal of Sound and Vibration*, vol. 226, no. 3, pp. 519–547, 1999.

[62] Cengel, Y.A. and Boles, M.A.: *Thermodynamics - An Engineering Approach*. 6th edn. McGraw-Hill, New York, 2007.

[63] Hughes-Hallett, D., Gleason, A.M., Flath, D., Gordon, S.P., Lomen, D.O., Lovelock, D., McCallum, W.G., Osgood, B.G., Pasquale, A., Tecosky-Feldman, J., Thrash, J.B., Thrash, R.K., Tucker, T.W., Quinney, D. and Bretscher, O.K.: *Calculus*. John Wiley & Sons, New York, 1994.

[64] Meriam, J.L. and Kraige, L.G.: *Engineering Mechanics Volume 2: Dynamics*. 6th edn. John Wiley & Sons, New York, 2008.

[65] Sze, K.Y., Yang, X. and Yao, L.Q.: Stabilized Plane and Axisymmetric Piezoelectric Finite Element Models. *Finite Elements in Analysis and Design*, vol. 40, pp. 1105–1122, 2004.

[66] Johnson, L.W., Riess, R.D. and Arnold, J.T.: *Introduction to Linear Algebra*. 2nd edn. Addison-Wesley Publishing Company, Inc., USA, 1989.

[67] Phillips, J.R.: Piezoelectric Technology: A Primer. 2000.
Available at: "`http://www.eetimes.com/document.asp?doc_id=1255166`

[68] Extreme Learning Machines.
Available at: `http://www.extreme-learning-machines.org/`

Appendix A

Material Properties

The material properties listed here are derived from the source literature as well as an extra source or 2. Table 1 is from Carrera *et al.* with the included problem data.

Table A.1: Carrera material properties[1]

Material: Producer:		PZT-5H Morgan	PZT-5A Morgan	PIC 515 PI Ceramics	PVDF Kynar
E_1	GPa	71	69	79	2
E_2	GPa	-	-	-	-
E_3	GPa	111	106	77	2
v_{13}	-	0.31	-	-	-
ρ	$\frac{kg}{m^3}$	7450	7700	7800	1800
$\gamma_{11}/\gamma_{\epsilon 0}$	-	-	1700	1980	12
$\gamma_{33}/\gamma_{\epsilon 0}$	-	3400	1730	2100	12
d_{33}	$\frac{m}{V} \times 10^{-12}$	593	374	140	-33
d_{31}	$\frac{m}{V} \times 10^{-12}$	-274	-171	-210	23
d_{15}	$\frac{m}{V} \times 10^{-12}$	741	575	580	-
T_C	°C	195	365	250	-

Table A.2: Carrera plate material properties[1]

Material:		PZT-4	Gr/Ep
E_1	GPa	81.3	132.38
E_2	GPa	81.3	10.756
E_3	GPa	64.5	10.756
v_{13}	-	0.432	0.24
v_{23}	-	0.432	0.49
v_{12}	-	0.329	0.24
G_{23}	GPa	25.6	3.606
G_{13}	GPa	25.6	5.6537
G_{12}	GPa	30.6	5.6537
e_{15}	$\frac{C}{m^2}$	12.72	-
e_{24}	$\frac{C}{m^2}$	12.72	-
e_{31}	$\frac{C}{m^2}$	-5.20	-
e_{32}	$\frac{C}{m^2}$	-5.20	-
e_{33}	$\frac{C}{m^2}$	15.08	-
γ_{11}	$\frac{pC}{V\,m}$	13060	30.9897
γ_{22}	$\frac{pC}{V\,m}$	13060	26.563
γ_{33}	$\frac{pC}{V\,m}$	11610	26.563

Table A.3: Piefort plate material properties[13]

Material:		PVDF
ρ	$\frac{kg}{m^3}$	1800
E_1	GPa	2
E_2	GPa	2
v	-	0.29
G_{12}	GPa	0.775
d_{31}	$\frac{C}{N}$	2.2×10^{-11}
d_{32}	$\frac{C}{N}$	0
γ	$\frac{F}{m}$	1.062×10^{-10}

Table A.4: Cen *et al.* plate material properties [10]

Material:		Composite	Piezoelctric
E_1	GPa	$25 \times E_2$	2
E_2	GPa	6.9	-
G_{23}	GPa	$0.5 \times E_2$	-
G_{13}	GPa	$0.5 \times E_2$	-
G_{12}	GPa	$0.2 \times E_2$	-
v	-	0.25	0.29
e_{31}	$\frac{C}{N}$	0	0.0046
e_{32}	$\frac{C}{N}$	0	0.0046
γ	$\frac{F}{m}$	8.85×10^{-12}	0.1062×10^{-9}

Appendix B

Code CD

Here a CD is supplied on which the program is situated. The file and folder make-up is as follows:

CD

- Fortran
  - + Fortran Version 1
  - + Regression testing
  - + Some Results and Plots Using Gnuplot
  - + Test_Cases
  - + THE PROGRAM
  - * SAOHPC_0.sub
  - * README.txt
- Matlabfiles
  - + GRNN - From Matt In MATLAB - REF Prof Green
  - + Individual Runs
  - + Optimisation
  - + Results
  - + Total Program
  - * README.txt

Please take note of the README in each folder as these will give further elaboration. The main program is in Fortran. The Matlab program was used as a learning tool in order to become proficient in the coding of the optimisation, FEM and regression.
The CD follows: